Experimental wave flume study: the stability of an artificial reef

Master of Science Thesis

C. Diederen

Delft University of Technology

TU Delft

Experimental wave flume study: the stability of an artificial reef

by

C. Diederen

to obtain the degree of

Master of Science

in Civil Engineering

at the Delft University of Technology.

Student number:	4374274	
Date:	June 23, 2022	
Thesis committee:	Prof. dr. ir. Marcel van Gent	TU Delft, Deltares (chair)
	Dr. ing. Mark Voorendt	TU Delft
	Ir. Jeroen van den Bos	TU Delft, Boskalis
	Ir. Menno de Ridder	Deltares
	Jesse de Bont	ReefSystems
	Max Dijkstra	ReefSystems
	Ir. Barend van den Bosch	Van Oord

TU Delft

Acknowledgements

This report presents the thesis research and is the final work to obtain the degree of Master of Science in Hydraulic Engineering at the Delft University of Technology. Of course, without the help of several people, this master thesis would not have been possible. Therefore, I would like to take this opportunity to thank everyone who contributed to this thesis.

First of all, I would like to express my gratitude to the thesis committee. Marcel van Gent, I really appreciate your pleasant guidance and helpfulness during the project. Our meetings gave me new insights, and you helped me back in the right direction where necessary. Mark Voorendt, your feedback on the report's structure has helped me be critical of my work and structure my research. Jeroen van den Bos, thank you for your input and suggestions during the progress meetings. And thank you, Menno de Ridder, especially for your help during the tests in the initial phase, when I was still very searching, and for your feedback and input during the meetings.

I would also like to thank Max Dijkstra and Jesse de Bont for giving me the opportunity and confidence to take on this project for ReefSystems. Although the two weeks of testing at Deltares were hard work, I enjoyed it together with you. Your enthusiasm and the critical questions you asked inspired me to bring the research to a successful conclusion. And thank you Barend van den Bosch for joining the supervisory team and attending the meetings.

This achievement, completing my study path, would not have been possible without the support of my family and friends. I want to thank my family for their unconditional love and support and our happy moments together, which always give me energy. Thank you to my friends and roommates, who provided distractions and fun activities after my laptop was closed or during the weekends. And last but not least, thank you, Pepijn, for your support and making my study days much more fun over the past few months.

C. Diederen
Delft, June 2022

Abstract

An artificial reef is a submerged structure placed on the seabed that mimics some characteristics of a natural reef. Artificial reefs have proven to be an optimal and effective solution in stabilizing coastlines worldwide, but they could also contribute to improving the ecology. The Modular Sealife System (MOSES) is a modular artificial reef created by ReefSystems using interlocking concrete blocks on top of a concrete plate. Although the research results on the added value of the Modular Sealife System (MOSES) for ecology seem promising, ReefSystems did not yet know whether the stability of this artificial reef is guaranteed. Knowledge of the effect the reef will have on the seabed or nearby structures is necessary, as damage can occur if the reef is not stable. Therefore, it is crucial to have information on the influence of different hydraulic conditions on the stability of the structure.

The objective of this master thesis is, therefore, to investigate experimentally how non-breaking wave loading affects the stability of the MOSES artificial reefs. Small scale wave flume tests with a length scale factor of 20 were conducted in the Scheldt flume at Deltares in Delft to determine the stability of three physical reef models with varying characteristics under multiple wave loading conditions. Based on this, a prediction of the stability of the reef prototype was investigated.

The main reef model, referred to as the grey reef, was constructed of 40 hexagonal tubes attached to a concrete plate with dimensions of 0.1 x 0.1 x 0.01 m. ReefSystems is most interested in the stability of this reef. For another reef model, referred to as the pink reef, the tubes are attached to a concrete plate with double the height of the grey one, resulting in dimensions of 0.1 x 0.1 x 0.02 m. Finally, the so-called 2x2 reef was made of four grey reefs attached, resulting in a surface area that is four times as large as the grey reef.

The experimental tests' conditions were based on varying parameters (the relative wave height, wave steepness, and water depth) to obtain the broadest possible range of conditions. Variations in regular or irregular waves, with or without foreshore, water depth, wave height, and period were used for the tests. For each experimental wave flume test, it was established whether the reef was stable, thus whether any displacement had occurred. The observed stability of the reef was related to the conditions during that test, determined by the resistance-type wave gauges that recorded the height of the free surface. With the use of the wave spectra, the most relevant parameters (the significant wave height H_{m0}, the peak period T_p, and the spectral wave period $T_{m-1,0}$) were obtained to give relevant data, which was used for the analysis.

Based on the data of the experimental flume test, a stability function was determined, giving the influence of three non-dimensional parameters (the relative wave height $d_{relative}$, the wave steepness s, and the relative water depth H_{m0}/d) on the stability of that reef. The stability function is based on the data points obtained from the experimental tests for the main grey reef model. Since non-dimensional parameters were used, the stability function can be used to give a stability prediction for an up-scaled version of that reef.

The tests with the grey reef were also used to compare with two stability prediction methods; the Morison method and a prediction method based on the mobility parameter θ. Some coefficients had to be determined based on literature for the Morison method. In contrast, for the mobility parameter prediction method, constants had to be determined based on curve fitting through the data points. Nevertheless, both prediction methods accurately describe the grey reef's stability. Because the Morison method uses dimensional parameters rather than dimensionless parameters like the mobility parameter prediction method, up-scaling is more complicated. This means that a separate prediction is required for each up-scaled version of the reef, but the mobility parameter prediction method could use the same prediction for all up-scaled versions of the reef. However, the Morison method includes more reef-specific property parameters, while for the mobility parameter method, some reef properties are included in the determined coefficients. Therefore, the Morison method is more applicable to reefs with property variations.

Tests with the pink and 2x2 reefs were conducted to determine the effect of a difference in height, weight, and surface area on the stability. A qualitative comparison of the reefs made it clear that the 2x2 reef is the most stable, followed by the pink reef, and the grey reef is the least stable. The determined stability function and the two prediction methods were also applied to the two other reefs. Both the stability function and the prediction method using the mobility parameter had to be calibrated on the wave flume data for those two reefs, but the Morison method could be applied without calibration, as it includes more reef-specific property parameters.

It was concluded that a prediction of the stability of an original MOSES single plate reef prototype can best be given based on the Morison method. Due to some manufacturing inaccuracies, the original MOSES prototypes are not precisely scaled versions of the models. Although both prediction methods (Morison method and mobility parameter method) are largely consistent with the data obtained from the flume tests, the Morison method seems best suitable for a stability prediction for reefs with deviating properties such as the MOSES artificial reef.

For further research, it is recommended to investigate the influence of scouring and currents on the stability of artificial reefs. Besides, examining the influence of multiple reefs close to each other was recommended, as it was found that it affects stability during testing. Morison's drag coefficient determination with flume tests is advisable. And lastly, research on the determination of the significant horizontal velocity is recommended.

Contents

1

Introduction

1.1. Research motivation

Coastlines define the transition between land and water. Coastal erosion and accretion have always existed, changing and shifting the coastlines worldwide, and contributed to the shaping of the present coastlines. This is, as such, not unfavorable since the movement was driven by forces that caused the coastlines to move to a new, natural equilibrium. However, in recent years, human activities and natural effects have intensified coastal erosion (Ma et al., 2020).

Nowadays, the erosion of beaches is a global problem (Luijendijk et al., 2018), which has led to the need to protect the coast. However, although some engineering projects are intended to solve erosion problems, these projects can also contribute to creating problems at nearby locations. Therefore, a coastal protection is a complicated and complex practice in which the solution should be friendly to natural, economic, and social elements in the particular region of interest.

The coastal zones, which serve as a habitat to many species of flora and fauna, are experiencing increasing pressure from both the sea and landward sides. The combination of sea-level rise due to climate change, and continuing economic development along coastlines, causes the Coastal Squeeze phenomenon (Pontee, 2013). Growing coastal communities cause human pressure to stress the need for a stable coastline. The rise of the sea level causes marine habitats to move landward to keep the physical environment unchanged. Protective measures to arm coastlines against sea-level rise interfere with the landward movement of marine habitats. Therefore, these coastal protection structures imply a strain on the natural habitat mitigation, causing the marine ecosystem to be 'squeezed' and thus causing intertidal habitat loss.

While this near-shore marine biodiversity is devastated by the Coastal Squeeze phenomenon, overfishing is generally considered the primary threat to marine biodiversity, especially when fishing methods also destroy the habitat (Reid et al., 2005). Besides, people are not only taking more fish than nature can sustainably yield annually but also too many high trophic levels and valuable fish species are taken, which thereby truncates the food web (Pauly et al., 2005). Figure 1.1 graphically shows this homogenization of the food web. These three aspects of overfishing cause the health weakening of both fish stocks and the marine ecosystem

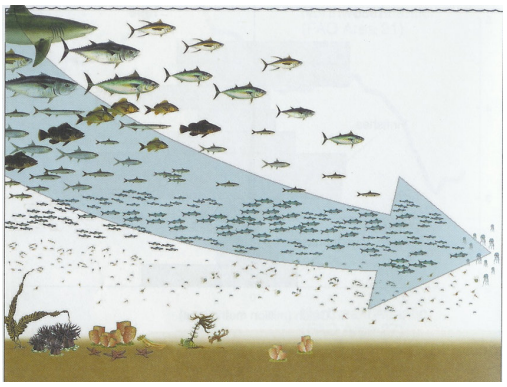

Figure 1.1: Fishing down the food web (Pauly et al., 2005). A graphical representation of the homogenisation process in the marine environment.

as a whole since fish are an essential part of marine ecosystems. Fish and life in the ocean face multiple threats, among which overfishing and climate change are the biggest.

An example of a coastal protection that is already used worldwide is an artificial reef, a submerged structure placed on the seabed which mimics some characteristics of a natural reef (Jensen et al., 2000). Artificial reefs have proven to be an optimal and effective solution in stabilizing coastlines worldwide, but also being an ecological solution (Cardenas-Rojas et al., 2021). Of course, implementing an artificial reef will not solve the problem of structural erosion, climate change, or overfishing, but it at least helps improve the consequences of it. This report studies the stability of artificial reefs.

1.2. Problem analysis

Currently, reefs are installed at some locations around the world. ReefSystems developed a modular artificial reef using interlocking blocks, the Modular Sealife System (MOSES). It is a structure that serves as a habitat for marine life to find food, shelter, and a safe space to reproduce. The MOSES reef aims to provide habitat for marine life, improve underwater biodiversity, and restore nature.

The first three pilot installations were installed in the Haringvliet, the Netherlands, in June 2019. After that, the reef was installed at two other locations in the Netherlands, both in the North Sea Channel and Shimoni, Kenya, and Portobelo, Panama. Much research has been done and is still in process about the effects on the biodiversity in these areas. Furthermore, in the case of Kenya, the coral reefs in this area have been damaged due to dynamite fishing, so a reef restoration project has been started to restore the damaged coral. Small pieces of living coral are placed on the MOSES artificial reefs, and after months of monitoring, it was observed that the corals are growing successfully (ReefSystems, 2021). The reefs are likely to be installed at different locations around the world with each location having a different water depth.

The connected blocks are made in such a way that they can be positioned differently, as shown in Figure 1.2. The structure consisting of the blocks is attached to a Stelcon concrete plate which has to be placed on the seabed, as can be seen in Figure 1.2a. The inside of the blocks have a smooth surface, so they will not become overgrown and will stay accessible to marine life. However, the outside surface has a rough texture, which functions as a hard substrate to grow on.

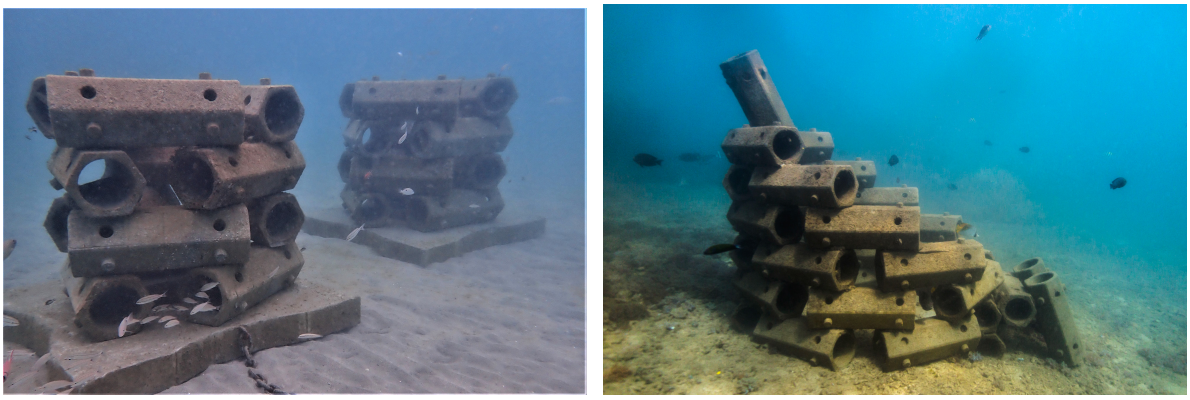

(a) MOSES project Portobelo, Panama in July 2021. Interlocking blocks are attached to a stelcon concrete plate.

(b) MOSES project Shimoni, Kenya in April 2021. Picture is made by Ewout Knoester.

Figure 1.2: Projects with different positioning of the interlocking blocks

Ideally, ReefSystems would like to install the MOSES reefs in many places around the world to improve underwater biodiversity and restore nature in as many areas as possible. Currently, the reef acts primarily as an environmentally friendly solution for ecology, but it has the potential to become a coastal structure. Although the results of the research on the added value for ecology seem promising, it is not yet known whether the stability of the reefs is guaranteed. Depending on the location of the construction of a reef, hydraulic conditions will vary, affecting the stability of the reefs. For clients looking to invest and include MOSES reefs in their construction projects, knowledge of the effect the reef will have on the seabed or nearby structures is necessary, as damage can occur if the reef is not stable. Therefore,

it is crucial to have information about the influence of different hydraulic conditions on the stability of the structure. This will be determined with the use of experimental tests in a wave flume.

1.3. Research objective and research questions

The objective of the study is to provide insight into whether or not the artificial reef is stable for a given location with known hydraulic circumstances during wave loading. Therefore, the research question that will be answered during this graduation project is:

> ***How does non-breaking wave loading affect the stability of the MOSES artificial reefs?***

The following sub-questions will function as a guideline to comprehensively answer the main question in the end. In other words, the main question has been split into the following questions:

1. What wave loading parameters are of importance to determine the stability of the artificial reef?
2. How can a wave flume experiment be designed to make relevant observations on the stability of the artificial reefs?
3. How can the results of the experimental tests be used to determine the influence of the wave loading parameters?
   (a) What is the influence of the relative wave height, the wave steepness, and the relative water depth on the stability of the reefs?
   (b) How can a prediction method be used to predict the stability characteristics of the artificial reefs?
   (c) How do the height, weight, and surface area of the reefs affect the stability?

1.4. Methodology

This section explains the methods applied to come to a comprehensive approach. These methods, as a whole, meet the objective of this research. The research is divided into three parts; a literature study, the experimental tests, and the analysis of these tests. Each part answers a research question.

Literature study - The first part of the research contains a literature study to get an overview of relevant information and a thorough view of the stability influencing parameters. This answers research sub-question 1. Qualitative data will be collected with the help of literature sources and study material about the wave loading parameters. Besides, prediction methods will be explained, which will be compared to the results of the tests in the analysis.

Experimental tests - In the second phase, scaling laws are used to interpret the model choices, and based on the earlier determined wave loading parameters, an experiment can be designed to make relevant observations. For this, previously conducted physical experimental studies regarding this topic will mainly be used. This answers research sub-question 2. Afterward, the design of the experimental set-up is used to perform the tests in the Scheldt flume at Deltares. The physical tests started on November 22nd, 2021, and lasted for two weeks.

Analysis - With the use of the defined relevant wave loading parameters from the first part of the research, the data obtained from the experimental tests are then analyzed and interpreted to answer the last sub-question, including sub-questions 3.a, 3.b, and 3.c. The data is stored in an Excel spreadsheet, and the graphs are made with the help of the computer programming language Python Notebook.

When all the sub-questions are answered, the research question can be answered, and conclusions can be drawn.

1.5. Research scope

The research will only focus on the stability of the MOSES artificial reef from the company ReefSystems, so no other reefs will be tested in the Scheldt flume. Additionally, in reality, the reef will be installed on

location-specific substrate composition, but this will not be taken into account when testing the reef. The tests will be conducted without substrate, so the reef will be placed on the concrete bed of the Scheldt Flume. The research will not include the study of the ecological value of the reef or the functioning of the coastal protection of the reef. Moreover, oceanic currents will not be taken into account during the experiments; the wave flume experiments will only expose the reef to non-breaking waves.

Due to the relatively short time of two weeks to use the Scheldt flume, the most important tests had to be conducted first. If time allowed, the intention was to assess the degree of wave energy dissipation, but there was not enough time to test this, and it will therefore not be further analyzed.

1.6. Reading guide

Details and content presented in the chapters of the thesis report are briefly described below. Besides, Figure 1.3 gives a detailed overview of the report's structure.

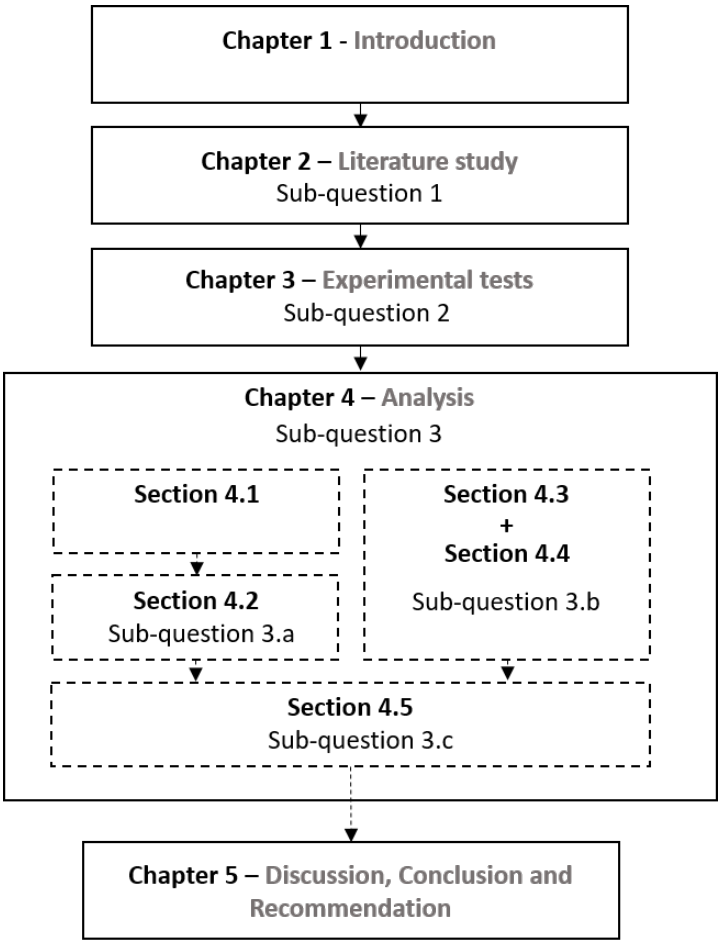

Figure 1.3: Structure of the report

Chapter 1: Gives a brief introduction of the research along with motivation, problem description, research objectives, methodology, research scope, and a reading guide of the report.

Chapter 2: A relevant literature overview is provided to put this research in proper perspective and to give the background information of valuable aspects. First, this chapter contains a description of the hydraulic conditions for an artificial reef. For instance, the depth at which these specific artificial reefs are normally placed and for what reason. Secondly, some important wave phenomena are explained, including the use and operation of wave spectra, which will be needed to interpret the outcome of the experiments to get usable data. Thirdly, dimensionless wave loading parameters are considered, which will be used for both the determination of the test plan and the analysis of the experimental data. And finally, two stability prediction methods are explained: the Morison method and the mobility parameter.

With this chapter, the first sub-question will be answered.

Chapter 3: The applied physical model will be presented. An explanation of the experimental set-up (including flume properties and the used instruments), the scaling of the model, and the layout of the tested reef models will be given. Afterward, the test configurations will be explained. Besides, the outcome of the experiments is interpreted using spectral parameters obtained from the literature study to get usable data to analyze. The second sub-question will be answered in this chapter.

Chapter 4: The data obtained from the experiments will be analyzed. The relation between the different non-dimensional parameters obtained from the literature study and the stability of the reef will be determined. The data from the experiments will be compared to two stability prediction methods to determine the suitability of these methods for a full-size prediction. And lastly, an analysis is performed about the effects of the height, weight, and surface area of the reefs on the stability. After this chapter, sub-questions 3.a, 3.b and 3.c will be answered.

Chapter 5: The results of the data analysis are discussed and a conclusion with regards to the research objective and questions is given. Finally, recommendations are provided for further research based on the outcomes.

2

Deriving relevant parameters

In this chapter, several relevant wave loading parameters will be obtained, which will be utilized to either determine the test plan of the experiments, interpret the measurements from the experiments to get valuable data or analyze the data from the experiments. In addition, relevant parameters for two stability prediction methods are given. Thus, this chapter provides an answer to research sub-question 1.

2.1. Hydraulic circumstances

Installation depth, wave height, currents, and tides are the main hydrographic elements to consider when choosing a site to construct an artificial reef. Wave forces and currents are responsible for loss of stability, such as sliding and overturning, and currents are responsible for the formation of local scour around the reef after installation (Grace, 2001; Düzbastılar et al., 2006). Therefore, the reef should withstand these forces and the effects of fishing, illegal trawling, anchoring, vessel draught, and other damages.

Many unsuccessful artificial reef applications have occurred over the last few decades due to a lack of knowledge and experience, resulting in unstable artificial units being installed at sites. Moreover, due to environmental design parameters like depth, wave and currents, sediment type, and slope, these artificial reefs pose significant dangers (Bell & Hall, 1994; Ingsrisawang et al., 1995).

Although reef stability is dependent on multiple conditions, this report focuses on stability due to non-breaking wave forces, as described in the scope of the study (Section 1.5). Other processes, such as scouring and flow currents, will not be considered for the experimental tests in the wave flume but may influence the stability of the reef.

The MOSES reefs will be constructed at sites with a wide variety of water depths. As a future project will be conducted near Aruba, where water depths are between approximately 3 to 9 meters, reef stability due to wave load should be determined for these values. For another future project in the Black Sea, the water depths vary from 9 to 20 meters. Lastly, a good option is to place the reefs in wind farms, as fishing is not allowed, but the water depth can be up to 50 meters at these locations.

2.2. Wave phenomena

In this section, a brief explanation of some wave theories is first given, particularly for what conditions these theories should be used. Next, the linear wave theory is explained, and finally, the use of a wave spectrum for irregular wave fields is given, including relevant wave spectra parameters arising from it. These parameters will be used to collect data from the wave records from the experimental tests.

2.2.1. Wave theories

Gravity dominates the movement of waves in water with a free fluid surface. It requires energy to make these movements happen. The wind can supply this energy and is the most fundamental cause of

wave formation in nature (Kolkman & Jongeling, 2007).

The Navier-Stokes equations can fully describe water in motion, although different terms can be ignored in different conditions. Figure 2.1 gives a well-known graphic of the application of several wave theories. The linear wave theory (or Airy wave theory) is an often-used theory to describe the motion of surface gravity waves. However, as can be seen in Figure 2.1, this theory should not be used for steep waves or waves in very shallow water, but non-linear theories are available, such as the *Stokes wave theory*, *cnoidal wave theory*, and the *stream-function theory*. However, the linear wave theory can still estimate the waves, even for situations where non-linear theories should be used, and will therefore be used within this research.

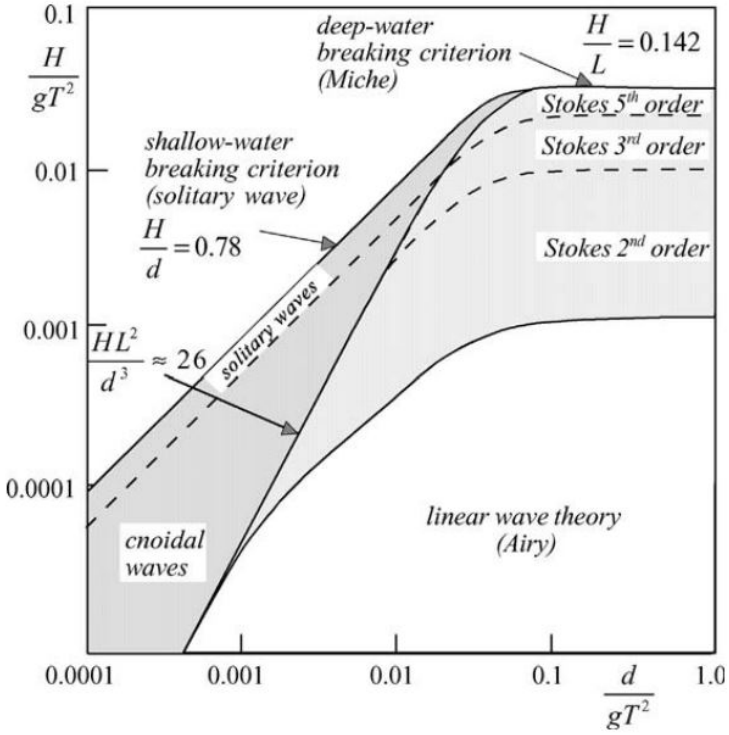

Figure 2.1: Validity of wave theories (LeMéhauté, 1976)

2.2.2. Linear wave theory

The linear wave theory is a theory for two-dimensional progressive gravity waves and is the basis for deriving the physical characteristics of wind-generated waves (Holthuijsen, 2007). The theory considers only the simplest conditions (such as constant depth and wave amplitude in space and time, neglecting viscous stresses). It ignores the effect of wind, dissipation, and other non-linear effects. Assumed is that the wave height H is much smaller than the wavelength L, so the wave steepness $H/L << 1$, and the non-linear terms are neglected (Svendsen, 2006). The continuity equation and momentum balance that define the free surface boundary conditions are linearized for the linear wave theory, which is shown in Appendix A.

The water depth d, the wave height H, the wavelength L, the wave celerity c, and the wave period T are needed to specify a wave motion. However, these parameters are linked by two relations; the definition of the wave celerity c, given in Equation 2.1, and the dispersion relation, given in Equation 2.2 (Svendsen, 2006).

$$c = \frac{L}{T} \tag{2.1}$$

$$\omega^2 = gk\ tanh\ kd \qquad \text{or} \qquad L = \frac{gT^2}{2\pi}\tanh\left(\frac{2\pi d}{L}\right) \tag{2.2}$$

Where:	c	[m/s]	=	Wave celerity (or phase velocity)
	L	[m]	=	Wave length
	T	[s]	=	Wave period
	ω	[rad/s]	=	Angular frequency ($\omega = \frac{2\pi}{T}$)
	g	[m/s^2]	=	Gravitational acceleration (= 9.81 m/s^2)
	k	[rad/m]	=	Wave number ($k = \frac{2\pi}{L}$)
	d	[m]	=	Water depth

With the two relations given above, three of the five parameters to specify a wave motion are enough to describe a wave motion. Therefore, wave conditions are described principally by:

- the incident wave height H (m), usually given as the significant wave height H_s or $H_{1/3}$ for irregular wave fields,
- the wave period T (m), usually given as the mean period T_m, the spectral mean energy period $T_{m-1,0}$, or the peak period T_p for irregular wave fields,
- the water depth d (m).

The horizontal and vertical components of the velocity of a water particle are given in Equation 2.3 and 2.4.

$$u(x,z,t) = \frac{\pi H}{T}\frac{cosh\ k(z+h)}{cosh\ kh}cos(\omega t - kx) \tag{2.3}$$

$$w(x,z,t) = \frac{\pi H}{T}\frac{sinh\ k(z+h)}{cosh\ kh}sin(\omega t - kx) \tag{2.4}$$

2.2.3. Wave spectra

Rather than describing the water surface with a wave-by-wave analysis, a wave spectrum presents it as a stochastic process. The irregular wave field at sea is often determined by measuring the surface elevation η over time, resulting in a so-called wave record. The spectrum contains all conceivable sea states, which may be deduced using a random-phase/amplitude model. This model describes the surface elevation as a sum of a large number of statistically independent, harmonic waves (a Fourier series), as given in Equation 2.5.

$$\eta(t) = \sum_{i=1}^{N} a_i cos(2\pi f_i t + \alpha_i) \tag{2.5}$$

Where a_i is the amplitude and α_i is the phase associated with the frequencies $f_i = i \cdot \Delta f$, in which i = 1,2,3,... and $\Delta f = 1/D_s$. A Fourier analysis of this recording yields the amplitude and phase values for each frequency. The amplitude a and phase α spectra for a certain record are obtained by plotting them against the frequency, as illustrated in Figure 2.2.

The surface elevation is considered Gaussian distributed in most wave record processing methods (as well as for the random-phase/amplitude model), with the average sea water level η set to 0. Furthermore, the spectral description of ocean waves is based on the assumption that the wave components are harmonic and independent. In other words, they behave as linear harmonic waves. Therefore the linear theory of surface gravity waves, as presented in the previous sections, is a theory that perfectly matches the spectral description of ocean waves.

To characterize the wave record, the phase spectrum will be ignored for waves in deep water, so only the amplitude spectrum remains. The linear wave theory (as described in Section 2.2.2) shows that

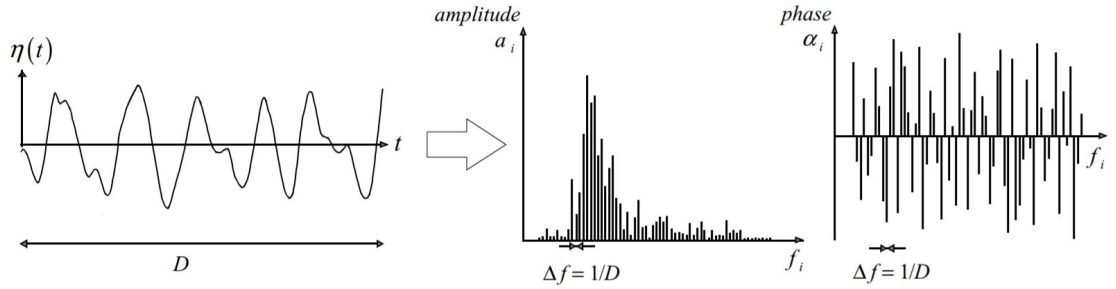

Figure 2.2: Observed surface elevation for a duration D and the corresponding amplitude and phase spectrum (Holthuijsen, 2007)

the energy of waves is proportional to the variance (Holthuijsen, 2007). Furthermore, the variance of each wave component $\frac{1}{2}\overline{a_i^2}$ is a more relevant (statistical) quantity than the amplitude. As a result, the variance spectrum is used instead of the amplitude spectrum. This seems to be trivial and also enough for describing the sea-surface elevation. By dividing the variance for each frequency by the frequency interval Δf, the variance density $\frac{1}{2}\overline{a_i^2}/\Delta f$ is obtained. To make the variance density spectrum continuous, the frequency interval Δf will approach zero ($\Delta f \to 0$). The definition of the variance density spectrum is given in Equation 2.6.

$$E(f) = \lim_{\Delta f \to 0} \frac{1}{\Delta f} E\{\frac{1}{2}\underline{a}^2\} \tag{2.6}$$

A variance density spectrum shows the distribution of the variance of the sea surface elevation over the frequencies. There are two different types of wind-generated waves: waves generated by the local wind, which are irregular and short crested at that location, and are called *wind sea*, and the waves that left the generation area, which take on a regular and long-crested appearance and is called *swell*. Two wave spectra with corresponding time series are given in Figure 2.3, in which the narrow spectrum gives an example of swell waves and the wide spectrum an example of wind sea. It is location dependent whether a wind sea spectrum, a swell spectrum, or a combination of these two spectra is present.

The JONSWAP spectrum gives wind sea conditions appropriate for the most severe sea states and will be used during the wave flume tests. On the other hand, moderate and low sea states are frequently made up of both wind-sea and swell and are not dominated by limited fetch, which is the case for wind sea. A two-peak spectrum should be considered if the swell is regarded as significant.

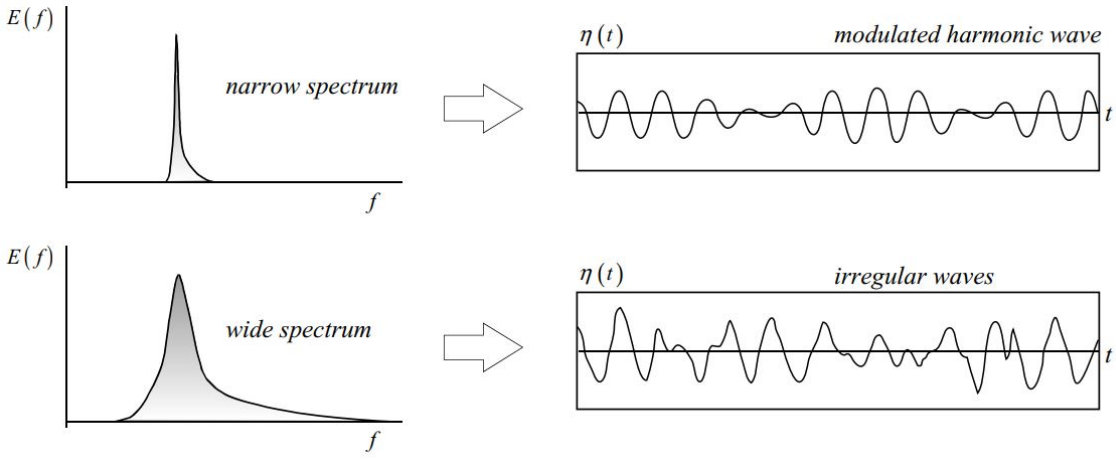

Figure 2.3: A narrow and a wide spectrum for swell waves and wind sea respectively with corresponding time series (Holthuijsen, 2007)

A wave spectrum represents an endless number of alternative time series of waves with the same statistical properties. This indicates that while the order of waves in a time series is unpredictable, all potential time series of a spectrum has the same statistical characteristics. All these statistical characteristics of a random sea-surface elevation (in case the elevation is treated as a stationary and Gaussian process) are expressed in terms of the *moments* of that spectrum, given with Equation 2.7.

The moment m_n is known as the 'nth-order moment' of $E(f)$. The zeroth moment of the spectrum m_0 is equal to the variance of the surface elevation $\overline{\eta^2}$. Due to the exponential influence of deviations in particular at higher frequencies, the greater the order of the moment, the more errors the value will contain.

$$m_n = \int_0^\infty f^n E(f)\, df \qquad \text{for } n = \ldots, -3, -2, -1, 0, 1, 2, 3, \ldots \tag{2.7}$$

The significant wave height is expressed in terms of the variance spectrum, specifically the zeroth moment of the spectrum, as given in Equation 2.8.

$$H_{m0} \approx 4\sqrt{m_0} \tag{2.8}$$

Various wave period definitions are used in approximations of wave processes. The peak frequency f_p is defined as the frequency at which the variance is at its maximum, with a corresponding peak period found by $T_p = 1/f_p$. The significant wave period (mean period of the highest third of the waves) $T_{1/3}$ can be empirically related to the peak period. For swell, the significant period is practically equal to the peak period of the spectrum as given in Equation 2.9 (Goda, 1988), and for wind sea, Equation 2.10 is used (Goda, 1978).

$$T_{1/3} \approx T_p \qquad \text{for swell} \tag{2.9}$$

$$T_{1/3} \approx 0.95 T_p \qquad \text{for wind sea} \tag{2.10}$$

The so-called spectral wave period $T_{m-1,0}$ (given in Equation 2.11) gives more weight to the lower frequencies (so longer periods) in a wave spectrum, than wave periods like the peak period T_p or significant period $T_{1/3}$. Therefore, the spectral period has become accepted as a characteristic wave period when describing the hydraulic attack on coastal structures, especially over shallow foreshores.

$$T_{m-1,0} = \frac{m_{-1}}{m_0} \tag{2.11}$$

During the experimental tests, the free surface elevation is recorded for each test using wave gauges (see Section 3.1 for information on flume set-up and the instrumentation during the tests). From these wave records, wave spectra are determined. The above-mentioned significant wave height H_{m0}, the peak period T_p, and the spectral wave period $T_{m-1,0}$ are relevant parameters obtained from these wave spectra and are used to interpret the results of the experiments to give relevant data, which will be used for the analysis.

2.3. Wave load parameters

This section first explains the use of dimensionless parameters, whereafter it provides the chosen dimensionless wave load parameters that will be utilized both in establishing the test plan and in analyzing the data from the wave flume tests. Lastly, two dimensionless parameters (Reynolds and Keulegan Carpenter number) are explained, which are relevant for stability determination and will be used for the stability prediction methods.

2.3.1. Dimensionless parameters

For the analysis of a physical phenomenon, in this case, the stability of the reef, one of the first steps is to decide which physical variables affect the process being studied (Hughes, 1993). Once this has been accomplished, experimental tests can be conducted to establish the functional relationship between all the important variables. If no theoretical formulation can be discovered, relevant and systematic experiments must be conducted to learn more about the relationship between variables. One variable in the experiment may be changed while all other variables remain constant in the set of experiments. As the number of variables grows, the number of experiments required grows rapidly.

To reduce the number of influencing parameters and therefore reduce test programs, these dimensional parameters are grouped into dimensionless parameters using a so-called dimensional analysis. Dimensional analysis is a method for rationally combining physical factors to create dimensionless parameters, decreasing the number of variables that must be evaluated (Hughes, 1993). Besides, the non-dimensional parameters are also useful since they allow easy comparison between engineering cases at various scales. The parameters can be used to establish a condition of similarity between a small-scale model and a full-scale prototype.

2.3.2. Evaluated parameters

The evaluated dimensionless parameters are the relative water depth, wave steepness, and relative wave height, and will each be discussed below. Figure 2.4 gives an overview of a propagating wave above the reef with the corresponding annotations to clarify the below given dimensionless parameters, which are based on these variables. With the evaluated parameters, the test plan for the wave flume tests was established, and the data obtained from the tests were analyzed using these parameters.

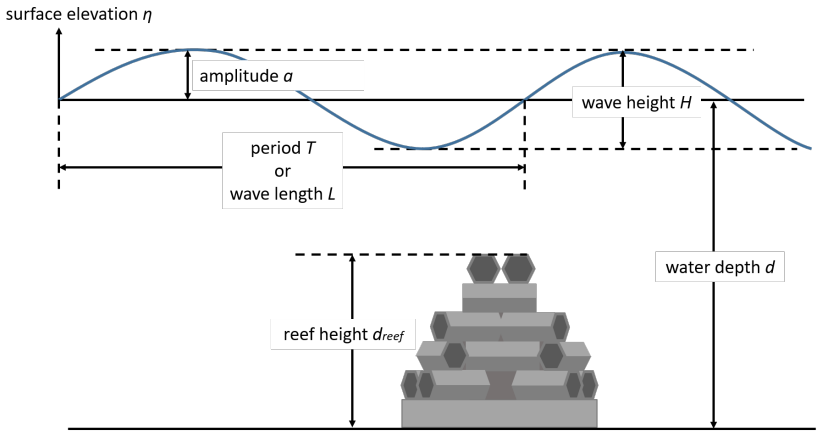

Figure 2.4: Overview of a propagating wave above a reef with reef height d_{reef}

Relative water depth - d/d_{reef}

The variable water-depth-over-reef-height d/d_{reef} or $d_{relative}$ will be evaluated. Several reefs are tested on stability, with different reef height d_{reef} (m). Section 3.3 contains an elaboration on the reef layout. The water depth at which the reefs will be constructed varies from 3 to 50 meters.

Wave steepness - s_0

The fictitious wave steepness s_0, based on the local wave height H (m) and the theoretical deepwater wavelength L_0 (m) or wave period T (s), is frequently used to describe the influence of the wave period, given in Equation 2.12. The wave steepness is a dimensionless parameter and is usually in the range of 0.03 to 0.04, with a maximum steepness of 0.14 for individual waves in deep water (Heineke & Verhagen, 2009). When the wave steepness exceeds this maximum value, it becomes unstable and breaks.

$$s_o = \frac{H}{L_0} = \frac{2\pi}{g}\frac{H}{T^2} \tag{2.12}$$

Relative wave height - H/d

The relative wave height, or wave-height-over-depth ratio, can be described as H/d and is a dimensionless number. The wave height limit in shallow water is 0.78 times the local water depth. Waves propagating over a horizontal and flat seabed, on the other hand, may break at a lower wave height. The breaking limit can be as low as 0.55 under idealized conditions, according to laboratory data (Nelson, 1994) and theoretical analysis (Massel, 1996).

2.3.3. Reynolds and Keulegan Carpenter number

The Reynolds number (Re) and Keulegan Carpenter number (KC) are dimensionless numbers and could be useful for stability determinations, and are given in Equation 2.13 and 2.14 respectively.

$$Re = \frac{UD}{\nu} \tag{2.13}$$

$$KC = \frac{U_m T}{D} \tag{2.14}$$

Where:
U	[m/s]	=	Representative velocity
D	[m]	=	Representative size of the reef along the direction of the prevailing current
ν	[m^2/s]	=	Kinematic viscosity of water (=10^{-6} m^2/s)
U_m	[m/s]	=	Maximum wave orbital velocity
T	[s]	=	Wave period

In practice, both the Reynolds number and the Keulegan Carpenter number change with the orbital velocities during the wave cycle, resulting in distinct values of KC and Re throughout the wave period. The Reynolds number Re and Keulegan Carpenter number KC for irregular oscillatory flow are given in Equation 2.15 and 2.16 respectively, in which σ_U is the deviation in velocity and T_p the peak wave period.

$$Re = \frac{\sqrt{2}\sigma_U D}{\nu} \tag{2.15}$$

$$KC = \frac{\sqrt{2}\sigma_U T_p}{D} \tag{2.16}$$

A smaller value of KC indicates inertia-dominated flow since the separation behind the reef will not occur because the orbital motion of the water particle is small relative to the significant length of the reef. A larger value for the Keulegan Carpenter number KC presents a drag-dominated flow, while separation and vortex-shedding occur.

2.4. Stability prediction methods

To determine the stability of an artificial reef, prediction methods such as the Morison method, which is based on forces, or a method with a mobility parameter can be used, which will both be explained in this section.

2.4.1. Morison

To estimate forces on a submerged reef, the Morison prediction (Morison et al., 1950) can be used, where the forces are estimated based on velocities and accelerations around the reef. For instance Harris & Gonzalez (2005), Düzbastılar & Şentürk (2009), Koudstaal & van Rijn (2020) or MIAO & XIE (2007) has used this method before to predict the stability of an artificial reef successfully.

The reef can become unstable due to the phenomena referred to as *lifting*, *sliding*, or *overturning*. The *lifting* stability criterion is based on vertical equilibrium and will be automatically verified if the horizontal stability equilibrium criterion for *sliding* is verified as well. For the reef to remain stable in terms of *sliding*, the total horizontal wave-induced force F_{wave} should be smaller than the resisting force $F_{resisting}$ of the reef (see Equation 2.17). A certain safety factor SF is added to compensate for some uncertainties. The determination of both the wave-induced force and the resisting force for the MOSES reef are given below.

$$F_{wave} \cdot SF < F_{resisting} \tag{2.17}$$

The wave force F_{wave} consists of two mobilizing forces; a force that acts on the submerged reef unit caused by the fluid stream and is due to the resistance between water and reef F_{drag}, and a force caused by the acceleration of the water past the reef $F_{inertia}$. As illustrated in Equation 2.18, the wave force is equal to the sum of the drag force and the inertial force. These two forces can be calculated with Equation 2.19 and Equation 2.20 respectively.

$$F_{wave} = F_{drag} + F_{inertia} \tag{2.18}$$

$$F_{drag} = C_D \rho_w A_p \frac{u^2}{2} \tag{2.19}$$

$$F_{inertia} = C_M \rho_w V a \tag{2.20}$$

Where:	C_D	[-]	=	Coefficient of drag
	ρ_w	[kg/m^3]	=	Water density
	A_p	[m^2]	=	Projected cross sectional area as seen from the direction of flow
	u	[m/s]	=	Horizontal water particle velocity
	C_M	[-]	=	Coefficient of inertia
	V	[m^3]	=	Volume of the submerged reef
	a	[m/s^2]	=	Water particle acceleration

The resisting forces $F_{resisting}$ prevent the submerged object from moving due to the wave-induced forces. The object's weight is the single resisting force in the event of an object resting on the seabed without any sort of anchoring. As given in Equation 2.21, the submerged object's resisting force is reduced by two forces; the buoyancy force $F_{buoyancy}$ by Archimedes, and the lift force F_{lift} given with Equation 2.22 and Equation 2.23 respectively.

$$F_{resisting} = \mu(W_{object,dry} g - F_{buoyancy} - F_{lift}) \tag{2.21}$$

$$F_{buoyancy} = \rho_w V g \tag{2.22}$$

$$F_{lift} = C_L \rho_w S \frac{u^2}{2} \tag{2.23}$$

Where:	μ	[-]	=	Coefficient of friction (assumed to be 0.5 for the flume)
	$W_{object,dry}$	[kg]	=	Dry weight of the reef
	C_L	[-]	=	Coefficient of lift
	S	[m^2]	=	Planform area of the submerged object

The lower the coefficient of friction, the lower the friction force becomes, and the easier the reef starts to slide. Multiple studies have looked into the friction coefficient of sand, which can vary depending on

the sand type and its moisture contents (Fall et al., 2014). The friction coefficient for wet sand is equal to 0.4 - 0.5, and rocks have an even higher friction coefficient (Koudstaal & van Rijn, 2020). During the experimental tests, the reefs are placed directly on top of the concrete flume, giving a friction coefficient of about 0.5. However, in reality, it is expected that the reef will not slide smoothly but will push itself into the sand. Therefore, it is assumed to have a friction coefficient of 0.6 for using the Morison prediction in real-life situations instead of flume experiments.

Since the drag coefficient C_D, the coefficient of inertia C_M, and the coefficient of lift C_L are case-specific, a value needs to be determined. Since there is little published data on values for these coefficients for complex three-dimensional shapes such as artificial reefs, it is necessary to estimate them.

- The coefficient of drag C_D is mostly dependent on the shape, the surface roughness of the reef and the Reynolds number (Re) of the flow, and the Keulegan Carpenter number (KC) (Seaman, 2000). The drag coefficient will increase over time due to the increased roughness caused by biological growth on the reef unit, resulting in an increase in the drag force. It will be assumed that the drag coefficient is equal to 2.0 based on Koudstaal & van Rijn (2020), since the shape of the reef they used to determine the drag coefficient is similar to the shape of the MOSES reefs.
- The coefficient of inertia C_M depends on the added mass to the structure; the extra inertia the structure will feel when water is accelerated. The value is based on the size and shape of the reef, with a general equation of $C_M = 1 + k_m$ where k_m is the added mass term. A widely used value for k_m is 1 (Harris & Gonzalez, 2005) for reefs with a circular cross-section, so C_m equals 2. However, according to Koudstaal & van Rijn (2020), the inertia (and added mass) coefficient is influenced by the presence of a fixed boundary; the closer the distance to the bed, the higher this coefficient becomes. With a reef placed at the seabed, the added mass term k_m becomes equal to 2, so C_m equals 3. This normative value will be used.
- The coefficient of lift C_L depends on the Keulegan Carpenter number as well, which means that the value varies for different wave conditions. It is assumed that the lift coefficient is equal to 2, since the drag forces are in the same order of magnitude as the lift forces, and while almost no experimental data on this coefficient is available. Besides, according to Tomasicchio et al. (2009), the lift coefficient for pipeline stability for $KC < 12$ is in the same order of magnitude.

For the horizontal water particle velocity (*u*), the characteristic peak bottom orbital velocity ($\hat{u}_\delta$) at the bed is used and can be calculated using Equation 2.24 based on linear wave theory. On the other hand, the horizontal acceleration (*a*) can be calculated with Equation 2.25. For the characteristic wave height and characteristic wave period, H_s and $T_{m-1,0}$ are used, based on Gent & Werf (2014).

$$\hat{u}_\delta = \frac{\pi H}{T} \frac{1}{\sinh kh} \tag{2.24}$$

$$a = \frac{2H\pi^2}{T^2} \frac{1}{\sinh kh} \tag{2.25}$$

Where: H [m] = Characteristic wave height
T [s] = Characteristic wave period
k [m^{-1}] = The wave number ($k = \frac{2\pi}{L} = \frac{2\pi}{\frac{g}{2\pi}T^2}$, where *L* is the wave length)
h [m] = Water depth

The wavelength L is determined with the dispersion relationship as given in Equation 2.2, which is an implicit expression in terms of wavenumber and requires an iteration procedure to calculate the wavelength.

From the previous, it is clear that there are still several uncertainties, particularly concerning the drag coefficient. For conservative considerations, a total safety factor of 1.2 is used in the Morison stability prediction based on these uncertainties (Koudstaal & van Rijn, 2020). In Section 4.3, the Morison

prediction will be compared to the results from the experimental tests in the flume to determine if this prediction method is correct for the MOSES reefs.

2.4.2. Method using the mobility parameter

A well-known non-dimensional parameter used to determine the initiation of motion of sediment in a fluid flow is the Shields parameter (also called the Shields criterion or Shields number). It is a nondimensionalization of a bed shear stress, where estimates of a characteristic velocity and a wave friction factor are used. The latter requires expressions for the bed roughness and the amplitude of the oscillating horizontal wave motion at the bed. However, in some cases, these expressions do not increase the accuracy of the predictions, so a method that only uses a characteristic velocity might be more appropriate. This yields the non-dimensional mobility parameter, given in Equation 4.6.

$$\theta = \frac{u^2}{g\Delta D_{n50}} \tag{2.26}$$

Where:	θ	[-]	=	Mobility parameter
	u	[m/s]	=	The characteristic velocity at the bed
	g	[m/s^2]	=	Gravitational acceleration (= 9.81 m/s^2)
	Δ	[-]	=	Relative density
	D_{n50}	[m]	=	Stone diameter

For the characteristic velocity the peak bottom velocity $\hat{u}_\delta$ is used (Equation 2.24). Since the mobility parameter θ is usually used for the motion of sediment, the equation is based on the stone diameter D_{n50}. However, for the stability prediction of the MOSES reefs, an estimate of this diameter should be provided, which gives a good representation of the reef. This characteristic reef diameter will be referred to as D_{reef}. The relative density can be determined as follows: $\Delta = (\rho_s - \rho_w)/\rho_w$ in which ρ_s is the density of the reef and ρ_w is the density of the water.

The outcome of a test in the wave flume is whether the reef is stable or not, and no distinction is made in the order of magnitude of the instability. The stability prediction should also give this qualitative outcome, so a stability curve should be created, representing the point at which the reef becomes unstable. A prediction method based on the mobility parameter could be of the following shape:

$$d_{relative} \leq r_1 \cdot \theta^{r_2} \cdot s^{r_3} \tag{2.27}$$

The mobility parameter prediction will be compared in Section 4.4 to the data obtained from the experiments, and based on that, the values for the constants r_1, r_2, and r_3 will be determined. Besides, a representative value for the stone diameter D_{n50} has to be estimated.

2.5. Relevant parameters overview

Several relevant wave loading parameters were obtained, which will be utilized to either determine the test plan of the experiments, interpret the measurements from the experiments to get valuable data, or analyze the data from the experiments. Table 2.1 gives an overview of the parameters with the corresponding purpose.

The test plan of the wave flume experiments will be based on the variation of three parameters to obtain the broadest possible range of conditions. These parameters are the relative wave height, wave steepness, and wave height.

During the wave flume tests, wave gauges record the free surface elevation. From these wave records, a wave spectrum will be conducted for each test, and based on this; relevant parameters can be obtained to **interpret the measurement** and be able to analyze the data. Parameters such as significant wave height, the peak period, and the spectral wave period are relevant parameters obtained from these wave spectra.

As can be seen in Table 2.1, the parameters used for **the analysis** of the data are split for a determined stability function, the Morison stability prediction method, and the prediction method based on the mobility parameter. The parameters used for the Morison method are dimensional, while for the stability function and mobility parameter prediction method, non-dimensional parameters will be used.

Table 2.1: Overview of the relevant wave load parameters with the corresponding purpose

		Parameters	**Expression**
Test plan determination		Relative wave height	H_{m0}/d [-]
		Wave steepness	$s_{m-1,0}$ [-]
		Wave height	H_{m0} [m]
Interpret measurements of experiments		Significant wave height	H_{m0} [m]
		Peak period	T_p [s]
		Spectral wave period	$T_{m-1,0}$ [s]
Analysis of the data	Stability function	Relative water depth	$d_{relative}$ [-]
		Relative wave height	H_{m0}/d [-]
		Wave steepness	$s_{m-1,0}$ [-]
	Morison method	Spectral wave period	$T_{m-1,0}$ [s]
		Significant wave height	H_{m0} [m]
		Water depth	d [m]
	Mobility parameter	Relative water depth	$d_{relative}$ [-]
		Mobility parameter	θ [-]
		Wave steepness	$s_{m-1,0}$ [-]

3

Physical model

This chapter contains specifications of the physical model tests. First, the experimental setup of the flume is given, including the instrumentation used during the tests. Secondly, a clarification of the scaling of the model is provided, which is used to determine the reef model set-up. Lastly, the test configurations will be explained. In this chapter, research sub-question 2 will be answered.

3.1. Experimental set-up

In this section, first, the characteristics of the flume are explained. Secondly, an explanation is given about how the wave height is measured with the wave gauges, and elaboration on the determination of the reef stability is provided.

3.1.1. Flume properties

During two weeks, the tests were carried out in the Scheldt Flume at Deltares, Delft. The flume has a length of 55 m, a width of 1 m, and a height of 1.25 m. After four days of testing, a structure was installed inside the flume where the reefs could be placed on top to model certain waves in a relatively small water depth, called a foreshore. Figure 3.1 shows a side and top view of the set-up of the flume, and a schematic overview of the flume, including the foreshore structure, is shown in Figure 3.2.

Both regular and irregular waves can be generated with the Piston type (translatory) wave board located at the beginning of the flume. The wave board is equipped with an Active Reflection Compensation (ARC) system, which prevents wave reflections from the structure to re-reflect from the wave board towards the structure. In addition, the wave board is equipped with three wave gauges measuring the wave height at the paddle. The ARC system identifies any reflected waves and instantaneously compensates the wave board motion to absorb these reflected waves (Deltares, 2021).

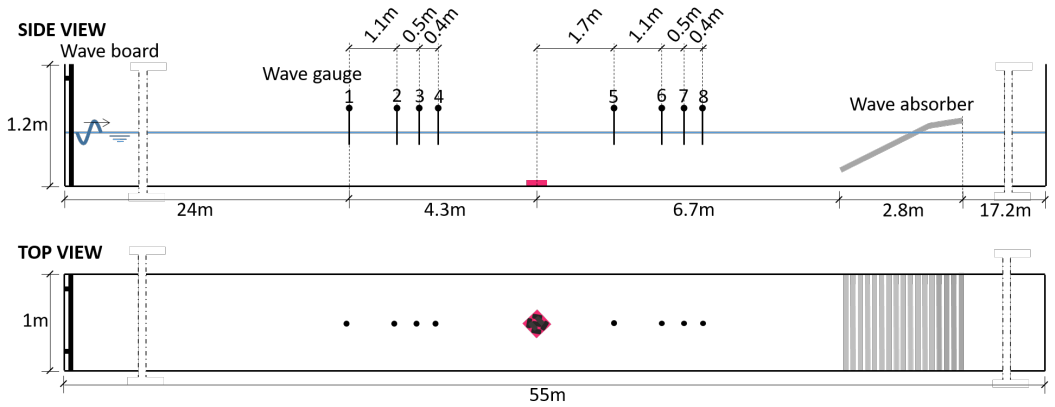

Figure 3.1: Experimental set-up of the flume

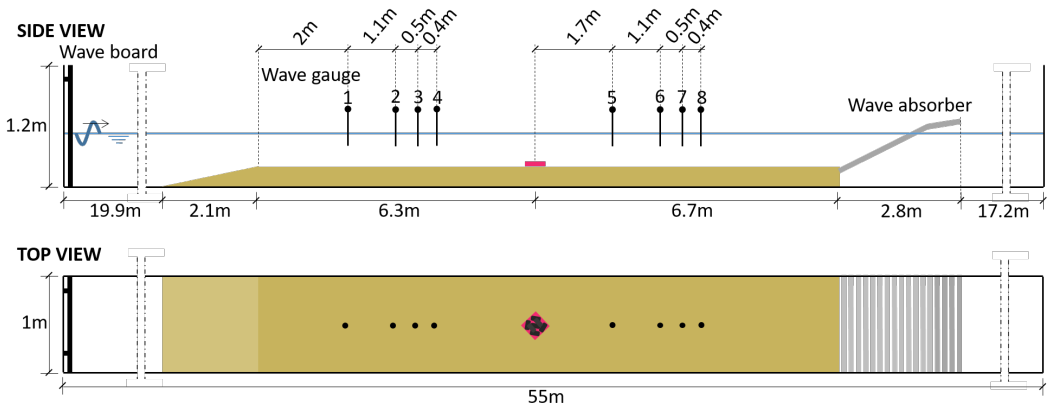

Figure 3.2: Experimental set-up of the flume including foreshore, which is installed after the fourth testing day. The foreshore is made of concrete and has a height of 20 cm

To generate a realistic natural wave field, the Scheldt flume is equipped with second-order wave computation software (Deltares, 2021). For the wave board motion, this considers the second-order effects of the first higher and first lower harmonics of the wave field. This way, spurious waves will be suppressed, and laboratory side effects will be minimized.

Besides, a wave absorber is placed at the end of the flume, so the measurements will be minimally influenced by the reflected waves. Figure 3.3 shows some pictures of the wave absorber taken during the tests. The absorber is placed in such a way that about half of the absorber surface is beneath the water level and half above. Since the water depth varied for each test, the absorber was adjusted for every test.

Figure 3.3: A wave absorber is positioned at the end of the flume to minimize reflected waves

3.1.2. Wave height measurement

Along the flume, resistance-type wave gauges record the free surface elevation. These wave gauges were installed in two sets of four probes, four close to the wave board for wave height analysis and four behind the artificial reef, to calculate the wave transmission. However, due to time constraints during testing, wave transmission is not within this study's scope. Figure 3.4 gives an impression of the wave gauges during the tests. The specific location of these probes can be seen in the experimental set-up of the flume in Figure 3.1.

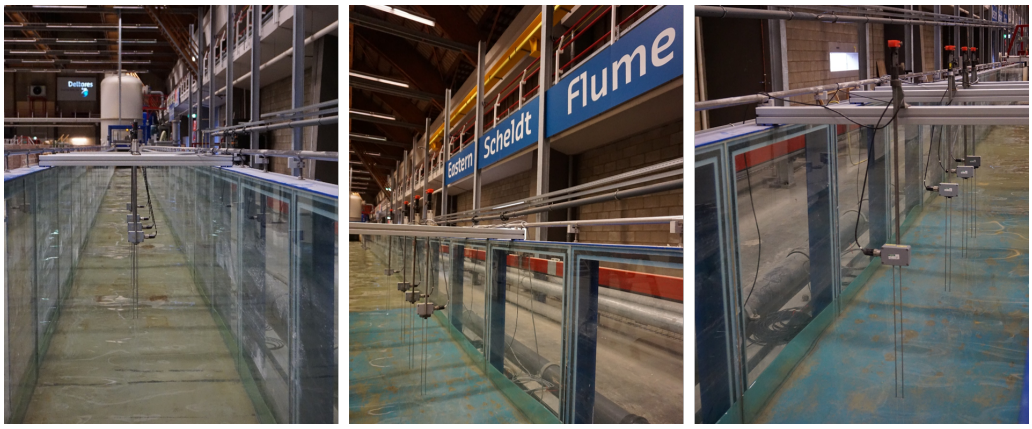

Figure 3.4: Impression of the wave gauges during the experiment

The probes are comprised of two parallel steel rods fixed at a set distance apart, mounted perpendicular to the flow direction, and a small box connecting the two rods at the bottom. The rods act as electrodes for this box; a high-frequency alternating voltage is passed through the rods, and the conductance between the rods is recorded (Hughes, 1993). The rod submergence varies depending on the water level, and so does the measured conductance. The measurements can be converted into a water surface elevation by following a calibration procedure, resulting in a linear correlation between water depth and instrument voltage.

The calibration process took place before the start of the experiments. For this purpose, the wave gauges were submerged in the water up to a certain level, which is set to zero in the voltmeter. Afterward, the instrument recorded the voltage for a range of water surface levels and established the linear correlation between water depth and instrument voltage.

3.1.3. Stability determination

To observe the stability of the reef, a camera was positioned to record the movement of the reefs. A good position had to be established for each test to have both the reefs and the moving water surface on camera. With the help of the videos, observed reef movements were related to the circumstances present at that moment of motion. In addition, during each test, it was checked whether the reef was stable or not, i.e., whether there had been any displacement. There should be no movement by any means when the artificial reef is on the seabed. Therefore, no distinction is made in the degree of movement, so a test is labeled ”not stable” if any movement is observed.

3.2. Model scaling

This section first explains the difference between the criteria of similitude and conditions of similarity between model and prototype, after which the scale selection is given, including an explanation.

3.2.1. Similitude vs. similarity

A physical model should be like a precision device that can predict the behavior of various physical phenomena (Yalin, 1989). If the model is not correctly scaled, or even a small error in measurement/instrumentation occurs, this leads to enormous inaccuracies in the predicted results. Therefore, it is very important to choose an appropriate scale that not only accurately represents the situation, but also reduces scale effects. For a better understanding of scaling, the following points should be kept

in mind;

- *Scale* is the ratio between prototype and model for certain parametric values. The ratio between the measurable characteristics of both model and prototype is constant (Yalin, 1971).
- *Scale effects* are differences in the response of the prototype and model, which is due to the inability to properly scale the two for all relevant mechanisms.
- *Laboratory effects* are the effects of the limitations in the laboratory facilities, such as solid model boundaries, wave and flow generation techniques, etc.

If well designed, a physical fluid model should show exactly similar behavior as the prototype, including the similitude in acceleration, velocity, mass transport, and fluid forces. When all the major factors related to fluid action are in proportion between model and prototype, this state of similitude is supposed to be reached (Hughes, 1993). A distinction is made between the similarity and the similitude of model and prototype. The **criteria of similitude** are based on physical relations between parameters, also referred to as 'scaling laws'. These parameters are mathematical conditions and must be met by a ratio between prototype and model. For the **conditions of similarity**, a set of rules is chosen to make the results of the models acceptable. For this, criteria of similitude can be chosen as a similarity condition.

A model and prototype are in "similarity" if both give a similar response, and this can be achieved even in a situation where the model does not strictly meet the similitude criteria (Hughes, 1993). Furthermore, similarity can be achieved without meeting similitude for situations where certain features of interest are satisfactorily represented in the model. To achieve similarity, three criteria have to be fulfilled: geometric, kinematic, and dynamic similarity.

3.2.2. Scale selection

For wave models, the most relevant forces include gravity, inertia, friction, and surface tension. To have a dynamic similarity, the Froude number (Fr), Reynolds number (Re), and Weber number (We) should be similar for the model and prototype. These numbers are defined as follows:

$$Fr = \sqrt{\frac{Inertial\ Force}{Gravitational\ Force}} \tag{3.1}$$

$$Re = \frac{Inertial\ Force}{Viscous\ Force} \tag{3.2}$$

$$We = \frac{Inertial\ Force}{Surface\ Tension\ Force} \tag{3.3}$$

However, it is not possible to satisfy the Froude number, the Reynolds number, and the Weber number for both model and prototype at the same time. As gravity and inertia are dominant parameters in the physical model wave field, Froude modeling is generally applied while keeping the Reynolds number in the same range (Frostick et al., 2019). Since surface tension is not dominant in wave action, the Weber number can be neglected for wave flume modeling. However, the model should satisfy certain conditions: the wavelength should be larger than 2 cm, and the water depth should be higher than 2 cm (Frostick et al., 2019).

Froude scaling can be used for surface waves because these are gravity-driven. Wave forces and other forces are properly translated from prototype to model by Froude laws. Therefore, for this research, Froude scaling laws will be used. The Froude number should be the same in model and prototype, and this leads to the following, in which the subscript 'p' refers to prototype and 'm' to model.

$$Fr = \sqrt{\frac{\rho L^2 V^2}{\rho L^3 g}} = \frac{V}{\sqrt{gL}} \tag{3.4}$$

$$\left(\frac{V}{\sqrt{gL}}\right)_p = \left(\frac{V}{\sqrt{gL}}\right)_m \tag{3.5}$$

Where: V [m/s] = velocity of the flow
g [m/s^2] = gravitational acceleration
L [m] = length

Rearranging results in:

$$\frac{V_p}{V_m} = \sqrt{\left(\frac{g_p}{g_m}\right)\left(\frac{L_p}{L_m}\right)} \tag{3.6}$$

Now Equation 3.6 can be rewritten in terms of scale ratios (N) as follows;

$$N_{Fr} = \frac{N_v}{\sqrt{N_g N_L}} = 1 \tag{3.7}$$

The relationship for scaling is expressed in the length scale factor (N_L). Other ratios in terms of this length scale factor are given in Table 3.1. For this research model, a length scale factor of 20 is applied. This means that all length scales in the model are 20 times smaller than their sizes in the prototype. Furthermore, for instance, the wave period will be $\sqrt{20}$ times smaller in the model than in real life. With this, the Froude number will be kept constant between model and prototype.

Table 3.1: Froude scaling parameters

Parameter	**Unit**	**Froude scaling**
Length	m	N_L
Area	m^2	N_L^2
Time	s	$N_L^{0.5}$
Velocity	m/s	$N_L^{0.5}$
Acceleration	m/s^2	1
Mass	kg	$N_L^3 \cdot N_\rho$
Volume	m^3	N_L^3
Discharge	m^3/s	$N_L^{1.5}$

3.3. Reef layout

A prototype of a MOSES reef contains a certain amount of fiberglass concrete modules placed on top of a Stelcon concrete plate. For the production of the modules, molds are used, which are made out of steel with a PU-rubber interior to enable a bio-receptive surface. Fiberglass, cement, aggregates, and water are mixed and placed into the molds, resulting in a product of concrete after 24 hours when the concrete is dry.

Three models of the MOSES reef with different weights and heights are tested during the tests. Figure 3.5 shows the different models with dimensions. For the models, 40 reef modules were constructed on a single, double or triple layer of Stelcon concrete plates, shown as the **GREY**, **PINK**, and **GREEN** model, respectively. Both the weight and the height increase with a higher amount of plates. The modules are modeled as 3D-printed hexagon tubes with a diameter of 1 cm and are attached to a thin iron plate to be able to connect it to the concrete. Concrete with fiberglass is used to model the Stelcon

plates to get the desired weight and density. All the parts of a reef model are glued together so that it does not get separated from each other during stability testing. The models of the reefs are shown in Figure 3.6.

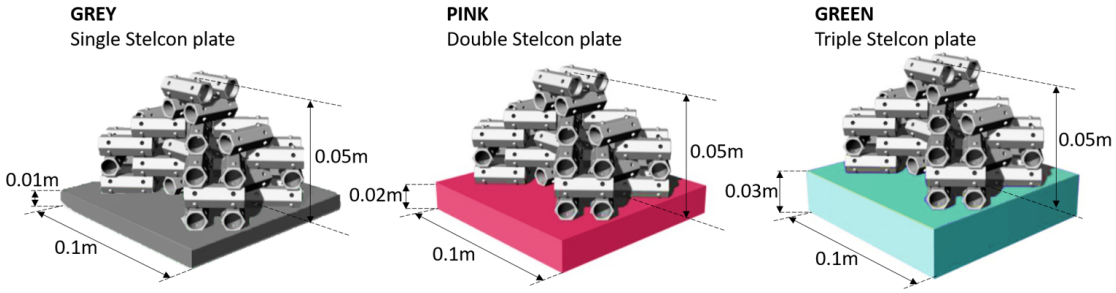

Figure 3.5: Schematic of the models of the reefs, with a single (left), double (middle), or triple (right) layer of Stelcon concrete plates

Figure 3.6: Models of the reefs, with a single (left), double (middle), or triple (right) layer of Stelcon concrete plates

In addition to the three reefs with different amounts of Stelcon plates, four reefs were glued together to create a larger reef. This two-by-two reef was made from the grey reef (see Figure 3.7) and was tested on stability as well. The reef has plate dimensions of approximately 0.2 m by 0.2 m and a height of 0.01 m. This reef was tested to get information about the impact of the contact surface on stability.

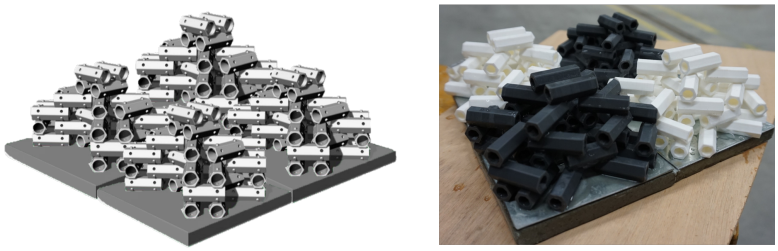

Figure 3.7: A schematic (left) and picture of the model (right) of the 2x2 reef. The deviation in color between the different reefs is due to the difference in printing material, but it has no further significance.

After the reefs were made, the density of the reefs was determined with Archimedes' principle, which states that: 'an object immersed in fluid experiences a buoyant force that is equal in magnitude to the force of gravity on the displaced fluid' (Mohazzab et al., 2017). To calculate the density of the models, Equation 3.8, 3.9 and 3.10 will be used.

$$\rho_r = \frac{m_r}{V_r} \tag{3.8}$$

$$V_r = V_w \tag{3.9}$$

$$V_w = \frac{m_w}{\rho_w} \tag{3.10}$$

Where:	ρ_r	[kg/m^3]	=	density of the reef
	m_r	[kg]	=	mass of the reef (measured above water)
	V_r	[m^3]	=	volume of the reef
	V_w	[m^3]	=	volume of the displaced water by the reef
	m_w	[kg]	=	mass of the displaced water, which equals $m_{r,above\ water} - m_{r,below\ water}$
	ρ_w	[kg/m^3]	=	density of water (1000 kg/m^3)

The masses of the three reef models are determined above and below water. To determine the mass of a reef below water, a string was tied to the bottom of a scale so that the reef could be hung underwater while measuring the weight. Table 3.2 shows the measured masses of the reefs above and below water and the corresponding calculated density.

After the manufacturing of the reef models, some inaccuracies appear. For example, the height of the green concrete plate is for the model 2.5 cm, while it should have been 3.0 cm according to the scaling factor. Besides, the density of the pink reef (with double plate) is expected to be between the densities of the grey and pink reefs, which is not the case. This is probably due to inaccuracies in the used concrete since the dimensions of the pink (double plate) reef are close to the dimensions it should be based on the scaling of the prototype. Lastly, the weight of the 2x2 reef should be four times as high as the grey reef, which is also not true.

Table 3.2: Density determination of the different reef models

	GREY	**PINK**	**GREEN**	**2x2**
	Single plate	Double plate	Triple plate	Four grey reefs
Weight above water [kg]	0.345	0.625	0.751	1.417
Weight below water [kg]	0.181	0.312	0.433	0.710
Reef volume [m^3]	0.000164	0.000313	0.000318	0.000707
Density [kg/m^3]	2104	1997	2362	2004

3.4. Test configurations

This section contains an explanation of the performed tests. An overview of all tests is shown in Appendix B. First, it will be explained why a distinction has been made between regular and irregular waves. Next, it will be presented which different positions of the reefs were used during the tests, the varying parameters will be discussed, and lastly, the accuracy and precision of the tests will be elaborated upon.

3.4.1. Regular and irregular waves

The tests with regular waves were conducted to estimate the conditions under which the reefs would become unstable. Figure B.1 shows the conducted tests with regular waves till the point it became clear that the reefs influenced the stability of each other (see Section 3.4.2 for explanation). These tests have the first TestID letter 'R', referring to 'regular' tests. However, most of the data of these tests on the reef stability are unreliable due to the consequences of the reefs influencing each other; an approximation of the instability conditions is known.

Stability tests with regular waves were conducted for the grey, pink, and 2x2 reef, but only one at a time. Table B.2 in Appendix B gives these conducted tests, with the first TestID letter 'D', referring to 'detailed' regular tests. These tests were mainly performed to study the effect of the height, weight, and contact area on the stability of a reef. The choice of the conditions for each test is based on the estimations from the tests with regular waves with TestID' R'.

The natural seaway on the oceans is irregular. The sea rarely shows a unidirectional, regular sinusoidal wave pattern, as with regular waves, but a mixture of waves of different lengths, heights, and directions is observed ("Chapter 1 - The Marine Environment", 2008). Therefore, for most of the tests, irregular waves were used. For the irregular waves, a Jonswap spectrum with a peak enhancement factor of 3.3 is assumed. Because the wave flume is two-dimensional, the effect of multi-directional waves is not tested. The maximum significant wave height in the flume is H_{m0} = 0.25 m and the maximum regular wave height is H_{max} = 0.4 m (Hydralab+, 2022). Table B.3 gives the experimental tests at which irregular waves are applied, with the first TestID letter' I', referring to' irregular' tests, and the first TestID letter' V', referring to tests with' Foreshore' (Voorland in Dutch), but also with irregular waves.

Table 3.3 gives an overview of all performed tests with their configurations. For the tests with regular waves, the test was ended the moment the reef started moving or after about ten waves for tests with a stable reef. However, for the tests with irregular waves, the test was completed until 1000 waves had passed, even if the reef was unstable before.

Table 3.3: Overview of tested configurations. *The grey reef is used for almost all tests, the pink and 2x2 reef is used for some of the tests.

	Specialties		**Reefs**				**Positioning**	
TestID	**Waves**	**Foreshore**	**Grey** Single	**Pink** Double	**Green** Triple	**2x2**	**Number**	**Separately/together**
Rxxx	Regular	No	x	x	x		1 and 2	Together
Dxxx	Regular	Yes	x	x		x	3	Separately
Ixxx	Irregular	No	x				3	Separately
Vxxx	Irregular	Yes	x*	x		x	3	Separately

3.4.2. Reef positioning

Figure 3.8 shows three options for the reef positioning. Initially, the leftmost option was used to test stability; three reefs next to each other with the sides of the squared reefs perpendicular and parallel to the flow direction. Shortly after testing began, it became apparent that the reefs were less stable when positioned as the middle option of Figure 3.8, and to create a situation with the most critical conditions, this positioning was used during the remainder of testing.

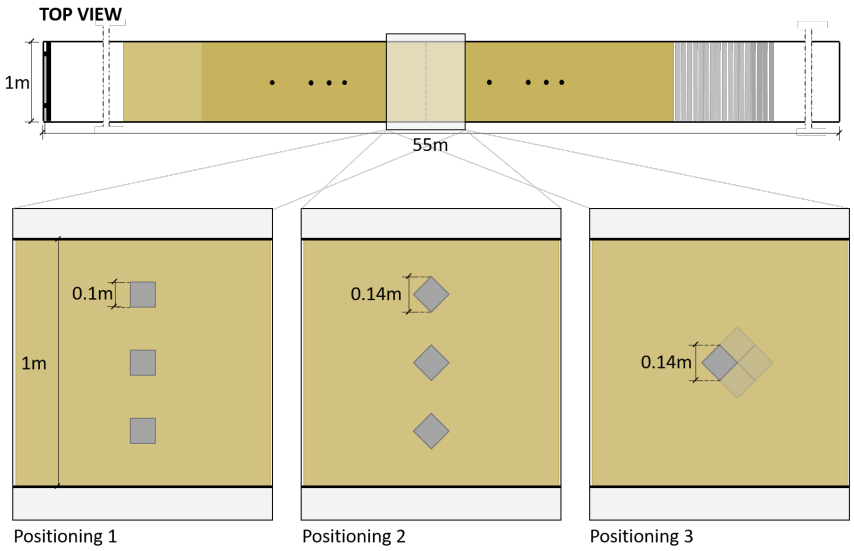

Figure 3.8: Reef positioning options

Furthermore, it became clear that the reefs were influenced by each other when testing with three reefs simultaniously. The middle reef became unstable the fastest, probably due to the current caused by the outer two. Therefore it was chosen to test only one reef at a time to get the most reliable results possible, shown in the right option (Positioning 3) of Figure 3.8.

Since the grey reef with only one Stelcon plate is most critical to be unstable and is the most likely to be used for ReefSystems, it was decided to do further testing primarily with this reef. The focus was generally on the grey reef, but the pink reef was tested for stability in a few conditions to compare the two. The same holds for the two-by-two reef (made out of four grey reefs). Due to the limited testing time at the Scheldt flume at Deltares, chosen is to eliminate the stability analysis of the green reef partially because it became clear that the green reef was highly stable and seldom moved under any of the circumstances.

3.4.3. Varying parameters for test plan

Based on the variation of three parameters (determined in Chapter 2), a test plan was prepared to obtain the broadest possible range of conditions, which is elaborated below. These parameters are:

- the relative wave height (H_{m0}/d),
- the wave steepness ($s_{m-1,0}$),
- the wave height (H_{m0}).

The relative wave height (RWH), or the wave-height-over-depth ratio, varied between 0.1 and 0.45. The ultimate wave-height-over-depth ratio possible for stable, shallow water oscillatory waves propagating in the water of constant depth is equal to 0.55 (Nelson, 1994). Waves with a larger wave-height-over-depth ratio can exist on these horizontal beds, but these would be turbulent breaking waves and therefore lose height rapidly due to the energy dissipation by the turbulence. According to the scope of this research, turbulent breaking waves are not considered, and therefore the maximum relative wave height is chosen to be 0.45.

Besides, the height of the wave flume and the range of waves that can be created by the wave board in certain water depths are limiting factors. This has also played a role in selecting the wave height parameter, which will vary between 0.05 m and 0.17 m. Based on the relevant parameters determined in Subsection 3.4.3 it is probable that the test plan is based on the variety of the relative water depth $d_{relative}$. However, the wave height was used instead to determine the test plan because of the limiting range of waves. By doing so, the relative water depth $d_{relative}$ still varies in the range between 2.5 and 14.

The wave steepness is defined according to Equation 3.11 and has realistic values from around 0.01 to around 0.05 (Hofland et al., 2017). The tests have conditions with wave steepnesses varying between these two values.

$$s_{m-1,0} = \frac{H_{m0}}{\frac{g}{2\pi} T_{m-1,0}^2} \tag{3.11}$$

In deep water, assuming a Rayleigh distribution there is a fixed ratio between the spectral period and sea-state period. The ratio of the peak period T_p over the mean energy (or spectral) period $T_{m-1,0}$ for a Jonswap spectrum with a peak enhancement factor γ of 3.3 is equal to 1.107 (Rock Manual, 2007). Besides, the ratio between the mean period T_m and spectral mean period $T_{m-1,0}$ is equal to 0.92 (Verhagen et al., 2009; Goda, 2010). The values for the T_p and T_m were necessary for controlling the wave flume; the peak period T_p was used as input for the control file and the mean period T_m was used to calculate the duration of a test T_{test} with 1000 waves as follows: $T_{test} = 1000 \cdot T_m$.

3.4.4. Accuracy and precision

The measurement precision of the wave gauges was 1 mm, meaning that a maximum deviation of the surface elevation of 1 mm is observed between several identical tests. As the wave gauges were calibrated before the start of the experiments, it is expected that the accuracy of the wave gauges is high, so the measured value is very close to the real value.

The wave board in the flume did not create conditions that exactly match the input values of the parameters, which caused the measured values to deviate from them. This happens due to wave transmission in the flume (i.e., wave breaking, shoaling, exchange of energy between frequencies). By performing calibration tests, it is possible to fix this and get exactly the same conditions as the input suggests. However, it was decided not to perform these calibration tests due to time constraints. Moreover, this calibration was deemed unnecessary since the measured values were used for the analysis. Table 3.4 gives an overview of the performed tests with varying parameters.

Table 3.4: Overview of tested configurations with varying parameters ranges

	Input values			**Measured values**		
TestID	**RWH**	**Steepness**	**Wave height**	**RWH**	**Steepness**	**Wave height**
	H_{m0}/d [-]	$s_{m-1,0}$ [-]	H_{m0} [m]	H_{m0}/d [-]	$s_{m-1,0}$ [-]	H_{m0} [m]
Rxxx	0.1 - 0.45	0.01 - 0.05	0.05 - 0.17	0.1 - 0.46	0.011 - 0.078	0.05 - 0.17
Dxxx	0.4 - 0.45	0.015 - 0.025	0.11 - 0.17	0.4 - 0.45	0.013 - 0.027	0.09 - 0.18
Ixxx	0.19 - 0.37	0.015 - 0.05	0.11 - 0.13	0.17 - 0.32	0.008 - 0.041	0.08 - 0.12
Vxxx	0.2 - 0.4	0.015 - 0.05	0.07 - 0.15	0.18 - 0.38	0.004 - 0.041	0.06 - 0.14

4

Experimental data analysis

For each test conducted in the wave flume, the result was a stable or unstable reef. Appendix B gives all tests with the corresponding outcome (stable or unstable), and the corresponding important spectral parameters from Subsection 2.2.3.

To investigate the stability of the MOSES reefs under wave forces, the reefs were subjected to several conditions with both regular and irregular waves during the experimental tests. This chapter first explains qualitatively the relation between the stability and some wave parameters, for which the tests with single plate reef and irregular waves will be considered. Accordingly, a stability function is determined based on the dimensionless parameters obtained from Chapter 1. Thirdly, the data from these irregular wave tests with a single plate reef will also be compared to two prediction methods: the Morison method and a method containing the mobility parameter, to investigate whether these methods are reliable to use for the reef stability. Lastly, a comparison between the three different reefs is given, for which the tests with the double-plated reef and the 2x2 reef will be used. This all answers the third research sub-question.

4.1. Qualitative description of the stability influencing parameters

In this section, some qualitative relations between the stability and wave parameters will be given. For the determination of the stability relations, the tests with irregular waves and the reef with one plate will be used. For the analysis with irregular waves, the tests with TestID letters ”I” and ”V” are used (see Appendix B), and no distinction is made between the tests with the foreshore and without foreshore.

The relation between the wave height H_{m0} and the water depth d for each test with the single Stelcon plate (grey) reef and irregular waves is given in Figure 4.1. The stable tests are displayed with the filled symbols, while the unstable tests have open ones. A test is labeled unstable if the reef has moved at any time during the 1000 waves. For each test, the corresponding wave steepness was calculated (according to Subsection 3.4.3), using the significant wave height H_{m0} and the spectral wave period $T_{m-1,0}$, which are both measured with the wave gauges just in front of the reef. Then the tests are grouped according to the rounding to two decimal places of these calculated wave steepnesses. Four plots are displayed, each with a different steepness: 0.01, 0.02, 0.03, and 0.04. Note that the points in, e.g., the plot for s = 0.01 do not specifically have wave steepnesses of 0.01, but the steepnesses of the points vary around that value.

The limiting height of the wave flume and the created range of waves by the wave board resulted in a certain field of wave conditions, excluding water depths of less than about 0.15 m or greater than 0.8 m. However, outside this range of water depth, it is uncertain whether the relationship between wave height and water depth is the same as within this range; therefore, these limits will be used.

However, some conclusions can be drawn for the given water depth range. For two situations with identical circumstances but only a difference in water depth, the reef will generally become unstable more easily in the case of shallower water. In addition, for two situations with similar conditions but

only a difference in wave height, the presence of higher wave heights will result in a less stable reef. Furthermore, there is a linear relationship between the wave height and water depth, and besides, with increasing wave steepness, the stability depends more strongly on the water depth.

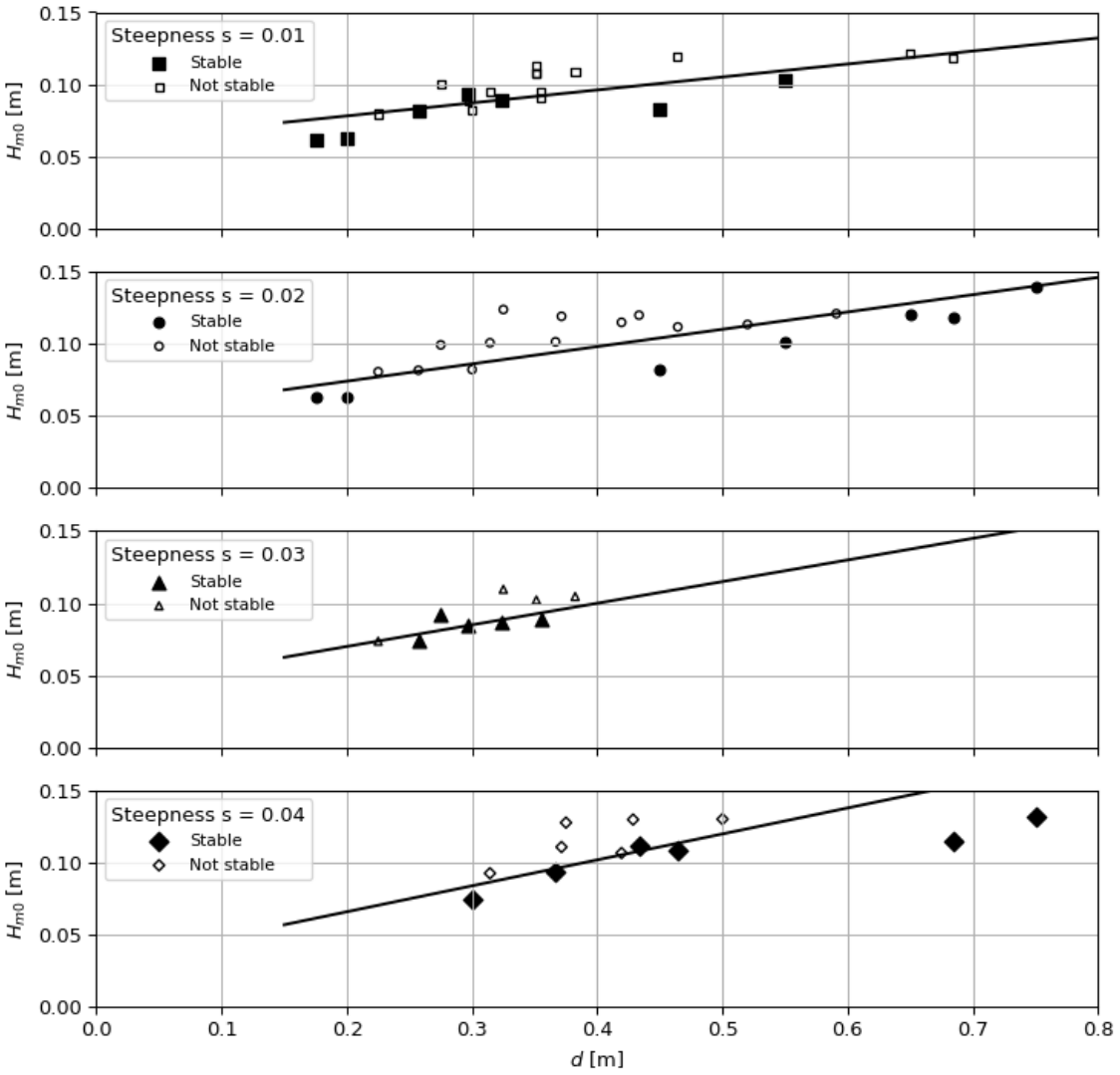

Figure 4.1: Linear relation between the wave height H_{m0} and the water depth d for four different wave steepnesses. The plotted trend lines indicate the linear relationship, suggesting the extreme limit at which the reef just remains stable, which is elaborated in Section 4.2.

4.2. Determining a stability function

The influence of the three dimensionless parameters, which are relative wave height, wave steepness, and relative water depth, on the stability of the (grey) single plate reef will be determined in this section.

4.2.1. Relative wave height influence

A trend line is plotted through the data points (see Figure 4.1) while having most of the unstable tests above this line and stable tests below. This line suggests a sort of ”tipping point” where the reef remains just stable but becomes unstable when the wave height for a given water depth increases or when the water depth for a given wave height decreases. The functions of the trend lines are given in Table 4.1, with each plot having a different trend line. The lines are estimated and are not derived from a linear regression method, such as the most common least-squares method. It is difficult to apply a linear regression method for these plots since they contain both stable and unstable data points, and therefore the lines are estimated.

Table 4.1 gives a rewrite of the determined trend line functions as well, giving the trend lines in terms of the relative wave height H_{m0}/d and the water depth d for the different wave steepnesses s. A general function for the rewritten relations can be described as follows: $\frac{H_{m0}}{d} = c_1\left(c_2 + \frac{1}{d}\right)$, with c_1 and c_2 being two constants which depend on the wave steepness. The dimensions of these functions are not correct yet, but this will be corrected while determining the constants in Subsection 4.2.3.

The trend lines give a linear relationship between the wave height and the water depth, with the wave steepness influencing the specifications of this relation. A high wave steepness results in a relatively high trend line slope, while a low wave steepness has a relatively low slope. This can be seen in Figure 4.1, where for the lowest plot with a wave steepness of 0.04 the trend line is steeper than for the upper plot with a wave steepness equal to 0.01. Besides the variation in slopes, the differences in wave steepnesses give different y-intercepts as well. The y-intercept of these linear functions is the value of the wave height H_{m0} at the point where the line crosses the y-axis (imaginary). However, the trend lines do not cross the y-axis due to the boundary conditions explained in Section 4.1, which means that the water depth range is between 0.15 and 0.8 m.

Table 4.1: Four steepnesses with corresponding trend line function and rewritten function for the relative wave height H_{m0}/d

Wave Steepness	**Function** Trend line	**Rewritten** Relative wave height
$s = 0.01$	$H_{m0} = 0.09d + 0.06$	$\frac{H_{m0}}{d} = 0.06\left(1.50 + \frac{1}{d}\right)$
$s = 0.02$	$H_{m0} = 0.12d + 0.05$	$\frac{H_{m0}}{d} = 0.05\left(2.40 + \frac{1}{d}\right)$
$s = 0.03$	$H_{m0} = 0.15d + 0.04$	$\frac{H_{m0}}{d} = 0.04\left(3.75 + \frac{1}{d}\right)$
$s = 0.04$	$H_{m0} = 0.18d + 0.03$	$\frac{H_{m0}}{d} = 0.03\left(6.00 + \frac{1}{d}\right)$

4.2.2. Wave steepness influence

Knowing the relations between wave height and water depth for different wave steepness, a single relation between these three parameters will be found in this subsection. The constants c_1 and c_2 from the general function for the rewritten relations (Subsection 4.2.1) will be determined. Since the values of the constants are different for varying wave steepnesses, the constants will be described as a function of the wave steepness.

For the constant c_1 a linear relation is found between the values and the corresponding wave steepness, resulting in $c_1 = 0.07 - s$. For the value of the c_2 constant, an exponential relation is found, resulting in $c_2 = 0.94 \cdot (1.17 \cdot 10^{20})^s$. These relations are found by plotting the values of the constants against the steepnesses and fitting a line through them. Appendix C provides an explanation of this.

With these relations for the constants, a general function for the relative wave height can be determined, which depends both on the wave steepness and the water depth, given in Equation 4.1.

$$\frac{H_{m0}}{d} = (0.07 - s) \cdot \left(0.94 \cdot (1.17 \cdot 10^{20})^s + \frac{1}{d}\right) \tag{4.1}$$

The range of the wave steepness for which the function is valid is between 0.01 and 0.04. It is uncertain whether the relationship holds outside this range since no tests have been done for these wave steepnesses.

4.2.3. Relative water depth influence

The relative wave height and the wave steepness are dimensionless parameters in Equation 3.10. However, the water depth is expressed in meters, and therefore the function is not useful for both the small-scale model and full-scale prototype situations. Using a non-dimensional parameter instead of the water depth, easy comparison between engineering cases at various scales is allowed. The relative

water depth d/d_{reef} or $d_{relative}$ will be used, for which a factor of 0.06 is necessary as given in Equation 4.2.

$$d = 0.06 \cdot \frac{d}{d_{reef}} = 0.06 \cdot d_{relative} \tag{4.2}$$

The factor 0.06 is based on the reef height of the grey single plate reef model. Therefore, the resulting determined stability function is only valid for the single plate reef or an up-scaled version, such as the full-size MOSES single plate reef prototype.

As the range of water depth for which the tests were performed is between 0.15 and 0.8 m, the relative water depth is also subject to a certain range. This is because the height of the reef is equal to 0.06 m, and therefore the range of the relative water depth $d_{relative}$ is approximately between 2.5 and 14.

4.2.4. Resulting stability function

Rewriting Equation 3.10 and substituting Equation 4.2 gives Equation 4.3, which is the resulting stability function for the single Stelcon plate (grey) reef, giving the relation between the dimensionless parameters; the relative wave height H_{m0}/d, the wave steepness s and the relative water depth d/d_{reef}. Figure 4.2 gives a plot of this relation and the data points from the tests, with the filled objects being the stable tests again and the open symbols being the tests that were not stable. As can be seen, most of the unstable tests are found above the stability function, while most of the stable tests are below it, with some outliers.

$$\begin{aligned} \frac{H_{m0}}{d} &\leq (0.07 - s) \cdot \left((0.06 \cdot d_{relative})^{-1} + 0.94 \cdot (1.17 \cdot 10^{20})^{s} \right) \\ &\leq (1.17 - 16.6s) \cdot d_{relative}^{-1} + (0.07 - 0.94s) \cdot (1.17 \cdot 10^{20})^{s} \end{aligned} \tag{4.3}$$

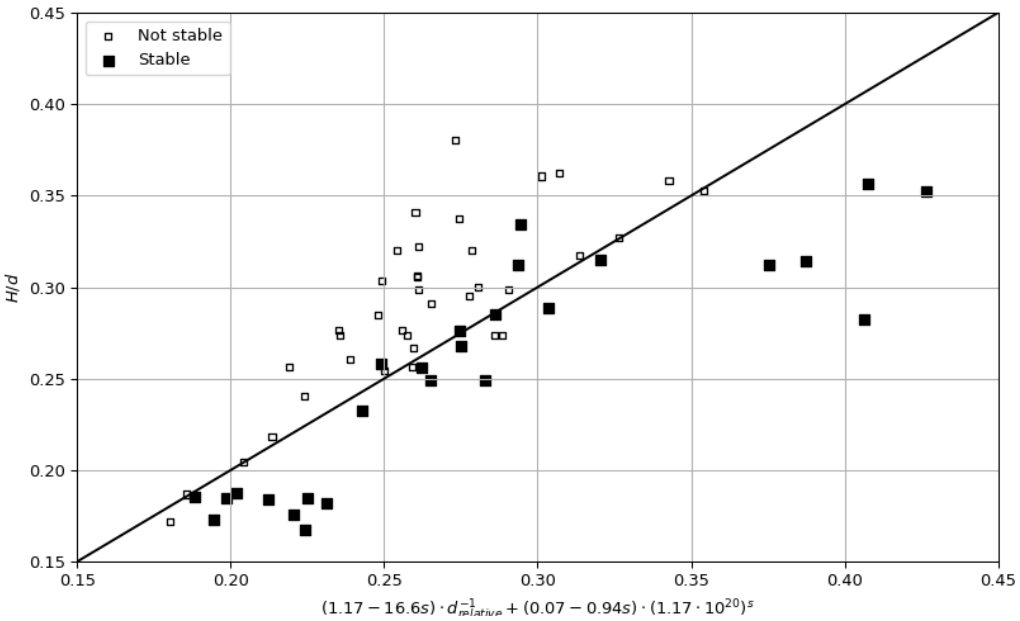

Figure 4.2: Relation of the resulting stability function for the single Stelcon plate (grey) reef with data points, with most of the unstable points above the line and stable points below

Lastly, a plot of the resulting stability function for the single Stelcon plate (grey) reef is provided in Figure 4.3, with the relative wave height on the y-axis and the wave steepness on the x-axis for various relative water depths. For a reef to remain stable, the circumstances should be such that the corresponding data point is below the associated relative water depth curve. The variation in curves for the relative water depth is based on the determined range between 2.5 and 14, and the range for the steepness is between 0.01 and 0.04.

From the figure, it is observed that for conditions with a relative water depth $d_{relative}$ of 6, the stability of the reef is independent of the wave steepness. For these conditions, the reef will be unstable if the relative water depth H/d is above a value of approximately 0.26 and stable if it is below 0.26. For lower relative water depths (below a value of 6), the stability is negative depending on the wave steepness, so when the steepness increases, the stability decreases. In addition, this relationship increases for higher wave steepness since the curves descend faster on the right-hand side of the graph. However, for higher relative water depths (above a value of 6), the stability is positively dependent on the wave steepness; a higher wave steepness results in a more stable reef.

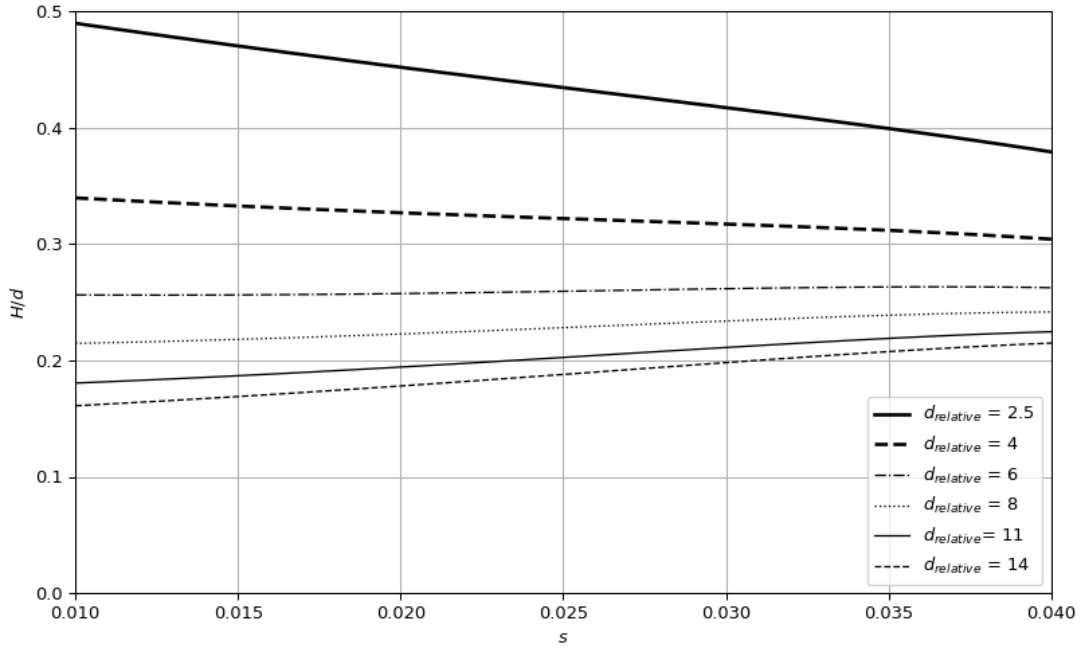

Figure 4.3: Plot for the resulting stability function for the single Stelcon plate (grey) reef

4.3. Suitability of the Morison method to predict stability

In this section, the data points obtained from the flume tests for the single plate (grey) reef with irregular waves will be compared to the Morison stability prediction. Each graph in this section was realized using Python Notebook, for which the scripts can be found in Appendix D.

4.3.1. The Morison model description

According to the theory explained in Subsection 2.4.1, a graph is plotted as depicted in Figure 4.4. The graph shows the relationship between the required dry weight of the reef model and the water depth for different significant wave heights, for which the expression is given in Equation 4.4.

$$W_{object} = \frac{\frac{F_{wave}}{\mu} + F_{buoyancy} + F_{lift}}{g}$$

$$= \frac{\frac{F_{drag}+F_{inertia}}{\mu} + F_{buoyancy} + F_{lift}}{g} \tag{4.4}$$

$$= \frac{\frac{C_D \rho_w A_p \frac{u^2}{2} + C_M \rho_w V a}{\mu} + \rho_w V g + C_L \rho_w S \frac{u^2}{2}}{g}$$

The used values to generate the graphs in Figure 4.4 are summarized in Table 4.2. For the coefficients

C_d, C_m, and C_l, and the coefficient of friction μ, the values are determined with data from the literature, given in Subsection 2.4.1. For the reef model, the planform area S equals a 0.1 meter by 0.1 meter square, resulting in an area of 0.01 m^2. For the projected cross-section seen from the flow direction A_p, the exact value is difficult to determine because the reef has a complicated structure; therefore, a slightly lower value than for the planform area of 0.009 m^2 is used, which is a rough estimate. The volume V of the reef model is determined in Section 3.3, and is equal to 0.000164 m^3. Lastly, for the spectral period $T_{m-1,0}$ a fixed value of 2 seconds is assumed.

By creating Figure 4.4, the limit of wave height due to water depth was taken into account. Laboratory data (Nelson, 1994) and theoretical analysis (Massel, 1996) indicate that under ideal conditions the breaking limit can be as low as 0.55. Thus, waves with wave heights higher than 0.55 times the water depth will not exist. This explains the linear relationship of the Morison method for low water depths.

Table 4.2: Values used to determine the graphs in Figure 4.4

C_d	C_m	C_l	μ	A_p [m^2]	V [m^3]	S [m^2]	$T_{m-1,0}$ [s]
2	3	2	0.5	0.009	0.000164	0.01	2

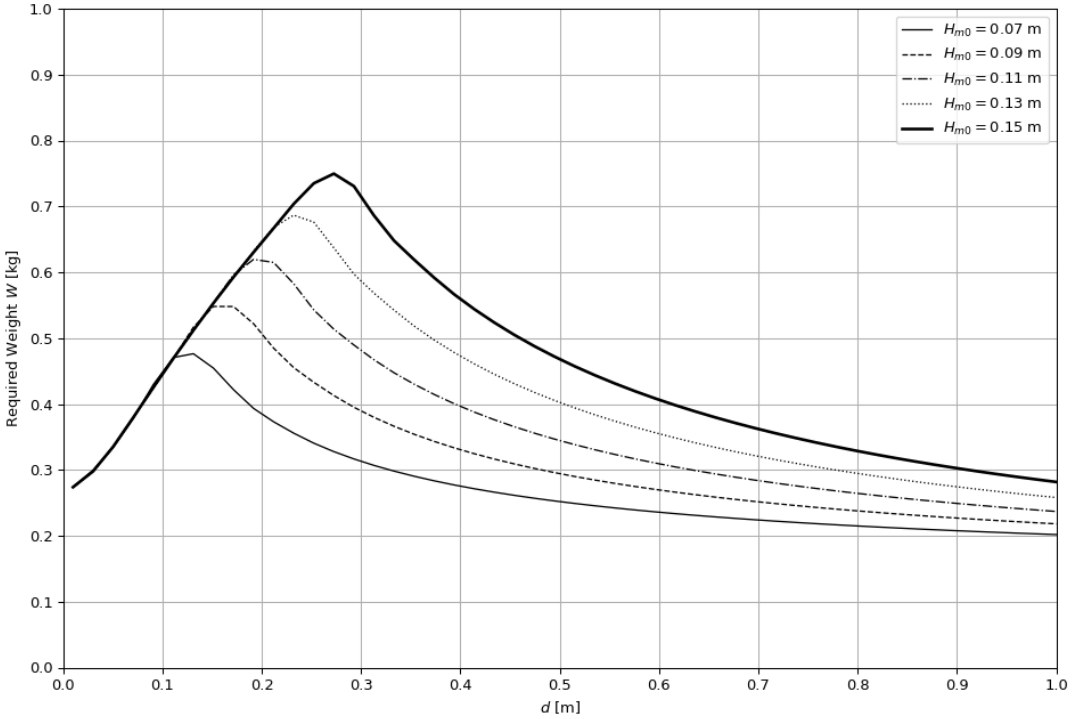

Figure 4.4: Relation between the required dry weight of the single plate (grey) reef model and the water depth for several significant wave heights according to the Morison stability prediction

4.3.2. Comparison with data points

Since the weight of the single plate reef model is a fixed value (W_{dry} = 0.345 kg), but the spectral period varies for different locations around the world, Figure 4.5 was created. While using the 'fsolve' function in Python, multiple graphs were made, giving the relation between the significant wave height and water depth for several spectral periods. The 'fsolve' function solves an equation by setting it equal to zero while giving a starting estimate of the unknown that has to be determined. In this case, the to-be-determined parameter is the wave height H_{m0}.

Most of the used values of the parameters have remained the same as the ones used before. However, the dry weight of the reef W_{dry} is now fixed and equal to 0.345 kg, and the spectral period $T_{m-1,0}$ is

varying with steps of 0.45 s between 1.00 and 2.80 s.

To determine the reliability of the Morison prediction, Figure 4.6 gives a graph for each specific spectral period $T_{m-1,0}$, with the flume test data points having approximately the same spectral period. The same spectral periods are used as for Figure 4.5, however, for each period, a separate plot is used. As can be seen, most of the unstable tests are above the lines, while most of the stable tests are below, with a few exceptions. Experimentation was done with the values of the coefficients to get the best possible fit, but it turned out that the values initially assumed formed the best fit. Here, the main focus was on the unstable points that should be above the line and less on the stable points that should be below the line to get the safest possible prediction. In addition, a safety factor has not yet been considered, but this will make the prediction even safer.

Only 4 of the 36 unstable points are below the curved lines. From this, it can be concluded that Morison's stability prediction is largely consistent with the stability data found in the experimental flume tests. In Table 4.3, the values used for the parameters for the graphs in both Figure 4.5 and Figure 4.6 are given.

Table 4.3: Values used to determine the graphs in Figure 4.5 and Figure 4.6

C_d	C_m	C_l	μ	A_p [m^2]	V [m^3]	S [m^2]	W_{dry} [kg]
2	3	2	0.5	0.009	0.000164	0.01	0.345

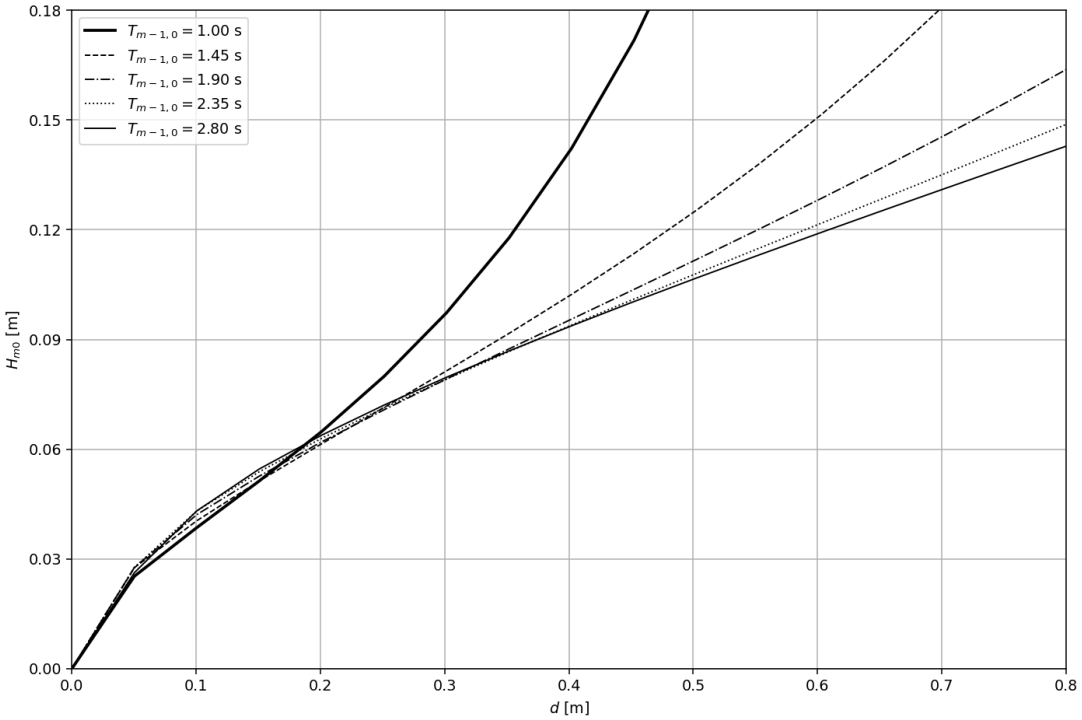

Figure 4.5: Relation between the significant wave height and the water depth for several spectral periods for the single plate (grey) reef model according to the Morison stability prediction

For the velocity u and acceleration a, the characteristic peak bottom orbital velocity and the horizontal acceleration at the bed are used, respectively, as given in Equation 2.24 and 2.25. However, according to some well-known design codes, the on-bottom stability of pipelines is also governed by the fundamental balance between loads and resistances, for which the velocity is determined with spectral analysis. This way of determining the velocity is applied to the Morison prediction too, and it appeared that the spectral velocity is less appropriate than using the peak bottom velocity. Appendix E provides a comprehensive explanation of the determination of the velocity with spectral analysis, including the suitability for the Morison stability prediction.

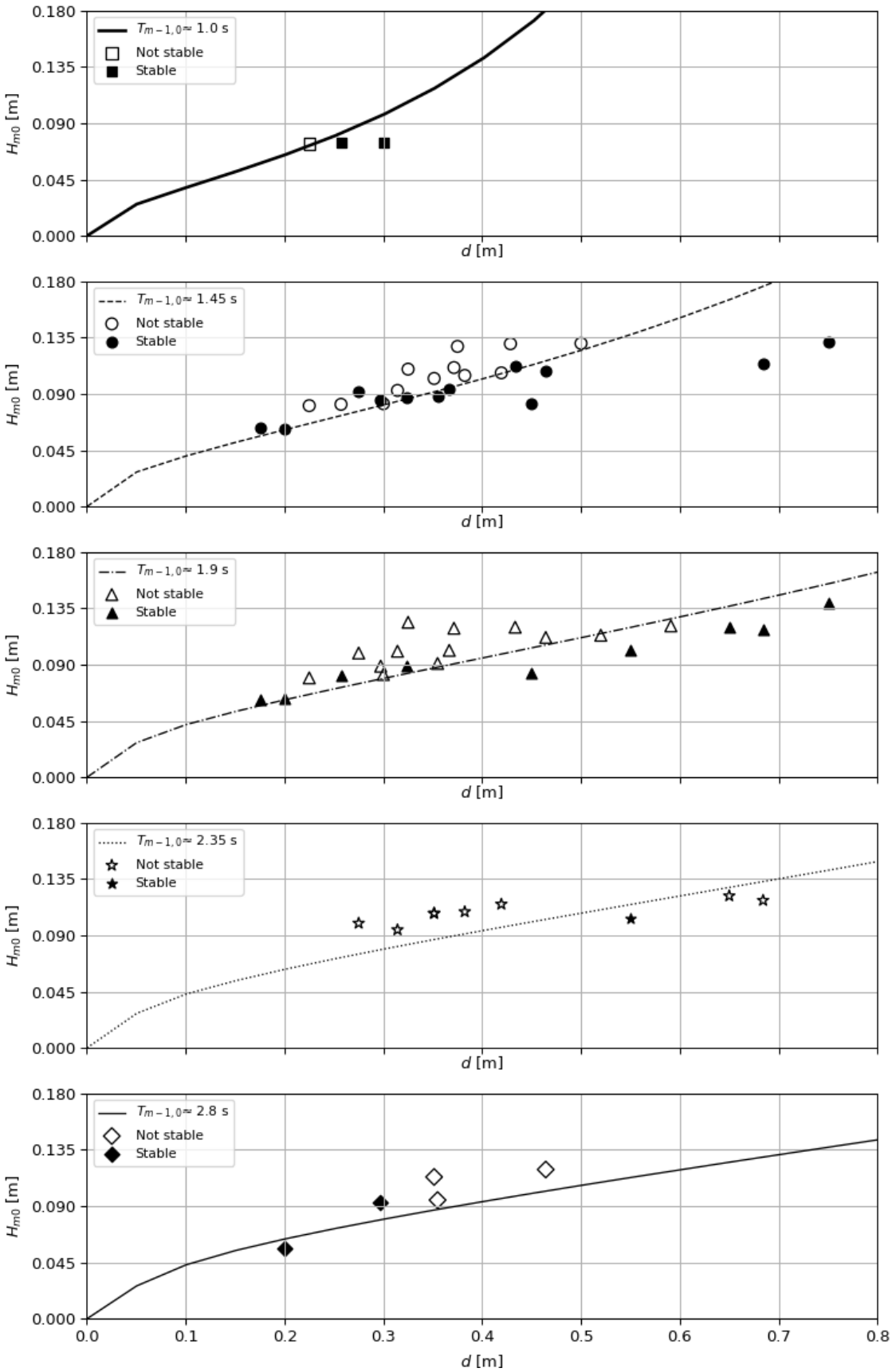

Figure 4.6: Separate plots for the relation between the significant wave height and the water depth for several spectral periods for the single plate (grey) reef model according to the Morison stability prediction, including the data points of the flume tests

4.3.3. Prediction for real size reefs

The above-given graphs for Morison's stability prediction are based on small-scale situations, but to predict the stability of the single plate reef prototype at full size, Figure 4.7 and Figure 4.8 are given. These figures give the relation between the required weight and the water depth and the significant wave height and water depth, respectively. A safety factor of 1.2 is used. Considering that the MOSES reefs are likely to be placed in the sea, the density is equal to 1025 kg/m^3 and the coefficient of friction μ is equal to 0.6 (according to Subsection 2.4.1). Appendix F gives the two figures without using a safety factor to obtain a best-estimate version of both.

The remaining values used to generate the graphs in Figure 4.7 are shown in Table 4.4. A value of 4 m^2 is used for the planform area S, which is based on the area of the model multiplied by the squared length scale factor N_L. The projected cross-sectional area, as seen from the direction of flow S of the reef, is calculated similarly, resulting in a value of 3.6 m^2. For the volume V, the volume of the model is multiplied by the length scale factor to the power three, which results in a value of 1.3 m^3. The used values for the areas and volume should correspond approximately to those of a real MOSES reef prototype. Here, for the spectral period $T_{m-1,0}$, a value of 10 seconds is assumed.

By creating Figure 4.7, again, the limit of wave height due to water depth was taken into account. The breaking limit is assumed to be equal to 0.55, resulting in waves with wave heights higher than 0.55 times the water depth that will not exist. This explains the almost linear relationship of the Morison method for low water depths.

Table 4.4: Values used to determine the graphs in Figure 4.7

C_d	C_m	C_l	μ	A_p [m^2]	V [m^3]	S [m^2]	$T_{m-1,0}$ [s]
2	3	2	0.6	3.6	1.3	4	10

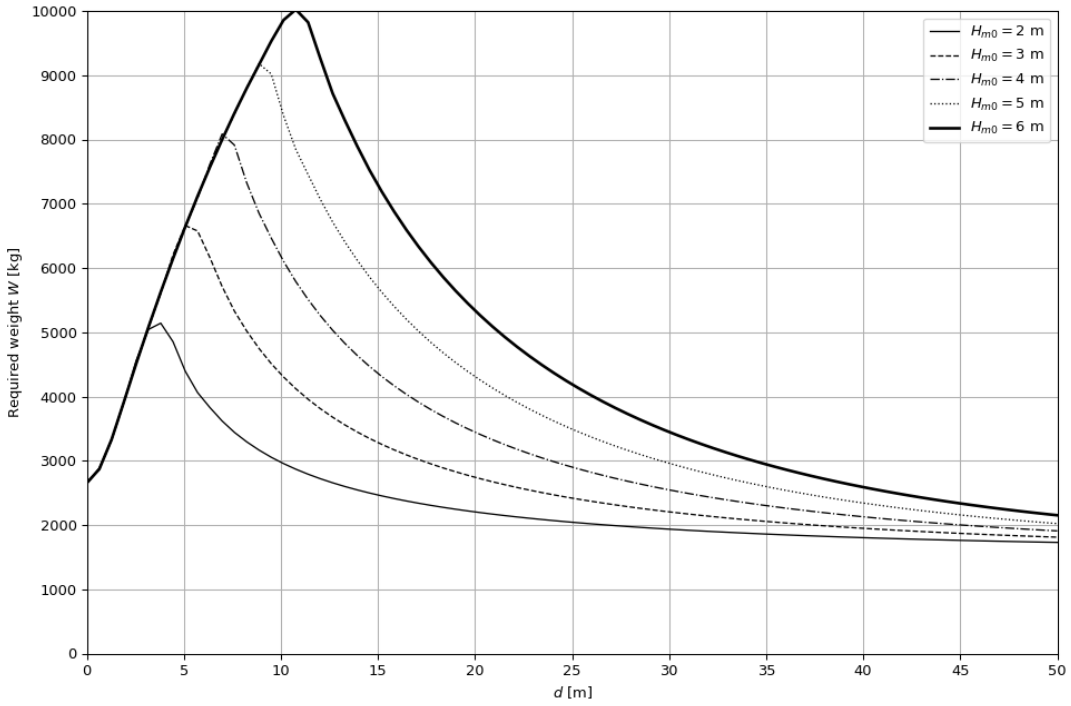

Figure 4.7: Relation between the required dry weight of the single plate reef prototype and the water depth for several significant wave heights according to the Morison stability prediction. A safety factor of 1.2 is used. The spectral period $T_{m-1,0}$ is equal to 10 s.

The values for the graphs in Figure 4.8 are given in Table 4.5. A dry weight of 2444 kg is used. A

Stelcon plate with dimensions of 0.2x0.2x0.02m weights 1900 kg (DE KEIJ Betonplaten, 2022). With 40 modules with a mass of about 14 kg, this results in a total reef weight of 2444 kg. The curve for the spectral period $T_{m-1,0}$ with a value of 5 seconds stops at the point where the wave steepness exceeds the maximum value of 0.14. When exceeding this value, the waves become unstable and will break, so waves with a wave steepness higher than 0.14 will not occur.

Table 4.5: Values used to determine the graphs in Figure 4.8

C_d	C_m	C_l	μ	A_p [m^2]	V [m^3]	S [m^2]	W_{dry} [kg]
2	3	2	0.6	3.6	1.3	4	2444

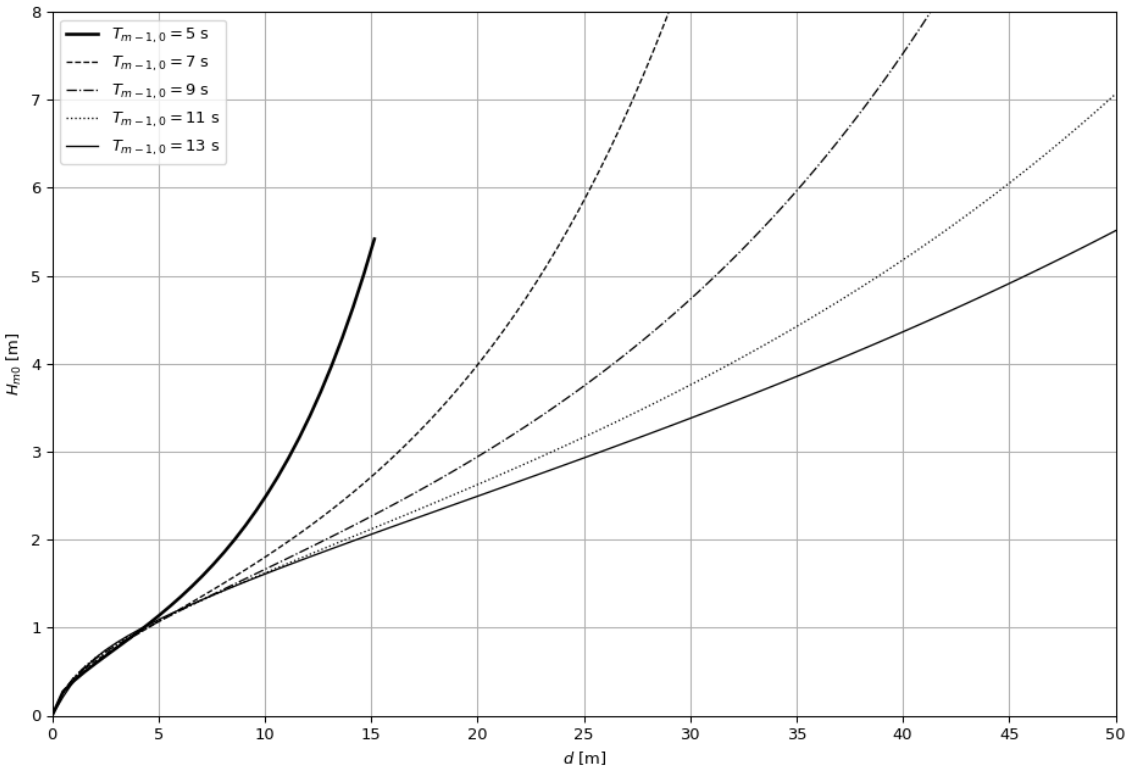

Figure 4.8: Relation between the significant wave height and the water depth for several spectral periods for the single plate reef prototype (2444 kg) according to the Morison stability prediction using a safety factor of 1.2. Above a curve, the reef is unstable, while below a curve the reef is stable.

4.4. Suitability of a prediction method using the mobility parameter

The mobility parameter prediction method is based on multiplying the dimensionless steepness s and mobility parameter θ. This section will first explain the influence of this θs-value on the stability of the reef. Next, the values for the constants r_1, r_2, and r_3 are determined.

4.4.1. Relations between stability and mobility parameter

According to the explanation in Subsection 2.4.2, a stability prediction method based on the mobility parameter could be as given in Equation 4.5. The mobility parameter θ depends in part on the diameter of a stone, or for this research on a characteristic diameter of the reef D_{reef}. This characteristic diameter is assumed to be equal to 0.14 m for the grey single plate reef, which is based on the largest dimension of the reef's surface, the diagonal. Besides, the mobility parameter depends on the relative density. As the density of the single plate reef equals 2104 kg/m^3 and assuming a water density of 1000 kg/m^3, the relative density will be equal to 1.104.

$$d_{relative} \leq r_1 \cdot \theta^{r_2} \cdot s^{r_3}$$
$$\leq r_1 \cdot \left(\frac{u^2}{g\Delta D_{reef}}\right)^{r_2} \cdot s^{r_3} \tag{4.5}$$

Figure 4.9 gives the data from the experiments with on the x-axis the water depth d in meters, and on the y-axis the multiplication of the non-dimensional steepness and mobility parameter, without taking the constants r_1, r_2, and r_3 into account. From this plot, it can be seen that there is a certain relation between the water depth and these two dimensionless parameters. Although this relation does not hold for each data point, a trend is visible between the stable and unstable data points; most unstable points have a higher θs-value than the stable points for a specific water depth. Besides, this trend is also showing that a deeper water depth results in a higher θs-value.

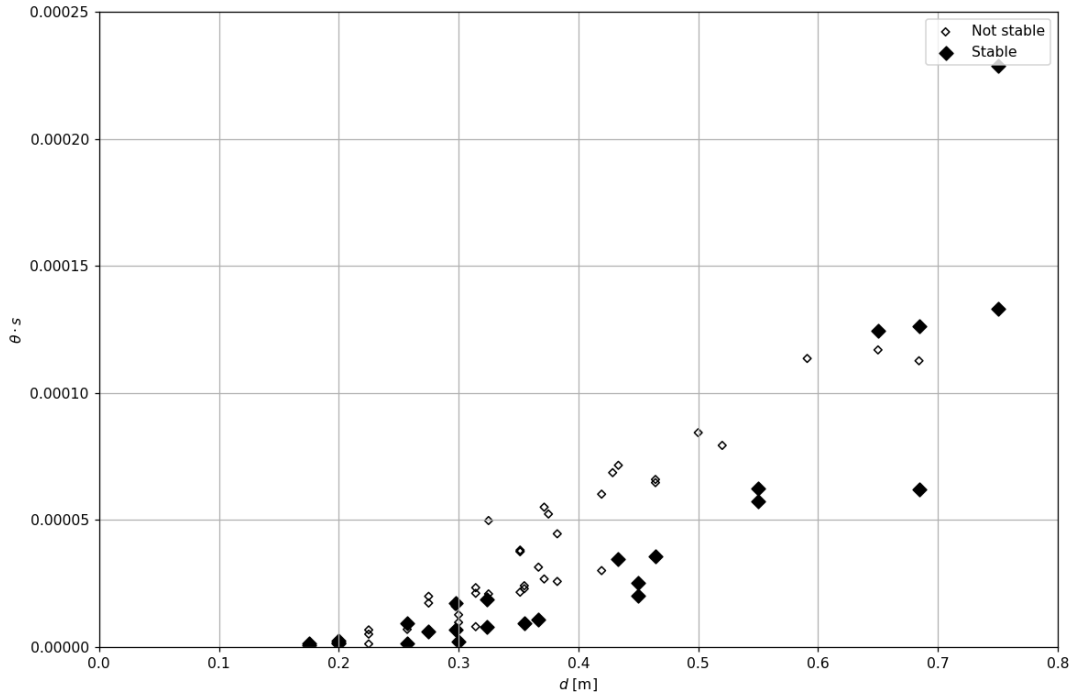

Figure 4.9: Data points from the experimental wave flume tests show the trend between the θs-value and the water depth d in meters

4.4.2. Determination of the constants

In Figure 4.9 the x-axis is indicated by the water depth d in meters. The non-dimensional relative water depth $d_{relative}$ is applied instead to use the graph as a prediction for the full-scale reef stability. The constants r_1, r_2, and r_3 are determined by varying the values to get the best possible fit. In doing so, the particular focus was on the unstable points that must be above the line and less on the stable points that should be below the line. This resulted in a value of 90 for r_1, 0.27 for r_2, and 0.21 for r_3, giving the stability prediction function as given in Equation 4.6. This relation of the prediction method using the mobility parameter against the relative water depth $d_{relative}$ is shown in Figure 4.10, including the data points for the single plate (grey) reef.

$$d_{relative} \leq 90 \cdot \theta^{0.27} \cdot s^{0.21} \tag{4.6}$$

For the data points, the order of magnitude of the values of the mobility parameter θ is 10^{-3}, while the order of magnitude of the values of the steepness s is 10^{-2}. In Equation 4.6, the mobility parameter is to the power of 0.27, and the steepness is to the power of 0.21. The combination of these two findings

shows that the influence of the steepness on the reef stability is greater than the influence of the mobility parameter.

The distinctive peak bottom orbital velocity and the horizontal acceleration at the bed, as given in Equation 2.24 and 2.25, are utilized for velocity u and acceleration a, respectively. According to several well-known design codes, the on-bottom stability of pipelines is also dictated by the fundamental balance between loads and resistances, for which the velocity is computed using spectrum analysis. Appendix E gives a detailed explanation of how to determine velocity using this spectral analysis, including whether it is suitable for the stability prediction using the mobility parameter. However, utilizing the spectrum velocity appeared less effective than using the peak bottom velocity.

Nevertheless, while using the peak orbital velocity, there are still some deviations visible, especially for the lower relative water depths ($d_{relative} < 6$), where six stable points are above the line, and two unstable points are below the trend line. This is expected to be partly due to the rough estimate of the characteristic velocity, for which the linear wave theory is assumed. For steep waves or waves in very shallow water, nonlinear theories are available. Overall, the prediction method is mainly consistent with the data obtained from the flume tests since only 4 of the 36 unstable points are below the line.

Because the experiments were conducted in a range of water depths between 0.15 and 0.8 meters, the relative water depth is also limited. Because the grey single plate reef's height is 0.06 m, the range of relative water depth $d_{relative}$ is between 2.5 to 14. Outside this range, it is uncertain if the given stability relation using the mobility parameter (Equation 4.6) is valid. The range for which the stability relation holds depends on the steepness s as well. Since the experimental tests were conducted for steepnesses between 0.01 and 0.04, the stability relation based on the mobility parameter is valid for steepnesses between these values. Moreover, the relation given in Equation 4.6 is only usable for a stability prediction of the single plate grey reef, or an up-scaled version of it, while it is based on the data points of this reef.

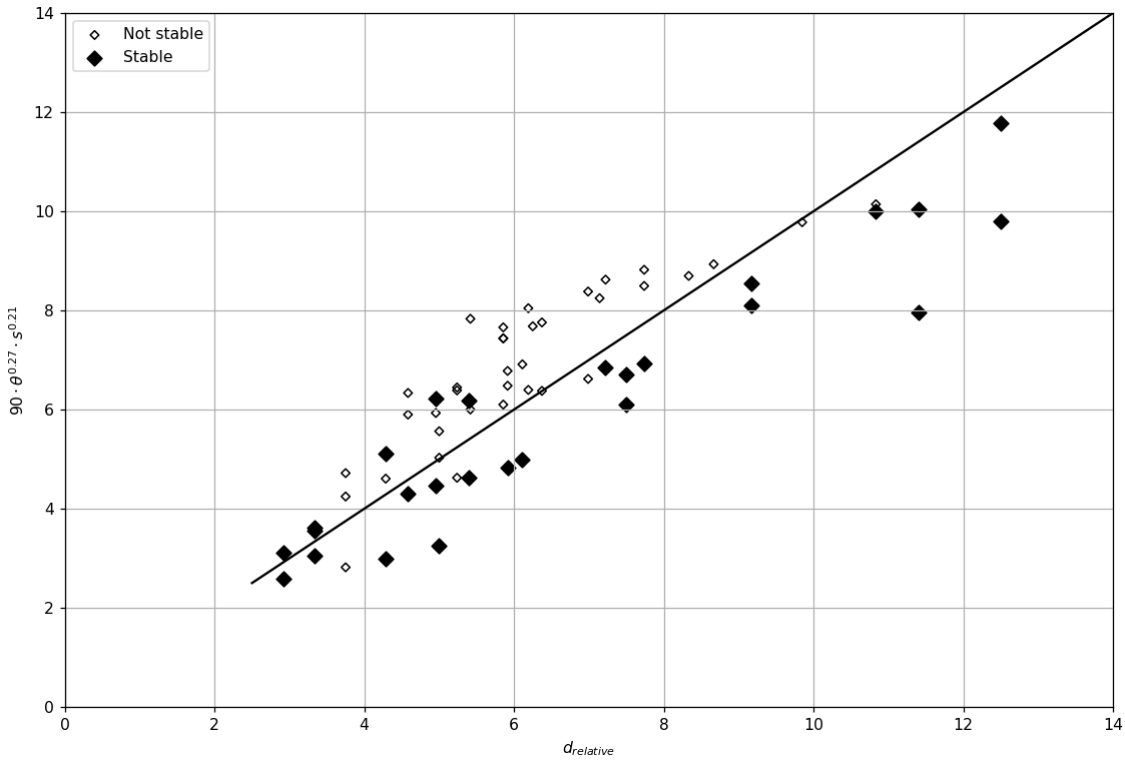

Figure 4.10: Relation of the prediction method using the mobility parameter for the single plate (grey) reef with data points, with most of the unstable points above the line and stable points below

4.5. Influence of reef property variations on stability

Three reefs are tested in the wave flume for the influence of some variations in reef properties on the stability. The specifications of these reefs are given in Section 3.3. Three reefs (single plate, double plate, and 2x2 reef) are tested on stability using regular and irregular waves. The regular wave tests will be used to first give a comparison between the three reefs quantitatively, whereafter, the irregular tests will be used for a quantitative comparison. Lastly, the method to determine the stability function, the Morison prediction method, and the mobility parameter prediction method is applied to the different reefs (Appendix G), and based on this, the differences in stability between the reefs will be given.

4.5.1. Qualitative comparison between the three reefs for regular wave tests

Table B.2 in Appendix B lists the tests performed for regular waves. Ten experiments under various conditions are conducted three times, each with one of the three reefs in the flume; the single plate grey reef, the double plate pink reef, or the 2x2 reef (made out of four grey reefs).

From the outcomes of these regular tests, so whether the reefs are stable or not, some observations can be made:

- For most conditions, the grey and pink reef have the same stability, so when the grey reef is stable, the pink reef is stable as well, and when the grey reef has become unstable, the pink reef has also become unstable.
- For only two conditions (the D113- and D112-tests), the grey and pink reefs did not respond the same. The reefs even showed the opposite outcome. For the D113-tests conditions, the grey reef was unstable, while the pink reef was stable, and for the D112-tests, the opposite happened, so the grey reef was unstable, while the pink reef was stable.
- The 2x2 reef is most stable compared to the grey and the pink reef. For most conditions where the grey or pink reef has become unstable, the 2x2 reef has not. In addition, no tests have taken place in which the pink or grey reef was stable while the 2x2 reef was unstable.
- The 2x2 reef is stable for each test, except for the D213-tests conditions, for which the input parameters are as follows: the water depth is 0.38, the relative water depth is 0.45, and the steepness is equal to 0.015.

Remarkable about the above observations is the behavior of the grey and pink reefs for the D113- and D112-tests conditions, stating that for a few conditions, the grey reef is more stable. In contrast, for other conditions, the pink reef is more stable. Compared to the grey reef, the pink reef is heavier and higher, and the volume is higher.

According to the Morison method, the height of a reef defines the projected cross-section seen from the direction of flow, which determines the drag force on the reef. The reef volume determines the inertial force and buoyancy force on the reef. The impact that these forces have on the required weight of the reef is different for several conditions due to the influence of the velocity u and acceleration a. Therefore, it is to be expected that the grey and pink reef can show opposite stability behavior for different wave conditions.

Additionally, the values of the parameters for tests with the same conditions but with another reef vary slightly, which is due to the variance in input values and measured values of the wave flume parameters. For example, the measured spectral period $T_{m-1,0}$ was slightly higher by testing the pink reef with D112 conditions than the period measured for the test with the grey reef. This could influence the test outcome.

4.5.2. Qualitative comparison between the three reefs for irregular wave tests

For some tests with irregular waves (Table B.3), next to the grey reef, the pink reef and 2x2 reef are tested as well. Table 4.6 gives an overview of these tests. Notably, both reefs show the same stability for the tests with irregular waves. Or in other words, for the tests where the pink reef is stable, the 2x2 reef is also stable, and when the pink reef is unstable, so is the 2x2 reef. The grey reef, however, is unstable for all of these tests with irregular waves, from which it can be concluded that the grey reef is less stable than the pink and 2x2 reefs.

Table 4.6: Overview of the tests performed for the single plate grey reef, double plate pink reef, and 2x2 reef with the corresponding outcome. Note: the grey reef has not been tested for V435 conditions due to time constraints. The reef is likely unstable under these conditions.

TestID	**GREY**	**PINK**	**2x2**
	Single plate	Double plate	Four grey reefs
V435	-	Not stable	Not stable
V415	Not stable	Stable	Stable
V432	Not stable	Stable	Stable
V323	Not stable	Stable	Stable
V224	Not stable	Stable	Stable
V134	Not stable	Stable	Stable

Since it is unknown at which moment the reefs became unstable during a test, it is still possible that the pink reef and 2x2 reef have varying stability. When they became unstable during the same test but by waves with different wave characteristics, there is a distinction in stability between the two.

4.5.3. Comparison between the three reefs based on stability function and prediction methods

Appendix G gives for both the double plate pink reef and the 2x2 reef the suitability of the method to establish the stability function, the Morison prediction method, and the mobility parameter prediction method. The application of these methods for the grey reef is given in Section 4.2, Section 4.3, and Section 4.4 respectively. According to the stability predictions, there certainly is a difference in stability between the three reefs. These differences will be discussed below.

The method used to establish the **stability function** for the grey reef is also applied to the pink and 2x2 reefs. According to this, two new stability functions are created, giving both a representative view of the stability of the reefs compared to the data points obtained from the flume tests for that reef. Comparing the resulting stability function of the grey reef to the stability function of the pink and 2x2 reef, the only difference is the relation for the c_1 constant. The relations for the c_1 constants are summarised below.

- Grey single plate reef: $c_1 = 0.07 - s$
- Pink double plate reef: $c_1 = 0.08 - s$
- 2x2 reef: $c_1 = 0.09 - s$

This difference initiates that the 2x2 reef should be more stable than the pink one, and the pink reef should be more stable than the grey reef, according to the established stability functions.

When applying the **Morison prediction method** to the pink and the 2x2 reef, it appears that it represents the stability of the reefs quite well when comparing the stability curves to the data points. However, the Morison method somewhat underestimated the stability of the 2x2 reef, as four of the five data points for stable trials are above the prediction curves when they should be below them. For the Morison method, the plotted curves to which the data points are compared depend on some reef properties, such as the reef height, weight, and volume, and therefore they deviate for the different reefs.

Even with underestimating the 2x2 reef, the Morison method states that the 2x2 reef should be the most stable of the three reefs, followed by the pink reef and the grey reef. This observation is based on the location of the Morison curves for the three reefs. For the 2x2 reef, these curves are the highest, while the curves for the grey reef are the lowest.

The variation in the **mobility parameter prediction method** for different reefs is in the difference

in reef height, a characteristic diameter (assumed as the diagonal of the surface area of the reefs), and the density of the reef. Besides, the value for the constant r_1 differs for the different reefs.

The reef height is included on the x-axis, and the density and diameter are included on the y-axis, so the data points are determined based on the reef properties. Applying the mobility parameter prediction method as used for the grey reef ($r_1 = 90$) to the pink reef gives an underestimation compared to the data points for that reef. The application of the grey reef method for the 2x2 reef gives an almost representative prediction of that reef's stability. An adjustment of the r_1-value from 90 to 55 for the pink reef and to 80 for the 2x2 reef gives a total representative prediction for both.

Rewriting the stability function (Equation 4.6) to get all reef property variables together at the front, gives:

$$d \leq d_{reef} \cdot (g\Delta D_{reef})^{-0.27} \cdot r_1 \cdot (u^2)^{0.27} \cdot s^{0.21}$$

The value of the first part of this equation, $d_{reef} \cdot (g\Delta D_{reef})^{-0.27} \cdot r_1$, is different for the grey, pink, and 2x2 reef, due to differences in reef properties and r_1. The rewritten stability functions for the three reefs are summarised below.

- Grey single plate reef: $d \leq 4.86 \cdot (u^2)^{0.27} \cdot s^{0.21}$
- Pink double plate reef: $d \leq 3.52 \cdot (u^2)^{0.27} \cdot s^{0.21}$
- 2x2 reef: $d \leq 3.68 \cdot (u^2)^{0.27} \cdot s^{0.21}$

The value is the smallest for the pink reef (3.52), which means that this reef should be the most stable. The 2x2 reef has the middle value (3.68), and the grey reef has the highest value (4.86), which means that this reef should be the least stable according to the mobility parameter prediction method. As the 2x2 reef has a value in between the values of the pink and grey reefs, the reef's stability should be in between those reefs as well. However, the qualitative comparison between the three reefs shows that the 2x2 should be the most stable instead.

5

Discussion, conclusions, and recommendations

This chapter discusses the uncertainties and limitations of the research, the conclusions, and several recommendations for further research.

5.1. Discussion

In general, this master thesis covered the following aspects:

1. Literature study about the relevant parameters to determine the reef stability
2. Set-up of the experiments
3. Performing the experimental tests
4. Analysis of the data from the flume experiments

Each of the processes outlined above had several uncertainties and limitations, which will be discussed in this section. Some of these uncertainties or constraints for a particular process have implications for subsequent processes.

Wave theory

The linear wave theory is a theory for two-dimensional progressive gravity waves. It assumes that the wave height is much smaller than the wavelength, so non-linear terms are neglected. In general, the theory should not be used for steep waves or waves in very shallow water. However, the linear wave theory can still estimate the waves, even in situations where non-linear theories should be used.

The linear wave theory was used in this research. However, for some tests, where the waves were too steep or the water depth too small, linear wave theory might not estimate the waves correctly by neglecting the non-linear terms, which might affect the results.

The determination of the velocity and acceleration, used for both the Morison prediction method and stability prediction method based on the mobility parameter, is based on the linear wave theory. In addition to the fact that the equations are approximations of the actual velocity and acceleration on the seafloor, since the values are based on the spectral parameters, are the equations for tests with low water depths or steep waves still used, even though they are based on linear wave theory.

The Morison coefficients

The Morison method uses several coefficients; the drag coefficient C_D, the inertia coefficient C_M, and the lift coefficient C_L. These coefficients are case-specific, so they depend on the shape of a reef, the surface roughness, the size of the reef, the Reynolds number (Re) of the flow, and the Keulegan Car-

penter number (KC). Based on the literature, an estimate of the values of the coefficients was made to apply the Morison approach to the MOSES reef models. However, the values used in the literature varied greatly, so only a rough approximation could be made. When comparing the applied method with the data points collected from the experimental flume testing, the coefficient values were varied to produce the best fit. However, it turned out that the values initially assumed according to the literature formed the best fit. If the assumed values are higher than in reality, the Morison prediction will underestimate the stability of the reef, so the reef will be more stable than the prediction suggest, while if the assumed values are too low, the stability will be overestimated.

Reef model scaling
The plan was to maintain a length scale factor of 20 between prototype and model. However, after manufacturing the models of the reefs, it was discovered that some properties, such as weight, size, and density, differed from the values determined using the scale factor. The manufacturing of the reef models was beyond the scope of this study.

The grey reef was too heavy, so the middle section had to be scraped off at the underside, resulting in a concave surface. In this way, the outer dimensions of the concrete plate remained the same, but the weight and the volume were reduced. This concave surface of the model had implications for the stability of the reef. Since less surface area of the reef model touched the bottom of the wave flume, the resistance to sliding was less, making the model more easily unstable compared to an original reef prototype with a flat bottom surface.

Furthermore, the pink reef was supposed to have a higher density than the grey reef but had a lower density. Because the dimensions of the pink reef model are close to the dimensions based on the scaling of the prototype, this difference is most likely due to inaccuracies in the used concrete. This under-dimensioning of the density leads to the pink reef model becoming more easily unstable than the double plate reef as an original MOSES prototype.

Finally, the weight of the 2x2 reef should be four times that of the grey reef, which was incorrect. Four times the weight of the grey reef model (0.345 kg) is equal to 1.38 kg. However, the 2x2 reef model weighs 1.417 kg, which is slightly higher. Besides, the density of the 2x2 reef model is lower than the grey reef model, which was expected to be the same. Therefore, due to the higher weight, the reef model will become unstable less quickly, while due to the lower density, the reef model will become unstable more easily.

Because of these inaccuracies, it is difficult to scale the conclusions drawn from the tests with the reef models to the original MOSES prototype reefs. Nonetheless, a conclusion based on a scaled version of the reef models is possible. However, the stability behavior of this scaled version of the models will likely not fully match the behavior of the original MOSES prototype reefs.

Velocity determination
A characteristic horizontal velocity was used for both the Morison stability prediction method and the prediction method using the mobility parameter. The spectral velocity and the peak bottom orbital velocity are methods to determine this characteristic velocity. Comparing the two velocity-determining methods makes it clear that the velocity based on the peak bottom orbital velocity has higher values than those calculated with the spectral velocity. The application of the spectral velocity to both the Morison stability prediction and the stability prediction using the mobility parameter (Appendix E) was less appropriate than using the peak bottom orbital velocity, and therefore the peak orbital velocity was used for the analysis of the wave flume data.

However, the peak bottom orbital velocity was expected to be less accurate than the spectral velocity. The peak orbital velocity determines the velocity at the seabed and does not consider the height of the reef. Since the velocity decreases further away from the water surface, the velocity at a certain height from the bottom will always be higher than at the bottom itself. More elevated reefs will therefore also be exposed to higher velocities. However, this is not included in the determination of the velocity with the peak bottom orbital velocity.

2DV model
A limitation is that the model was set up in 2DV, which does not consider the system's full complexity in

3D. Because the wave flume is two-dimensional, the effect of multi-directional waves was not tested. However, the sea rarely shows a unidirectional, regular sinusoidal wave pattern but rather a mix of waves of various lengths, heights, and directions. The mixing of waves of different lengths and heights was accounted for with irregular waves, but waves with different directions were not included during the tests. Nonetheless, during testing, the most critical configuration concerning the wave direction became apparent and was applied to the remainder of the tests.

Wave reflection
While testing the stability of the reefs, a wave absorber was located at the end of the wave channel to ensure that the least possible reflection of the waves would occur. Since approximately half of the absorber had to be below the water surface, the absorber had to be adjusted to the water level for each experimental test. Nonetheless, since adjusting the location of the absorber was not a very accurate operation, variation in the degree of absorption for each test was the result. The variation in wave reflection varies between 0.2 and 0.45. Since the amount of absorbed energy affects the measured wave height, the test results may differ slightly from reality. It is unclear how these different wave reflections affect the results of the tests and how they influence the stability of the reefs.

Different bed roughness with and without foreshore
The tests were conducted both with and without a foreshore. The foreshore was installed to create relatively high waves in a relatively small water depth at the location of the reef models. No distinction was made between the tests with and without the foreshore. Nonetheless, the waves are affected by the slope of the foreshore due to a water depth change when testing with the foreshore in the flume. The reefs are located at a distance of 6.3 m from the beginning of the straight section of the foreshore, with wave gauges on both sides. Since the data analysis was based on the measured values rather than the input values, and since the wave gauges in front- and behind the reef gave almost the same values, it was assumed that the wave changes are no longer present at the location of the reef.

Still, the bed friction was different in both situations. The bed was made of smooth concrete without foreshore, while the bed was rougher for the tests with foreshore. This is because the foreshore was made from sand-cement, with a relatively higher grain diameter. This difference in bed roughness may influence the stability of the reefs; a high bed roughness results in a higher coefficient of friction and a more stable reef. Therefore, the reefs tested with foreshore may become unstable less quickly than the reefs tested without foreshore. However, it was assumed that this difference is negligible, so it was not considered. Besides, for the Morison method, the same coefficient of friction was used for both tests with and without foreshore.

Measurement inaccuracy
The results of the experimental wave channel tests, i.e., whether or not the reefs are stable, are based on observations that can be seen with the naked eye. It could be that for some tests, there was an error in determining whether the reef was stable or not. For example, the displacement of the reef may have been so small that it could not be seen with the naked eye, or there may have been both a displacement in a certain direction and a displacement in the opposite direction at a time when no one was observing. Upon return, it would then appear as if the reef had not moved while it actually had moved. Since all tests were recorded with a video camera, some results were determined afterward to be unstable, which increased the accuracy. However, it is possible that some of the tests still have false results, but it is expected that this will only be the case to a minimal extent.

Approximation of area for Morison method
For the Morison method, the exact value of the projected cross-section seen from the flow direction A_p is challenging to determine because the reef has a complicated structure. For the grey reef, it was assumed that a slightly lower value (0.009 m^2) than for the planform area S was used, which is a rough estimate. The value for the pink reef is slightly larger (0.01 m^2), as the pink reef is higher. Finally, the 2x2 reef uses a value (0.027 m^2) which is three times greater than the grey reef. Since these values are rough estimates, the comparisons between the Morison stability prediction method and the data points obtained from the experimental tests are not entirely accurate.

5.2. Conclusions

This study aims to provide insight into whether or not the artificial reef is stable for a given location with known hydraulic circumstances during wave loading. Damage to the reef itself or its surroundings can occur if it is not stable, so knowledge of the stability is necessary. Therefore, it is crucial to have information about the influence of different hydraulic conditions on the stability of the structure. To be able to answer the main research question, answers to the sub-questions will be given below.

1. ***What wave loading parameters are of importance to determine the stability of the artificial reefs?***

   Several relevant wave loading parameters were obtained, which were used to define the experiment's test plan, interpret the measurements from the tests to gain valuable data, or analyze the data from the experiments. The relevant wave loading parameters are:

- Water depth	d	[m]
- Significant wave height	H_{m0}	[m]
- Peak period	T_p	[s]
- Spectral wave period	$T_{m-1,0}$	[s]
- Relative wave height	H_{m0}/d	[-]
- Wave steepness	$s_{m-1,0}$	[-]
- Relative water depth	$d_{relative}$	[-]
- Mobility parameter	θ	[-]

2. ***How can a wave flume experiment be designed to make relevant observations on the stability of the artificial reefs?***

   Small-scale wave flume experiments were conducted with a length scale factor of 20. Three reefs with different characteristics were tested. The primary model was constructed of 40 FDM-printed hexagonal tubes attached to a concrete plate. For the second model, the plate was double the height of the grey reef and the third model was made by attaching four of the primary models to each other.

   Experimental flume tests with both regular and irregular waves were conducted to determine if the reef models were stable or not. The experimental tests' conditions were based on varying parameters (determined in sub-question 1) to obtain the broadest possible range of conditions. Tests were done both with and without foreshore to create relatively high waves in a relatively small water depth. For each experimental wave flume test, determined was whether the reef was stable. According to resistance-type wave gauges that recorded the free surface elevation, the observed reef stability was connected to the circumstances during that test.

3. ***How can the results of the experimental tests be used to determine the influence of the wave loading parameters?***

   According to the results of the experimental wave flume tests with a MOSES reef attached to a single concrete Stelcon plate, the stability is partly influenced by the water depth d, the significant wave height H_{m0}, and the dimensionless steepness s of the waves. There is a linear relationship between wave height and water depth for a given wave steepness, for which the reef becomes unstable. The reef became unstable more easily in shallow water than in deep water. Also, the bigger wave heights will often result in a less stable reef. Lastly, the stability becomes more dependent on water depth as wave steepness increases.

   (a) ***What is the influence of the relative wave height, the wave steepness, and the relative water depth on the stability of the reefs?***

   A resulting stability function (Equation 4.3) was determined based on the data points obtained from the experimental flume tests with the single plate grey reef model. The function is depending on three non-dimensional parameters; the relative wave height (H_{m0}/d), the relative water depth (d/d_{reef} or $d_{relative}$), and the wave steepness (s). Since non-dimensional

parameters were used, this function can be used for a scaled-up version of the reef model as well. The function is not valid for reefs with different properties, such as height or weight variations. The ranges of the parameters for which the function can be used are as follows:

- The relative wave height (H_{m0}/d) 0 - 0.5
- The relative water depth (d/d_{reef} or $d_{relative}$) 2.5 - 14
- The wave steepness (s) 0.01 - 0.04

(b) ***How can a prediction method be used to predict the stability characteristics of the artificial reefs?***

The data from the experimental flume tests are compared to two stability prediction methods: the Morison stability method and a prediction method using the mobility parameter.

The prediction method using the mobility parameter shows a good representation of the stability of the single plate reef as well, according to the wave flume tests. As for reef properties, the mobility parameter prediction method takes into account the height of the reef d, the specific density Δ, and a characteristic diameter of the reef D_{reef}. The prediction method using the mobility parameter is based on dimensionless parameters, so the same prediction can be used for all up-scaled versions of the reef. For deviating reef properties, the function is not valid.

It can be concluded that Morison's stability prediction is largely consistent with the stability data from the single plate reef model. The method is based on forces on the reef, which are derived from velocities and accelerations created by the waves. The stability prediction uses a couple of reef-specific properties, such as the planform area S, the projected cross-section seen from the flow direction A_s, the volume V, and the weight W. The Morison method uses dimensional parameters, so up-scaling is complicated, meaning that for each specific up-scaled version of the reef, a new prediction is necessary. On the other hand, the Morison method includes more reef-specific property parameters, while some reef properties are included in the determined coefficients for the mobility parameter method. Therefore, the Morison method is more applicable to reefs with variations in reef properties.

(c) ***How do the height, weight, and surface area of the reefs affect the stability?***

For the influence of some variations in reef properties on the stability, three reefs were tested in the wave flume, having varying height, weight, and surface area. From the qualitative comparison between the three reefs, based on the tests with regular waves, it can be concluded that the 2x2 reef (with the largest surface area) is the most stable. The single plate grey reef model and the double plate pink reef model have the same stability behavior for these tests. From the tests with irregular waves, it became clear that the single plate grey reef is the least stable, and the outcome of the double plate pink reef and the 2x2 reef is the same for all tests. Based on these two findings, it can be concluded that the 2x2 reef is the most stable, followed by the pink reef, and the grey reef is the least stable.

The method used to obtain the stability function for the grey reef is applied for the pink and 2x2 reef as well. Although only six data points with irregular waves are available for the pink and 2x2 reef, the determined functions give both a good representation of the reef stability based on the data points. This difference in the stability functions initiates that the 2x2 reef should be more stable than the pink reef, and the pink reef should be more stable than the grey reef, which is in line with the qualitative observations.

The Morison and mobility parameter prediction methods were also applied to both reefs. According to the Morison method, the 2x2 reef should be the most stable, followed by the pink reef, and the grey reef should be the least stable. For the mobility parameter method, the function had to be calibrated on the flume data of the specific reefs. However, it predicts that the pink reef is most stable, which is not in line with what was expected. As the mobility parameter prediction method is strongly dependent on velocity, this unexpected outcome could be due to the use of the peak bottom orbital velocity, which does not include the impact of the height of the reef.

The main research question was formulated as follows: "***How does non-breaking wave loading affect the stability of the MOSES artificial reef?***"

As explained in the discussion, the original MOSES prototypes are not exactly scaled versions of the models due to some manufacturing inaccuracies. Although both prediction methods (Morison method and mobility parameter method) are largely consistent with the data obtained from the flume tests, the Morison method seems best suitable for a stability prediction for reefs with deviating properties such as the MOSES artificial reef.

Moreover, the relationships for the specific stability equation from Section 4.2 are similar to Morison's relationships. In both cases, a higher wave steepness, or a smaller period, leads to a less stable reef. Besides, a higher water depth, or a lower wave height, results in a more stable reef according to both methods. This confirms the likelihood of the Morison method.

As ReefSystems is most interested in the stability of the original single plate reef prototype, the prediction in Figure 4.8 is normative. According to Morison's stability prediction, this figure shows the relationship between significant wave height and water depth for several spectral periods for the original single plate reef prototype's stability. A total reef weight of 2444 kg was used for the prediction, and Table 4.5 shows the other relevant values of the reef characteristics.

A stability prediction for reefs with other characteristics is possible as well. However, since the Morison method is not based on non-dimensional parameters, a separate prediction has to be made for each specific reef. Furthermore, as the coefficients for the Morison method are case-specific, the reef characteristics may not deviate too much from that of the grey single plate reef; otherwise, the prediction becomes too inaccurate.

5.3. Recommendations for further research

Based on the discussed limitations and uncertainties discussed in Section 5.1 and the conclusions summarized in Section 5.2, the following recommendations are made for further research.

- **Investigate the influence of scouring and currents on the stability**

  It is advisable to investigate the influence of stability influencing parameters, such as scour and currents. The reef will likely be placed on a sandy seabed, so the chances of erosion are high, and in addition, water currents can be found in many places around the world. These processes were not taken into account in the experimental tests in the wave flume, as only the influence of non-breaking waves was tested, but the processes certainly affect the stability of the reef. A conclusion was drawn based on stability due to waves, but to know for sure if the reef is stable for certain conditions, all stability-influencing processes must be included. A small-scale experiment could be the solution for determining the influence of both waves and currents, and a small-scale experiment using a sandy flume bed could also be conducted to help assess stability due to scour.

- **Investigate the influence of multiple reefs close to each other**

  Simultaneous testing of the three reefs showed that the stability of the reefs was affected by each other, so from then on, only tests with one reef in the flume were conducted. In reality, however, the reefs could also be positioned close together and therefore influence each other. The influence on the stability of placing them close together should be investigated, resulting in knowledge at what distance the reefs no longer influence each other's stability.

- **Morison's drag coefficient determination with flume tests**

  The conclusions showed that the Morison method is suitable for predicting the stability of prototype MOSES artificial reefs. Literature was used to determine the coefficients (the drag coefficient C_D, the inertia coefficient C_M, and the lift coefficient C_L) used for the Morison method. Although, as the coefficients are based on reef-specific properties, only a rough estimate could be made. To make the prediction more accurate, the drag coefficient C_D for the specific MOSES reef can

be determined using flume experiments, according to Koudstaal & van Rijn (2020), who used flume experiments for the determination of the drag coefficient. The flume's flow velocity must be increased in steps until the structure becomes unstable. By measuring the flow velocities and assuming the accelerations are zero, the only unknown parameter in the Morison equation is the drag coefficient.

These tests may be helpful, especially when certain reef properties will change in the future. Proven is that the Morison method is applicable for a stability prediction, but for changes to the reef, the coefficients will change too. The flume tests determining the drag coefficient will be helpful since by this it is not necessary to redo all the tests conducted during this study.

- **Research on the significant horizontal velocity determination**

  The peak bottom velocity was applied for this study for the characteristic velocity. However, reef height is not taken into account when applying this determination. Especially for the mobility parameter method for the pink reef, this probably resulted in an unexpected outcome. Since the velocity determination is used for both the Morison method and the mobility parameter method, it is recommended to do more research on the determination of the characteristic velocity.

References

Bell, M., & Hall, W. J. (1994). Effects of hurricane hugo on south carolina's marine artificial reefs. *Bulletin of Marine Science*, *55*(2-3), 836–847.

Cardenas-Rojas, D., Mendoza, E., Escudero, M., & Verduzco-Zapata, M. (2021). Assessment of the performance of an artificial reef made of modular elements through small scale experiments. *Journal of Marine Science and Engineering*, *9*(2). doi: 10.3390/jmse9020130

Chapter 1 - the marine environment. (2008). In A. F. Molland (Ed.), *The maritime engineering reference book* (p. 1-42). Oxford: Butterworth-Heinemann. doi: https://doi.org/10.1016/B978-0-7506-8987-8.00001-9

DE KEIJ Betonplaten. (2022). *Gewicht stelconplaat.* Retrieved 2022-04-02, from `https://www.dekeij.nl/gewicht-stelconplaat/`

Deltares. (2021). *Scheldt Flume.* Retrieved 2021-11-05, from `https://www.deltares.nl/en/facilities/scheldt-flume/`

DNV. (1988). On-Bottom Stability Design of Submarine Pipelines (RP E305). Veritas Offshore Technology and Services A/S..

DNV. (2006). Submarine Pipeline Systems (OS F101). Det Norkse Veritas AS..

DNV. (2010). On-Bottom Stability Design of Submarine Pipelines (RP F109). Det Norske Veritas AS..

Düzbastılar, F. O., Lök, A., Ulaş, A., & Metin, C. (2006). Recent developments on artificial reef applications in turkey: Hydraulic experiments. *Bulletin of Marine Science*, *78*(1), 195–202.

Düzbastılar, F., & Şentürk, U. (2009). Determining the weights of two types of artificial reefs required to resist wave action in different water depths and bottom slopes. *Ocean Engineering*, *36*(12), 900-913. doi: https://doi.org/10.1016/j.oceaneng.2009.06.008

Fall, A., Weber, B., Pakpour, M., Lenoir, N., Shahidzadeh, N., Fiscina, J., … Bonn, D. (2014, Apr). Sliding friction on wet and dry sand. *Phys. Rev. Lett.*, *112*, 175502. doi: 10.1103/PhysRevLett.112.175502

Frostick, L. E., McLelland, S. J., & Mercer, T. G. (2019). *Users guide to physical modelling and experimentation: Experience of the hydralab network*. CRC Press.

Gent, M., & Werf, I. (2014, 06). Toe stability of rubble mound breakwaters.. doi: 10.13140/2.1.2158.8481

Goda, Y. (1978, Jan.). The observed joint distribution of periods and heights of sea waves. *Coastal Engineering Proceedings*, *1*(16), 11. doi: 10.9753/icce.v16.11

Goda, Y. (1988). Statistical variability of sea state parameters as a function of wave spectrum. *Coastal Engineering in Japan*, *31*(1), 39-52. doi: 10.1080/05785634.1988.11924482

Goda, Y. (2010). *Random seas and design of maritime structures* (Vol. 33). World Scientific Publishing Company.

Grace, R. (2001, 06). The factors and processes that influence artificial reef longevity. *Marine Technology Society Journal*, *35*, 3-13. doi: 10.4031/002533201788001910

Harris, L., & Gonzalez, J. (2005). *Stability analysis for the submerged reef ball breakwater proposed for the mayan palace resort, quintana roo, mexico.* (http://www.reefball.org/album/mexico/mayanriviara/mayanpalaceproject/anchoringrequirementstudy/mayan_palace_rbstability.pdf)

Heineke, D., & Verhagen, H. (2009, 06). On the use of the fictitious wave steepness and related surf-similarity parameters in methods that describe the hydraulic and structural response to waves. *Coastal Structures 2007: Proceedings of the 5th International Conference, Venice, Italy, 2-4 July 2007*. doi: 10.1142/9789814282024_0093

Hofland, B., Chen, X., Altomare, C., & Oosterlo, P. (2017). Prediction formula for the spectral wave period tm-1,0 on mildly sloping shallow foreshores. *Coastal Engineering*, *123*, 21-28. doi: https://doi.org/10.1016/j.coastaleng.2017.02.005

Holthuijsen, L. (2007). *Waves in oceanic and coastal waters*. United Kingdom: Cambridge University Press.

Hughes, S. A. (1993). *Physical models and laboratory techniques in coastal engineering* (Vol. 7). World Scientific.

Hydralab+. (2022). *Schelde Flume.* Retrieved 2022-01-13, from https://hydralab.eu/facilities--instruments/facilities-in-hydralab/Special-Purpose-Wave-Flumes/Schelde-Flume/

Ingsrisawang, V., Ban, M., & Kimura, H. (1995). Comparative study on the sinking of artificial reefs by local scour between laboratory and field experiments..

Jensen, A., Collins, K., & Lockwood, A. (2000). *Artificial reefs in european seas*. doi: 10.1007/978-94-011-4215-1

Kolkman, P., & Jongeling, T. (2007). Dynamic behaviour of hydraulic structures. *WL| Delft Hydraulics publication*.

Koudstaal, K., & van Rijn, L. (2020). Artificial reef structures north sea, structure stability analyses in borssele owf and nsil.

LeMéhauté. (1976). An introduction to hydrodynamics and water waves.

Luijendijk, A., Hagenaars, G., Ranasinghe, R., Baart, F., Donchyts, G., & Aarninkhof, S. (2018, 04). The state of the world's beaches. *Scientific Reports*, *8*. doi: 10.1038/s41598-018-24630-6

Ma, Y., Kuang, C., Han, X., Niu, H., Zheng, Y., & Shen, C. (2020). Experimental study on the influence of an artificial reef on cross-shore morphodynamic processes of a wave-dominated beach. *Water*, *12*(10). doi: 10.3390/w12102947

Massel, S. (1996). On the largest wave height in water of constant depth. *Ocean Engineering*, *23*(7), 553-573. doi: https://doi.org/10.1016/0029-8018(95)00049-6

MIAO, Z., & XIE, Y. (2007). Effects of water-depth on hydrodynamic force of artificial reef. *Journal of Hydrodynamics, Ser. B*, *19*(3), 372-377. doi: https://doi.org/10.1016/S1001-6058(07)60072-9

Mohazzab, P., et al. (2017). Archimedes' principle revisited. *Journal of Applied Mathematics and Physics*, *5*(04), 836.

Morison, J. R., Johnson, J. W., & Schaaf, S. A. (1950). The force exerted by surface waves on piles. *Journal of Petroleum Technology*, *2*, 149-154.

Nelson, R. (1994). Depth limited design wave heights in very flat regions. *Coastal Engineering*, *23*(1), 43-59. doi: https://doi.org/10.1016/0378-3839(94)90014-0

Pauly, D., Watson, R. A., & Alder, J. (2005). Global trends in world fisheries: impacts on marine ecosystems and food security. *Philosophical Transactions of the Royal Society B: Biological Sciences*, *360*, 12 - 5.

Pontee, N. (2013). Defining coastal squeeze: A discussion. *Ocean and Coastal Management*, *84*, 204-207. doi: https://doi.org/10.1016/j.ocecoaman.2013.07.010

ReefSystems. (2021). *Shimoni, Kenya.* Retrieved 2021-10-28, from `https://www.reefsystems.org/projects/shimoni-kenya`

Reid, W., Mooney, H., Cropper, A., Capistrano, D., Carpenter, S., & Chopra, K. (2005). *Millennium ecosystem assessment. ecosystems and human well-being: synthesis*.

Rock Manual. (2007). *CIRIA, CUR, CETMEF. The Rock Manual. The use of rock in hydraulic engineering (2nd edition). C683, CIRIA, London*.

Seaman, J. (2000). *Artificial reef evaluation: With application to natural marine habitats*.

Svendsen, I. A. (2006). *Introduction to nearshore hydrodynamics* (Vol. 24). World Scientific.

Tomasicchio, G., Aristodemo, F., & Veltri, P. (2009, 06). Wave and current hydrodynamic coefficients for bottom pipeline stability. In (p. 1067-1078). doi: 10.1142/9789814282024_0094

Verhagen, H. J., van Vledder, G. P., & Arab, S. E. (2009). A practical method for design of coastal structures in shallow water..

Yalin, M. S. (1971). *Theory of hydraulic models*. Macmillan International Higher Education.

Yalin, M. S. (1989). Fundamentals of hydraulic physical modelling..

Appendices

A

Important wave theory

First, the balance equations that define the free surface boundary conditions are given in this appendix. After, the equations are linearized for the linear wave theory.

A.1. Balance equations

Balance equations are used as the basis for the linear wave theory and will be given in this section. The derivations can be found in Holthuijsen (2007).

Equation A.1 gives the continuity equation, and Equation A.2 and A.3 give the momentum balance equations in x and z direction respectively, for a constant density. Only the expressions for u and w are presented because this study is conducted in a 2D frame of reference with zero flow in the y-direction.

$$\frac{\partial u}{\partial x} + \frac{\partial w}{\partial z} = 0 \tag{A.1}$$

$$\frac{\partial u}{\partial t} + \frac{\partial (uu)}{\partial x} + \frac{\partial (wu)}{\partial z} = -\frac{1}{\rho}\frac{\partial P}{\partial x} \tag{A.2}$$

$$\frac{\partial w}{\partial t} + \frac{\partial (uw)}{\partial x} + \frac{\partial (ww)}{\partial z} = -\frac{1}{\rho}\frac{\partial P}{\partial z} - g \tag{A.3}$$

By combining both the continuity equation (A.1) and differentiation of the momentum equations (A.2 and A.3), Equation A.4 and A.5 are acquired which give the Eulerian equations of motion in x- and y-direction respectively.

$$\frac{\partial u}{\partial t} + u\frac{\partial u}{\partial x} + w\frac{\partial u}{\partial z} = -\frac{1}{\rho}\frac{\partial P}{\partial x} \tag{A.4}$$

$$\frac{\partial w}{\partial t} + u\frac{\partial w}{\partial x} + w\frac{\partial w}{\partial z} = -\frac{1}{\rho}\frac{\partial P}{\partial z} - g \tag{A.5}$$

The associated boundary conditions consist of one dynamic condition and two kinematic conditions. The kinematic surface boundary condition (Equation A.6) states that if a particle is to remain on the surface, its velocity component in the direction normal to the surface must equal the velocity of the surface in that direction. The kinematic bottom boundary condition (Equation A.7) states that the water may not penetrate the fixed, horizontal bottom, and the dynamic surface boundary (Equation A.8) is simply that the pressure is zero.

$$w = \frac{\partial \eta}{\partial t} + u\frac{\partial \eta}{\partial x} \qquad \text{at } z = \eta \tag{A.6}$$

$$w = 0 \qquad \text{at } z = -d \tag{A.7}$$

$$P = 0 \qquad \text{at } z = \eta \tag{A.8}$$

A.2. Linear Wave Theory

For the linear wave theory the continuity equation and momentum balance given in Section A.1 are linearized, which results in the following equations. Equation A.9 gives the continuity equation for the linear wave theory, Equation A.10 the linearized momentum in x-direction and Equation A.11 in y-direction.

$$\frac{\partial u}{\partial x} + \frac{\partial w}{\partial z} = 0 \tag{A.9}$$

$$\frac{\partial u}{\partial t} = -\frac{1}{\rho}\frac{\partial P}{\partial x} \tag{A.10}$$

$$\frac{\partial w}{\partial t} = -\frac{1}{\rho}\frac{\partial P}{\partial z} - g \tag{A.11}$$

The linearized boundary conditions are given below (Equation A.12, A.13 and A.14)

$$w = \frac{\partial \eta}{\partial t} \qquad \text{at } z = \eta \tag{A.12}$$

$$w = 0 \qquad \text{at } z = -d \tag{A.13}$$

$$P = 0 \qquad \text{at } z = \eta \tag{A.14}$$

B

Performed tests

This appendix contains the results of all tests conducted during the two weeks of testing in the flume. The tables in this appendix show the flume input and measured values, which may vary slightly.

B.1. With regular waves - three reefs side to side

Table B.1 gives an overview of the performed tests for regular waves for the grey, pink and green reef side to side. Because the reefs got influenced by each other, the data obtained from these tests are unreliable and will therefore not be used for the data analysis.

Table B.1: Experimental tests for regular waves with three reefs side to side (the (grey) single plate, (pink) double plate, and (green) triple plate reef)

		INPUT				MEASURED				
TestID	d	H_{m0}/d	$s_{m-1,0}$	H_{m0}	$T_{m-1,0}$	H_{m0}/d	$s_{m-1,0}$	H_{m0}	$T_{m-1,0}$	T_p
	[m]	[-]	[-]	[m]	[s]	[-]	[-]	[m]	[s]	[s]
R314	0.33	0.45	0.01	0.15	2.53	0.42	0.017	0.14	2.28	2.53
R513	0.40	0.43	0.01	0.17	3.30	0.44	0.011	0.17	3.10	3.30
R517	0.33	0.43	0.01	0.14	2.99	0.41	0.017	0.13	2.22	2.97
R317	0.33	0.43	0.014	0.14	2.53	0.45	0.019	0.15	2.22	2.51
R523	0.40	0.43	0.0175	0.17	2.49	0.44	0.019	0.17	2.43	2.47
R527	0.33	0.43	0.0175	0.14	2.26	0.46	0.035	0.15	1.64	2.23
R533	0.40	0.43	0.025	0.17	2.09	0.43	0.028	0.17	1.97	2.09
R417	0.33	0.43	0.025	0.14	1.89	0.44	0.023	0.14	2.00	1.88
R613	0.43	0.4	0.01	0.17	3.30	0.37	0.011	0.16	3.11	3.29
R612	0.35	0.4	0.01	0.14	2.99	0.39	0.015	0.14	2.38	3.01
R611	0.28	0.4	0.01	0.11	2.65	0.35	0.015	0.10	2.00	2.63
R316	0.33	0.4	0.013	0.13	2.53	0.42	0.018	0.14	2.21	2.51
R623	0.43	0.4	0.0175	0.17	2.49	0.33	0.012	0.14	2.71	2.47
R622	0.35	0.4	0.0175	0.14	2.26	0.41	0.031	0.14	1.71	2.26
R621	0.28	0.4	0.0175	0.11	2.01	0.30	0.011	0.08	2.15	2.00

R633	0.43	0.4	0.025	0.17	2.09	0.39	0.027	0.17	1.99	2.10
R632	0.35	0.4	0.025	0.14	1.89	0.36	0.018	0.13	2.13	1.91
R631	0.28	0.4	0.025	0.11	1.68	0.28	0.016	0.08	1.76	1.67
R731	0.30	0.37	0.025	0.11	1.68	0.32	0.016	0.09	1.94	1.68
R315	0.33	0.36	0.012	0.12	2.53	0.40	0.017	0.13	2.26	2.50
R311	0.50	0.3	0.01	0.15	3.10	0.32	0.012	0.16	2.92	3.14
R312	0.33	0.3	0.01	0.1	2.53	0.33	0.015	0.11	2.21	2.55
R321	0.50	0.3	0.025	0.15	1.96	0.33	0.028	0.16	1.95	1.96
R322	0.33	0.3	0.025	0.1	1.60	0.30	0.026	0.10	1.58	1.61
R331	0.50	0.3	0.05	0.15	1.39	0.31	0.078	0.16	1.13	1.12
R332	0.33	0.3	0.05	0.1	1.13	0.28	0.047	0.09	1.13	1.13
R212	0.50	0.2	0.01	0.1	2.53	0.22	0.011	0.11	2.52	2.51
R222	0.50	0.2	0.025	0.1	1.60	0.21	0.025	0.11	1.65	1.58
R232	0.50	0.2	0.05	0.1	1.13	0.21	0.053	0.10	1.13	1.13
R112	0.50	0.1	0.01	0.05	1.79	0.11	0.008	0.05	2.08	1.80
R122	0.50	0.1	0.025	0.05	1.13	0.11	0.028	0.06	1.13	1.12
R132	0.50	0.1	0.05	0.05	0.80	0.10	0.052	0.05	0.80	0.80

B.2. With regular waves - reefs tested separately

Table B.2 gives an overview of the performed tests for regular waves.

Table B.2: Experimental tests for regular waves. Each test is conducted for the grey, pink, and 2x2 reef separately. For the experiments with the TestID consisting of Dxxx.b, then the pink reef was tested, and if it consists of Dxxx.c the 2x2 reef was tested. If no extra letter is added to the TestID, so just Dxxx, then the grey reef has been tested.

			INPUT				MEASURED				
TestID	Stability	d	H_{m0}/d	$s_{m-1,0}$	H_{m0}	$T_{m-1,0}$	H_{m0}/d	$s_{m-1,0}$	H_{m0}	$T_{m-1,0}$	T_p
		[m]	[-]	[-]	[m]	[s]	[-]	[-]	[m]	[s]	[s]
D213	Unstable	0.38	0.45	0.015	0.17	2.69	0.45	0.0131	0.17	2.88	2.71
D213.b	Unstable	0.38	0.45	0.015	0.17	2.69	0.44	0.0135	0.17	2.81	2.66
D213.c	Unstable	0.38	0.45	0.015	0.17	2.69	0.49	0.0212	0.18	2.36	2.71
D211	Stable	0.24	0.45	0.015	0.11	2.17	0.36	0.0167	0.09	1.85	2.16
D211.b	Stable	0.24	0.45	0.015	0.11	2.17	0.41	0.0200	0.10	1.80	2.19
D211.c	Stable	0.24	0.45	0.015	0.11	2.17	0.39	0.0205	0.10	1.73	2.16
D223	Unstable	0.38	0.45	0.025	0.17	2.09	0.43	0.0315	0.16	1.81	2.10
D223.b	Unstable	0.38	0.45	0.025	0.17	2.09	0.44	0.0333	0.17	1.78	2.10
D223.c	Unstable	0.38	0.45	0.025	0.17	2.09	0.47	0.0383	0.18	1.73	2.08
D221	Stable	0.24	0.45	0.025	0.11	1.68	0.36	0.0186	0.09	1.75	1.68
D221.b	Stable	0.24	0.45	0.025	0.11	1.68	0.41	0.0287	0.10	1.50	1.69
D221.c	Stable	0.24	0.45	0.025	0.11	1.68	0.39	0.0273	0.10	1.50	1.68
D113	Unstable	0.43	0.4	0.015	0.17	2.69	0.40	0.0123	0.17	2.97	2.66
D113.b	Stable	0.43	0.4	0.015	0.17	2.69	0.42	0.0187	0.18	2.48	2.68
D113.c	Stable	0.43	0.4	0.015	0.17	2.69	0.39	0.0157	0.16	2.59	2.68
D112	Stable	0.35	0.4	0.015	0.14	2.45	0.36	0.0177	0.13	2.14	2.45
D112.b	Unstable	0.35	0.4	0.015	0.14	2.45	0.35	0.0167	0.12	2.17	2.45
D112.c	Stable	0.35	0.4	0.015	0.14	2.45	0.34	0.0178	0.12	2.08	2.47
D111	Stable	0.28	0.4	0.015	0.11	2.17	0.36	0.0186	0.10	1.85	2.16
D111.b	Stable	0.28	0.4	0.015	0.11	2.17	0.35	0.0191	0.10	1.80	2.19
D111.c	Stable	0.28	0.4	0.015	0.11	2.17	0.32	0.0186	0.09	1.73	2.16
D123	Unstable	0.43	0.4	0.025	0.17	2.09	0.43	0.0305	0.18	1.95	2.09
D123.b	Unstable	0.43	0.4	0.025	0.17	2.09	0.39	0.0241	0.17	2.10	2.07
D123.c	Stable	0.43	0.4	0.025	0.17	2.09	0.42	0.0310	0.18	1.93	2.09
D122	Stable	0.35	0.4	0.025	0.14	1.89	0.37	0.0272	0.13	1.75	1.90
D122.b	Stable	0.35	0.4	0.025	0.14	1.89	0.38	0.0248	0.13	1.85	1.91
D122.c	Stable	0.35	0.4	0.025	0.14	1.89	0.40	0.0305	0.14	1.71	1.90
D121	Stable	0.28	0.4	0.025	0.11	1.68	0.34	0.0238	0.09	1.59	1.67
D121.b	Stable	0.28	0.4	0.025	0.11	1.68	0.37	0.0265	0.10	1.58	1.70
D121.c	Stable	0.28	0.4	0.025	0.11	1.68	0.36	0.0254	0.10	1.58	1.69

B.3. With irregular waves - reefs tested separately

Table B.3 summarizes the tests conducted for irregular waves, mainly for the single plate (grey) reef. Some tests are conducted for the double plate (pink) and 2x2 reef as well.

Table B.3: Experimental tests for irregular waves. For the TestID, the first letter 'I' refers to the irregular wave tests and the 'V' to the irregular wave tests at which also a foreshore ('voorland' in Dutch) was being used. The (grey) single plate reef is used for almost all tests, and some tests are repeated for the (pink) double plate and 2x2 reef, and for these tests '.b,' or '.c' has been added to the TestID, respectively.

TestID	Stability	d	INPUT				MEASURED				
			H_{m0}/d	$s_{m-1,0}$	H_{m0}	$T_{m-1,0}$	H_{m0}/d	$s_{m-1,0}$	H_{m0}	$T_{m-1,0}$	T_p
		[m]	[-]	[-]	[m]	[s]	[-]	[-]	[m]	[s]	[s]
V435.b	Unstable	0.38	0.4	0.015	0.15	2.53	0.36	0.011	0.13	2.82	2.82
V435.c	Unstable	0.38	0.4	0.015	0.15	2.53	0.36	0.011	0.13	2.82	2.82
V433	Unstable	0.28	0.4	0.015	0.11	2.17	0.36	0.011	0.10	2.36	2.34
V432	Unstable	0.23	0.4	0.015	0.09	1.96	0.35	0.012	0.08	2.07	2.22
V432.b	Stable	0.23	0.4	0.015	0.09	1.96	0.37	0.013	0.08	2.04	2.22
V432.c	Stable	0.23	0.4	0.015	0.09	1.96	0.37	0.013	0.08	2.05	2.22
V431	Stable	0.18	0.4	0.015	0.07	1.73	0.35	0.012	0.06	1.79	1.92
V424	Unstable	0.33	0.4	0.025	0.13	1.83	0.38	0.020	0.12	1.97	1.92
V423	Unstable	0.28	0.4	0.025	0.11	1.68	0.36	0.020	0.10	1.79	1.86
V422	Unstable	0.23	0.4	0.025	0.09	1.52	0.36	0.019	0.08	1.63	1.72
V421	Stable	0.18	0.4	0.025	0.07	1.34	0.36	0.019	0.06	1.44	1.51
V415	Unstable	0.38	0.4	0.05	0.15	1.39	0.34	0.036	0.13	1.52	1.52
V415.b	Stable	0.38	0.4	0.05	0.15	1.39	0.34	0.035	0.13	1.53	1.52
V415.c	Stable	0.38	0.4	0.05	0.15	1.39	0.34	0.035	0.13	1.52	1.52
V414	Unstable	0.33	0.4	0.05	0.13	1.29	0.34	0.035	0.11	1.42	1.43
V413	Stable	0.28	0.4	0.05	0.11	1.19	0.33	0.035	0.09	1.30	1.32
V412	Unstable	0.23	0.4	0.05	0.09	1.07	0.33	0.032	0.07	1.21	1.19
I713	Unstable	0.35	0.37	0.015	0.13	2.36	0.32	0.009	0.11	2.84	2.61
I711	Stable	0.30	0.37	0.015	0.11	2.17	0.31	0.008	0.09	2.71	2.41
I733	Unstable	0.35	0.37	0.025	0.13	1.83	0.31	0.014	0.11	2.24	2.04
I731	Unstable	0.30	0.37	0.025	0.11	1.68	0.30	0.013	0.09	2.10	1.90
I723	Unstable	0.35	0.37	0.05	0.13	1.29	0.29	0.031	0.10	1.46	1.47
I721	Stable	0.30	0.37	0.05	0.11	1.19	0.29	0.030	0.08	1.35	1.32
V333	Unstable	0.31	0.35	0.015	0.11	2.17	0.30	0.011	0.09	2.32	2.46
V332	Stable	0.26	0.35	0.015	0.09	1.96	0.32	0.013	0.08	2.01	2.22
V331	Stable	0.20	0.35	0.015	0.07	1.73	0.31	0.011	0.06	1.88	1.85
V324	Unstable	0.37	0.35	0.025	0.13	1.83	0.32	0.021	0.12	1.93	2.04
V323	Unstable	0.31	0.35	0.025	0.11	1.68	0.32	0.020	0.10	1.78	1.90
V323.b	Stable	0.31	0.35	0.025	0.11	1.68	0.32	0.021	0.10	1.77	1.90

V323.c	Stable	0.31	0.35	0.025	0.11	1.68	0.32	0.020	0.10	1.78	1.90
V322	Unstable	0.26	0.35	0.025	0.09	1.52	0.32	0.020	0.08	1.60	1.72
V321	Stable	0.20	0.35	0.025	0.07	1.34	0.31	0.017	0.06	1.52	1.51
V315	Unstable	0.43	0.35	0.05	0.15	1.39	0.30	0.037	0.13	1.51	1.52
V314	Unstable	0.37	0.35	0.05	0.13	1.29	0.30	0.037	0.11	1.39	1.43
V313	Unstable	0.31	0.35	0.05	0.11	1.19	0.29	0.036	0.09	1.28	1.29
V312	Stable	0.26	0.35	0.05	0.09	1.07	0.29	0.035	0.07	1.17	1.19
V311	Stable	0.20	0.35	0.05	0.07	0.95	0.28	0.004	0.06	3.10	1.06
I833	Unstable	0.38	0.34	0.025	0.13	1.83	0.28	0.015	0.11	2.19	2.04
I831	Stable	0.32	0.34	0.025	0.11	1.68	0.28	0.014	0.09	2.06	1.90
I823	Unstable	0.38	0.34	0.05	0.13	1.29	0.27	0.033	0.10	1.43	1.45
I821	Stable	0.32	0.34	0.05	0.11	1.19	0.27	0.032	0.09	1.31	1.32
I911	Unstable	0.35	0.31	0.015	0.11	2.17	0.27	0.009	0.09	2.64	2.41
I933	Unstable	0.42	0.31	0.025	0.13	1.83	0.27	0.015	0.11	2.18	2.07
I931	Unstable	0.35	0.31	0.025	0.11	1.68	0.26	0.015	0.09	1.98	1.90
I923	Unstable	0.42	0.31	0.05	0.13	1.29	0.25	0.035	0.11	1.40	1.43
I921	Stable	0.35	0.31	0.05	0.11	1.19	0.25	0.034	0.09	1.29	1.32
V232	Unstable	0.30	0.3	0.015	0.09	1.96	0.27	0.013	0.08	2.00	2.17
V224	Unstable	0.43	0.3	0.025	0.13	1.83	0.28	0.021	0.12	1.91	2.04
V224.b	Stable	0.43	0.3	0.025	0.13	1.83	0.28	0.022	0.12	1.89	2.04
V224.c	Stable	0.43	0.3	0.025	0.13	1.83	0.28	0.021	0.12	1.89	2.04
V223	Unstable	0.37	0.3	0.025	0.11	1.68	0.28	0.021	0.10	1.77	1.90
V222	Unstable	0.30	0.3	0.025	0.09	1.52	0.27	0.021	0.08	1.58	1.72
V215	Unstable	0.50	0.3	0.05	0.15	1.39	0.26	0.038	0.13	1.48	1.52
V214	Stable	0.43	0.3	0.05	0.13	1.29	0.26	0.038	0.11	1.37	1.43
V213	Stable	0.37	0.3	0.05	0.11	1.19	0.26	0.038	0.09	1.26	1.32
V212	Stable	0.30	0.3	0.05	0.09	1.07	0.25	0.036	0.07	1.15	1.19
I1013	Unstable	0.46	0.28	0.015	0.13	2.36	0.26	0.010	0.12	2.76	2.56
I1033	Unstable	0.46	0.28	0.025	0.13	1.83	0.24	0.017	0.11	2.04	2.04
I1023	Stable	0.46	0.28	0.05	0.13	1.29	0.23	0.036	0.11	1.38	1.43
I1133	Unstable	0.52	0.25	0.025	0.13	1.83	0.22	0.019	0.11	1.98	2.04
I1233	Unstable	0.59	0.22	0.025	0.13	1.83	0.20	0.021	0.12	1.94	2.01
V134	Unstable	0.65	0.2	0.015	0.13	2.36	0.19	0.013	0.12	2.46	2.61
V134.b	Stable	0.65	0.2	0.015	0.13	2.36	0.19	0.013	0.12	2.47	2.61
V134.c	Stable	0.65	0.2	0.015	0.13	2.36	0.19	0.013	0.12	2.47	2.61
V133	Stable	0.55	0.2	0.015	0.11	2.17	0.19	0.013	0.10	2.24	2.41
V132	Stable	0.45	0.2	0.015	0.09	1.96	0.18	0.013	0.08	2.02	2.22

V125	Stable	0.75	0.2	0.025	0.15	1.96	0.19	0.022	0.14	2.03	2.22
V124	Stable	0.65	0.2	0.025	0.13	1.83	0.18	0.022	0.12	1.88	2.04
V123	Stable	0.55	0.2	0.025	0.11	1.68	0.18	0.022	0.10	1.72	1.90
V122	Stable	0.45	0.2	0.025	0.09	1.52	0.18	0.021	0.08	1.57	1.72
V115	Stable	0.75	0.2	0.05	0.15	1.39	0.18	0.041	0.13	1.44	1.52
I1313	Unstable	0.68	0.19	0.015	0.13	2.36	0.17	0.012	0.12	2.48	2.61
I1333	Stable	0.68	0.19	0.025	0.13	1.83	0.17	0.022	0.12	1.88	2.04
I1323	Stable	0.68	0.19	0.05	0.13	1.29	0.17	0.041	0.11	1.33	1.43

C

Determination of constants for the stability prediction function

The constants c_1 and c_2 (from Subsection 4.2.2) depend on the wave steepness. In this appendix, a relationship between the constants and the wave steepness will be established.

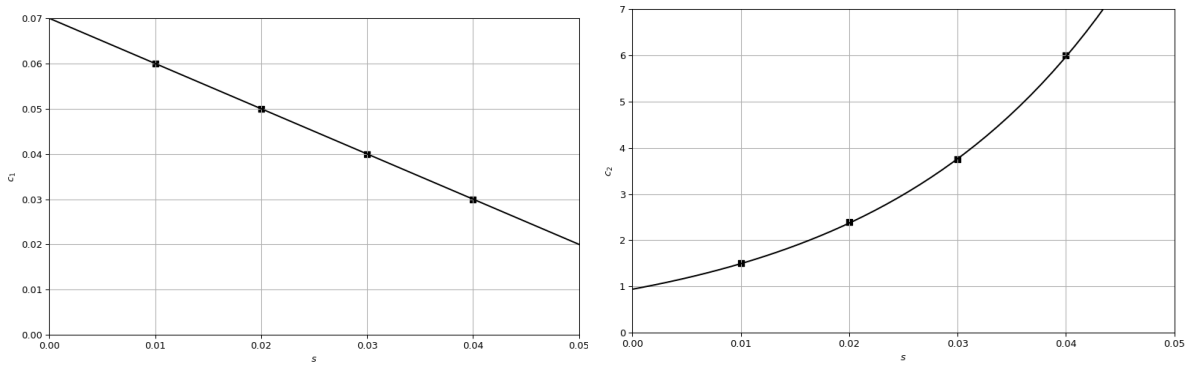

(a) The relation between the constant c_1 and wave steepness s, which is equal to $c_1 = 0.07 - s$

(b) The relation between the constant c_2 and wave steepness s, which is equal to $c_2 = 0.94 \cdot (1.17 \cdot 10^{20})^s$

Figure C.1: Graphs used to determine the relationship between the constants c_1 and c_2, and the wave steepness s. A line is plotted through the points, which are derived from the corresponding values for wave steepness and constants, from Table 4.1 with rewritten functions.

Figure C.1a shows the points for which the values of the constant c_1 are related to the values of the corresponding wave steepness. The points are located on a line, so there is a linear relationship between the constant c_1 and the wave steepness s. The equation of the line has the form $c_1 = b + a \cdot s$, in which a is the slope of the line and b is the y-intercept. For this case, the value of a is equal to -1, and the y-intercept b is equal to 0.07. This results in the following equation: $c_1 = 0.07 - s$.

Figure C.1b shows the points for the constant c_2 related to the corresponding wave steepness, between which an exponential relationship is visible. The equation of the exponential line has the form $c_2 = a \cdot b^x$. With two data points, you can define the exponential function that passes through these points by substituting them in the equation.

- Substituting data point (0.01, 1.5) gives $1.5 = a \cdot b^{0.01}$
- Substituting data point (0.04, 6.0) gives $6.0 = a \cdot b^{0.04}$

Solving the first equation for a in terms of b gives $a = 1.5 \cdot b^{-0.01}$. When substituting this in the second equation, and solving for b:

$6.0 = a \cdot b^{0.04}$
$6.0 = 1.5 \cdot b^{-0.01} \cdot b^{0.04}$
$6.0 = 1.5 \cdot b^{0.03}$
$b = (6.0/1.5)^{1/0.03}$
$b \approx 1.17 \cdot 10^{20}$

The value of b is used in the first equation to solve for the value of a:

$a = 1.5 \cdot b^{-0.01}$
$a = 1.5 \cdot (1.17 \cdot 10^{20})^{-0.01}$
$a \approx 0.94$

With the values of a and b known, the exponential equation becomes $c_2 = 0.94 \cdot (1.17 \cdot 10^{20})^{s}$.

D

Python scripts

```
C_d = 2
rho = 1000
A_p = 0.009
g = 9.81
C_m = 3
V = 0.000164
C_l = 2
S = 0.01
mu = 0.5

def func(d,H,T_m10):
    L1 = g * T_m10**2/(2*np.pi)
    for i in range(100):
        L1 = g * T_m10**2/(2*np.pi) * np.tanh(2*np.pi*d/L1)
    H1 = 0.55*d
    H = min(H1, H)
    U = ( np.pi * H )/ ( T_m10 * np.sinh((2*np.pi/L1)*d))
    F_drag = C_d * rho * A_p * U**2/2
    a = 2* np.pi**2 * H / T_m10**2 * (1/np.sinh((2*np.pi/L1)*d))
    F_inertia = C_m * rho * V * a
    F_wave = F_drag + F_inertia
    F_bouy = rho * V * g
    F_lift = C_l * rho * S * U**2/2
    W_object = ((F_wave/mu) + F_bouy + F_lift)/g
    return W_object

H = [0.07, 0.09, 0.11, 0.13, 0.15]
d = np.linspace(0.01,1,30)
H_index = 0
weight = [[],[],[],[],[]]
for H_value in H:
    for i in range(len(d)):
        weightt = func(d[i],H[H_index],2)
        weight[H_index].append(weightt)
    H_index = H_index+1

fig = plt.figure(figsize = (12,8))
ax = fig.subplots()

a = [0, 1, 2, 3, 4]
line = ['-', '--', '-.', ':', '-']
width = ['1','1','1','1','2',]
for i in a:
    d_new = np.linspace(d.min(), d.max(), 50)
    a_BSpline = make_interp_spline(d, weight[i])
    y_new = a_BSpline(d_new)
    plt.plot(d_new, y_new,linestyle = line[i], color = 'k', linewidth= width[i], label =r'$H_{m0} = $'f'{H[i]} m' )

ax.set_xlabel(r'$d$ [m]')
ax.set_ylabel(r'Required Weight $W$ [kg]')
ax.legend()
xnumbers = np.linspace(0, 1, 11)
ynumbers = np.linspace(0, 1, 11)
plt.xticks(xnumbers)
plt.yticks(ynumbers)
plt.axis([0, 1, 0, 1])
ax.grid(True)
```

Figure D.1: Python script for Figure 4.4

```
C_d = 2.5
rho = 1000
A_p = 0.01
g = 9.81
C_m = 3
V = 0.000164
C_l = 2.5
S = 0.0009
mu = 0.5
W_object = 0.345

def func(H):
    L1 = g * T_p**2/(2*np.pi)
    for i in range(100):
        L1 = g * T_p**2/(2*np.pi) * np.tanh(2*np.pi*d/L1)
    U = ( np.pi * H )/ ( T_p * np.sinh((2*np.pi/L1)*d))
    F_drag = C_d * rho * A_p * U**2/2
    a = 2* np.pi**2 * H / T_p**2 * (1/np.sinh((2*np.pi/L1)*d))
    F_inertia = C_m * rho * V * a
    F_wave = F_drag + F_inertia
    F_bouy = rho * V * g
    F_lift = C_l * rho * S * U**2/2
    stability = W_object*g - (F_wave/mu) - F_bouy - F_lift
    return stability

T_p2 = [1.0, 1.45, 1.90, 2.35, 2.80]
d2 = np.linspace(0.0001, 10,200)
T_p_index = 0
weight = [[],[],[],[],[],[]]
for T_p_value in T_p2:
    for i in range(len(d2)):
        T_p = T_p_value
        d = d2[i]
        H = abs(fsolve(func, 5) )
        H1 = 0.55*d
        H = min(H1, H)
        weight[T_p_index].append(H)
    T_p_index = T_p_index+1

fig = plt.figure(figsize = (10,6))
ax = fig.subplots()
plt.plot(d2,weight[0],linestyle = "-", color = 'k', linewidth= '2', label=r'$T_p=$1.00 s')
plt.plot(d2,weight[1],linestyle = "--", color = 'k', linewidth= '1', label=r'$T_p=$1.45 s')
plt.plot(d2,weight[2],linestyle = "-.", color = 'k', linewidth= '1', label=r'$T_p=$1.90 s')
plt.plot(d2,weight[3],linestyle = ":", color = 'k', linewidth= '1', label=r'$T_p=$2.35 s')
plt.plot(d2,weight[4],linestyle = "-", color = 'k', linewidth= '1', label=r'$T_p=$2.80 s')

ax.set_ylabel(r'$H_{m0}$ [m]')
ax.set_xlabel(r'$d$ [m]')
xnumbers = np.linspace(0, 0.8, 9)
ynumbers = np.linspace(0, 0.18, 7)
plt.xticks(xnumbers)
plt.yticks(ynumbers)
plt.axis([0, 0.8, 0, 0.18])
ax.legend()
```

Figure D.2: Python script for Figure 4.5

```
C_d = 2
rho = 1000
A_p = 0.009
g = 9.81
C_m = 3
V = 0.000164
C_l = 2
S = 0.01
mu = 0.5
W_object = 0.345

def func(H):
    L1 = g * T_m10**2/(2*np.pi)
    for i in range(100):
        L1 = g * T_m10**2/(2*np.pi) * np.tanh(2*np.pi*d/L1)
    U = ( np.pi * H )/ ( T_m10 * np.sinh((2*np.pi/L1)*d))
    F_drag = C_d * rho * A_p * U**2/2
    a = 2* np.pi**2 * H / T_m10**2 * (1/np.sinh((2*np.pi/L1)*d))
    F_inertia = C_m * rho * V * a
    F_wave = F_drag + F_inertia
    F_bouy = rho * V * g
    F_lift = C_l * rho * S * U**2/2
    stability = W_object*g - (F_wave/mu) - F_bouy - F_lift
    return stability

T_m102 = [1.0, 1.45, 1.90, 2.35, 2.80]
d2 = np.linspace(0.0001, 10,200)
T_m10_index = 0
weight = [[],[],[],[],[],[]]
for T_m10_value in T_m102:
    for i in range(len(d2)):
        T_m10 = T_m10_value
        d = d2[i]
        H = abs(fsolve(func, 5))
        H1 = 0.55*d*np.ones(1)
        H = min(H1, H)
        if 2*np.pi/g * H / T_m10**2 > 0.14:
            H = np.nan*np.ones(1)
        weight[T_m10_index].append(H)
    T_m10_index = T_m10_index+1

S001 = df.loc[(df['T_m-1,0'] >= 1.0) & (df['T_m-1,0'] <= 1.225)]
S002 = df.loc[(df['T_m-1,0'] >= 1.226) & (df['T_m-1,0'] <= 1.675)]
S003 = df.loc[(df['T_m-1,0'] >= 1.676) & (df['T_m-1,0'] <= 2.125)]
S004 = df.loc[(df['T_m-1,0'] >= 2.126) & (df['T_m-1,0'] <= 2.575)]
S005 = df.loc[(df['T_m-1,0'] >= 2.576) & (df['T_m-1,0'] <= 3.2)]

S001stabiel = S001.loc[S001['Stabiliteit'] == 'Stabiel']
S001nietstabiel = S001.loc[S001['Stabiliteit'] == 'Niet stabiel']
S002stabiel = S002.loc[S002['Stabiliteit'] == 'Stabiel']
S002nietstabiel = S002.loc[S002['Stabiliteit'] == 'Niet stabiel']
S003stabiel = S003.loc[S003['Stabiliteit'] == 'Stabiel']
S003nietstabiel = S003.loc[S003['Stabiliteit'] == 'Niet stabiel']
S004stabiel = S004.loc[S004['Stabiliteit'] == 'Stabiel']
S004nietstabiel = S004.loc[S004['Stabiliteit'] == 'Niet stabiel']
S005stabiel = S005.loc[S005['Stabiliteit'] == 'Stabiel']
S005nietstabiel = S005.loc[S005['Stabiliteit'] == 'Niet stabiel']


fig, axs = plt.subplots(5, figsize=(9, 15), sharex=True, sharey=True)
axs = axs.ravel()
line = ['-','--','-.',':','-',]
width = [2,1,1,1,1]
marker = ['s','o','^','*','D']
stabiel = [S001stabiel,S002stabiel,S003stabiel,S004stabiel,S005stabiel]
nietstabiel = [S001nietstabiel,S002nietstabiel,S003nietstabiel,S004nietstabiel,S005nietstabiel]

for i in range(5):
    axs[i].plot(d2,weight[i],linestyle = line[i], color = 'k', linewidth= width[i], label=r'$T_{m-1,0} ≈ $'f' {T_m102[i]} s')
    axs[i].set_ylabel(r'$H_{m0}$ [m]')
    axs[i].scatter(nietstabiel[i]['d'], nietstabiel[i]['H_m0'] , color = 'k', s =55, marker = marker[i], facecolors='none', labe
l = 'Not stable')
    axs[i].scatter(stabiel[i]['d'], stabiel[i]['H_m0'] , color = 'k', s =45, marker = marker[i], label = 'Stable')
    axs[i].legend(loc=2, fontsize='small', fancybox=True)
    axs[i].grid(True)
    axs[i].set_xlabel(r'$d$ [m]')
xnumbers = np.linspace(0, 0.8, 9)
ynumbers = np.linspace(0, 0.18, 5)
plt.xticks(xnumbers)
plt.yticks(ynumbers)
plt.axis([0, 0.8, 0, 0.18])
```

Figure D.3: Python script for Figure 4.6, in which ’df’ is a dataframe containing the test results

```
C_d = 2
rho = 1025
A_p = 0.009*20**2
g = 9.81
C_m = 3
V = 0.000164*20**3
C_l = 2
S = 0.01*20**2
mu = 0.6

def func(d,H,T_m10):
    H1 = 0.55*d
    H = min(H1, H)
    L1 = g * T_m10**2/(2*np.pi)
    for i in range(100):
        L1 = g * T_m10**2/(2*np.pi) * np.tanh(2*np.pi*d/L1)
    U = ( np.pi * H )/ ( T_m10 * np.sinh((2*np.pi/L1)*d))
    F_drag = C_d * rho * A_p * U**2/2
    a = 2* np.pi**2 * H / T_m10**2 * (1/np.sinh((2*np.pi/L1)*d))
    F_inertia = C_m * rho * V * a
    F_wave = F_drag + F_inertia
    F_bouy = rho * V * g
    F_lift = C_l * rho * S * U**2/2
    W_object = ((F_wave/mu) + F_bouy + F_lift)/g
    return W_object

H = [2, 3, 4, 5, 6]
d = np.linspace(0.01,50,50)
H_index = 0
weight = [[],[],[],[],[]]
for H_value in H:
    for i in range(len(d)):
        weightt = func(d[i],H[H_index],10)
        weight[H_index].append(weightt*1.2)
    H_index = H_index+1

fig = plt.figure(figsize = (12,8))
ax = fig.subplots()

a = [0, 1, 2, 3, 4]
line = ['-', '--', '-.', ':', '-']
width = ['1','1','1','1','2',]
for i in a:
    d_new = np.linspace(d.min(), d.max(), 80)
    a_BSpline = make_interp_spline(d, weight[i])
    y_new = a_BSpline(d_new)
    plt.plot(d_new, y_new,linestyle = line[i], color = 'k', linewidth= width[i], label = r'$H_{m0} = $'f'{H[i]} m' )

ax.set_xlabel(r'$d$ [m]')
ax.set_ylabel(r'Required weight $W$ [kg]')
ax.legend()
xnumbers = np.linspace(0, 50, 11)
ynumbers = np.linspace(0, 10000, 11)
plt.xticks(xnumbers)
plt.yticks(ynumbers)
plt.axis([0, 50, 0, 10000])
ax.grid(True)
```

Figure D.4: Python script for Figure 4.7

```
C_d = 2
rho = 1025
A_p = 0.009*20**2
g = 9.81
C_m = 3
V = 0.000164*20**3
C_l = 2
S = 0.01*20**2
mu = 0.6
W_object = 2444

def func(H):
    L1 = g * T_m10**2/(2*np.pi)
    for i in range(100):
        L1 = g * T_m10**2/(2*np.pi) * np.tanh(2*np.pi*d/L1)
    U = ( np.pi * H )/ ( T_m10 * np.sinh((2*np.pi/L1)*d))
    F_drag = C_d * rho * A_p * U**2/2
    a = 2* np.pi**2 * H / T_m10**2 * (1/np.sinh((2*np.pi/L1)*d))
    F_inertia = C_m * rho * V * a
    F_wave = F_drag + F_inertia
    F_bouy = rho * V * g
    F_lift = C_l * rho * S * U**2/2
    stability = W_object*g - (F_wave/mu) - F_bouy - F_lift
    return stability

T_m102 = [5, 7, 9, 11, 13]
d2 = np.linspace(0.0001, 50, 100)
T_m10_index = 0
weight = [[],[],[],[],[]]
for T_m10_value in T_m102:
    for i in range(len(d2)):
        T_m10 = T_m10_value
        d = d2[i]
        H = abs(fsolve(func, 5))/1.2
        H1 = 0.55*d*np.ones(1)
        H = min(H1, H)
        if 2*np.pi/g * H / T_m10**2 > 0.14:
            H = np.nan
        weight[T_m10_index].append(H)
    T_m10_index = T_m10_index+1

fig = plt.figure(figsize = (12,8))
ax = fig.subplots()
plt.plot(d2,weight[0],linestyle = "-", color = 'k', linewidth= '2', label=r'$T_{m-1,0}=$5 s')
plt.plot(d2,weight[1],linestyle = "--", color = 'k', linewidth= '1', label=r'$T_{m-1,0}=$7 s')
plt.plot(d2,weight[2],linestyle = "-.", color = 'k', linewidth= '1', label=r'$T_{m-1,0}=$9 s')
plt.plot(d2,weight[3],linestyle = ":", color = 'k', linewidth= '1', label=r'$T_{m-1,0}=$11 s')
plt.plot(d2,weight[4],linestyle = "-", color = 'k', linewidth= '1', label=r'$T_{m-1,0}=$13 s')

ax.set_ylabel(r'$H_{m0}$ [m]')
ax.set_xlabel(r'$d$ [m]')
xnumbers = np.linspace(0, 50, 11)
ynumbers = np.linspace(0, 8, 9)
plt.xticks(xnumbers)
plt.yticks(ynumbers)
plt.axis([0, 50, 0, 8])
ax.legend()
ax.grid(True)
```

Figure D.5: Python script for Figure 4.8

E

Velocity determination with spectral analysis

In this appendix, first, some important theory of the spectral velocity determination will be given, whereafter the spectral velocity will be compared to the peak bottom orbital velocity. Lastly, the theory will be applied for the analysis of the data from the stability experiments of the reefs for both the Morison stability prediction method and the stability method using the mobility parameter.

E.1. Velocity spectrum theory

Like the stability of artificial reefs, the on-bottom stability of pipelines is governed by the fundamental balance between loads and resistances as well. In offshore pipelines, these loads are hydrodynamic loads induced by waves and currents. This load-resistance relationship has formed the basis for various design codes governing the stability of submarine pipelines such as the DNV RP E305 (DNV, 1988), DNV RP F109 (DNV, 2006), and DNV OS F101 (DNV, 2010). Based on these design codes, a characteristic velocity can be determined, which may be useful for the determination of the stability of the reefs. For both the Morison stability prediction method and the stability method using the mobility parameter, a characteristic velocity is needed.

The wave-induced velocity spectrum at the sea bed $S_{UU}(\omega)$ may be obtained through a spectral transformation of the waves at sea level, as shown in Equation E.1.

$$S_{UU}(\omega) = G^2(\omega) \cdot S_{\eta\eta}(\omega) \tag{E.1}$$

The transfer function G transforms sea surface elevation to wave-induced flow velocities at the sea bed. It is given with Equation E.2, in which d is the water depth, ω is the circular wave frequency of the wave motion ($= 2\pi/T$), and k is the wavenumber ($= 2\pi/L$).

$$G(\omega) = \frac{\omega}{\sinh kd} \tag{E.2}$$

The spectral moments of order n is defined in Equation E.3.

$$M_n = \omega^n \cdot S_{UU}(\omega) \tag{E.3}$$

Assuming linear wave theory, the design spectral velocity amplitude U_s can be obtained analytically as described with Equation E.4, or from Figure E.2 in which T_n is given with Equation E.5 and γ is equal to 3.3 for the used Jonswap spectrum.

$$U_s = 2\sqrt{M_0} \tag{E.4}$$

$$T_n = \sqrt{\frac{d}{g}} \tag{E.5}$$

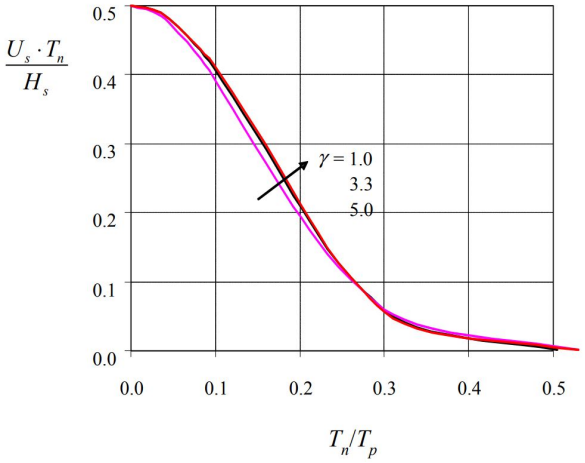

(a) By fitting a curve through some characteristic points on the graph for $\gamma = 3.3$, the relation between the x- and y-axis is determined and is as follows: $y = 564.7x^6 - 857.3x^5 + 441.4x^4 - 73.92x^3 - 3.073x^2 - 0.2279x + 0.5009$, in which $x = T_n/T_p$ and $y = U_s \cdot T_n/H_s$.

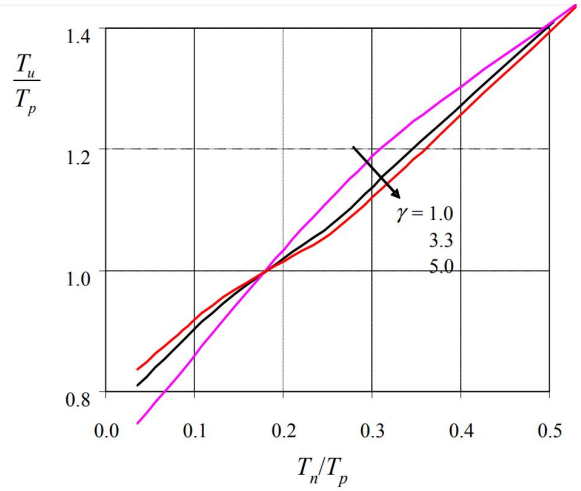

(b) By fitting a curve through some characteristic points on the graph for $\gamma = 3.3$, the relation between the x- and y-axis is determined and is as follows: $y = -19.56x^4 + 21.86x^3 - 7.966x^2 + 2.296x + 0.7362$, in which $x = T_n/T_p$ and $y = T_u/T_p$.

Figure E.1: Graphs to determine significant flow velocity amplitude U_s and mean zero up-crossing period of oscillating flow T_u at sea bed level (DNV, 2006)

For analytical determination, the mean zero up-crossing period T_u of oscillating flow at the sea bed is given in Equation E.6. However, from Figure E.1b the mean zero up-crossing period can be obtained as well.

$$T_u = 2\pi \sqrt{\frac{M_0}{M_2}} \tag{E.6}$$

The significant acceleration can be determined with Equation E.7.

$$a_s = \frac{2\pi U_s}{T_u} \tag{E.7}$$

The design spectral velocity amplitude U_s and the significant acceleration a_s can be used instead of the peak bottom orbital velocity $\hat{u}_\delta$ and the horizontal acceleration a from Equation 2.24 and 2.25 respectively.

E.2. Comparison with peak bottom orbital velocity

In addition to the spectral analysis method of determining the velocity at the bed, a more simplistic method consists in using the characteristic peak bottom orbital velocity $\hat{u}_\delta$ as given in Equation 2.24. For the characteristic wave height and period, the significant wave height H_s and spectral wave period $T_{m-1,0}$ are used.

Figure E.2 shows the data points for both of these velocity determination methods, where the points that are close to each other refer to the same wave flume test (indicated by an encircling for some of the tests). It can be concluded from the figure that the velocity based on the peak bottom orbital velocity has higher values than the ones calculated with the spectral velocity, as the red points have higher velocity values than the black ones.

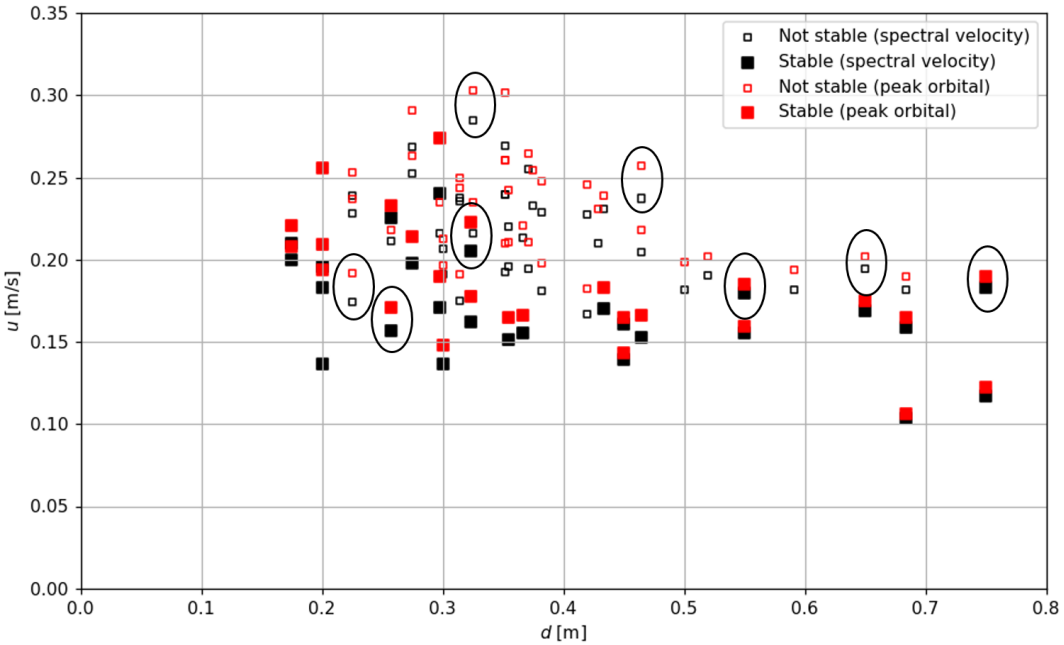

Figure E.2: Data points for which the velocity u is calculated with different methods; the black points are determined using the spectral velocity and the red points are determined using the peak orbital velocity as given in Equation 2.24, for which the significant wave height and spectral wave period, H_s and $T_{m-1,0}$ are used.

E.3. Morison suitability with spectral velocity

The comparison between the Morison stability prediction and the data from the experiments (as described in Section 4.3.2) is performed again. However, the spectral velocity is used instead of the peak bottom orbital velocity. All other values of the parameters used for the graphs are the same as the ones for the comparison using the peak orbital velocity (Table 4.3).

Figure E.3 shows the result of the comparison between the Morison method using the spectral velocity and the data points from the tests. Compared with the method using the peak orbital velocity, the data points did not change, but the curves depicting the Morison stability prediction differ. Due to the relatively lower spectral velocity, predicted is that the reef will become unstable at lower wave heights, and therefore the Morison curves are lower.

The data points deviate relatively much from the Morison curves compared to the Morison curves using peak orbital velocity. The Morison curves are too low, resulting in an overly safe stability prediction. Almost all stable data points are above the Morison curves. An option is to vary the values of the coefficients C_d, C_m, and C_l to get a better fit. However, these values are obtained from the literature, so too much variance would no longer match these values. From this, it can be concluded that using the spectral velocity for the Morison stability prediction is less appropriate than using the peak bottom orbital velocity and will therefore not be used to analyze the data with the Morison method.

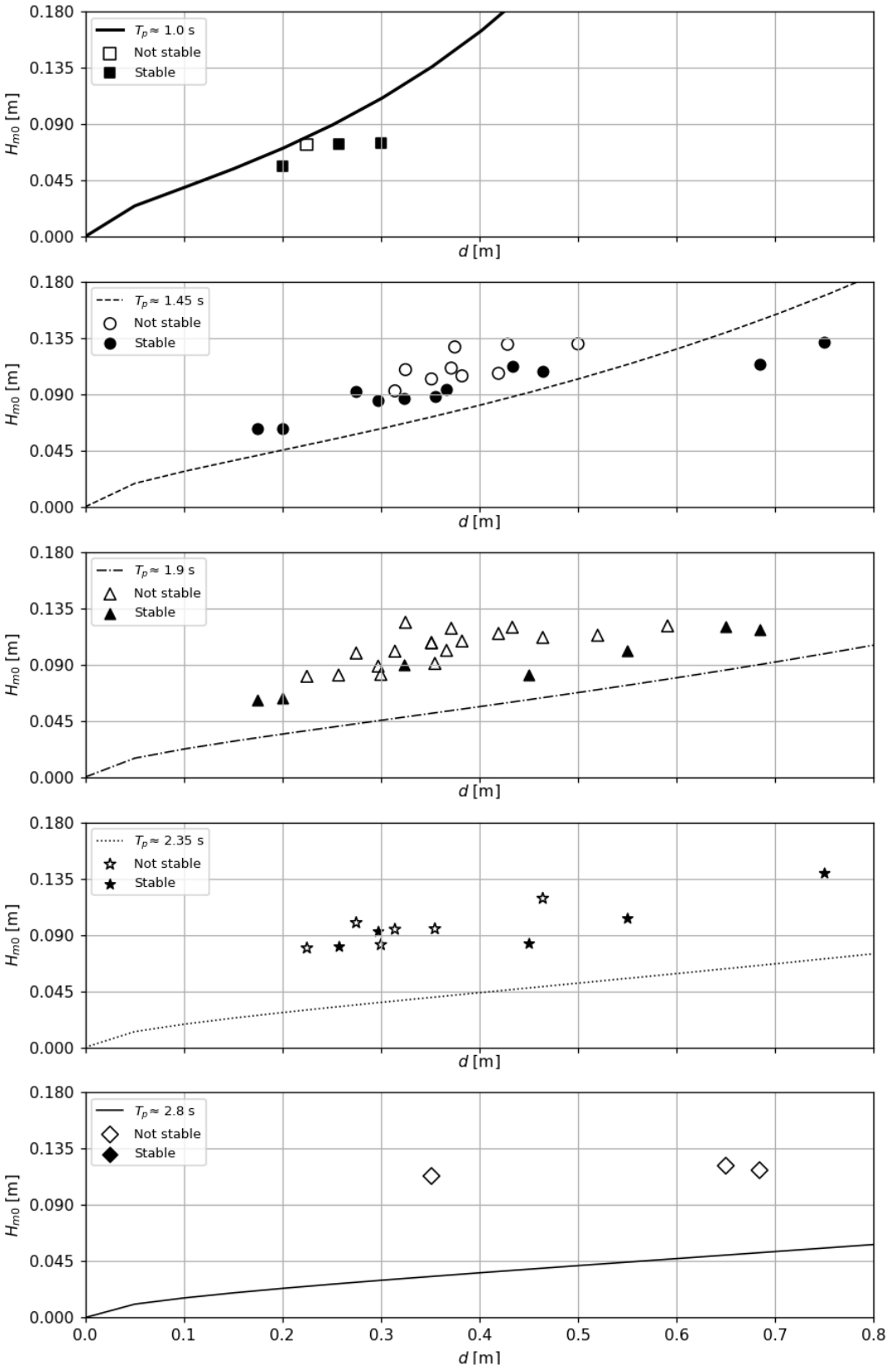

Figure E.3: Relation between the significant wave height and the water depth for several peak periods for the single plate (grey) reef model according to the Morison stability prediction using the spectral velocity

E.4. Suitability of mobility parameter prediction method using spectral velocity

The mobility parameter prediction method, as explained in Section 4.4 makes use of the peak bottom orbital velocity. Figure E.4 gives the data points again from the experimental wave flume tests with the θs-value (the multiplication of the non-dimensional mobility parameter and steepness) on the y-axis, but this time using the spectral velocity. While a certain trend was visible with the prediction method based on the peak orbital velocity, this trend is not visible when using spectral velocity. Both stable and unstable points are scattered, with no specific limit indicating at what value the reef would become unstable.

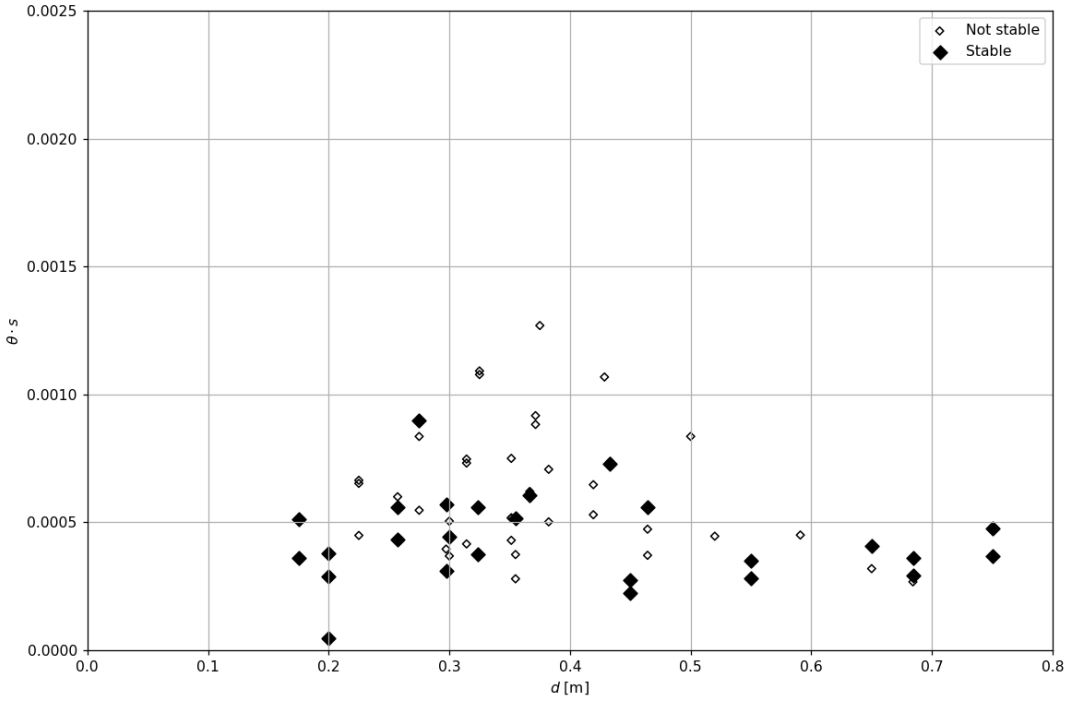

Figure E.4: Data points from the experimental wave flume tests showing the trend between the θs-value and the water depth d in meters using the spectral velocity determination

Knowing that no specific instability limit is visible between the stable and unstable points, and no clear trend is visible between the θs-value and the water depth, a relation for the prediction method using the mobility parameter is hard to find. Figure E.5 shows the relation of the mobility parameter prediction method from Section 4.4, for which the peak orbital velocity is being used, and the data points are determined with the spectral velocity.

A big deviation between the prediction line and data points is visible. Changing the values for r_1, r_2, and r_3 could reduce this deviation; however, since the trends in Figure E.4 are already not properly represented, using the spectral velocity for the mobility parameter stability prediction would be less appropriate than using the peak orbital velocity.

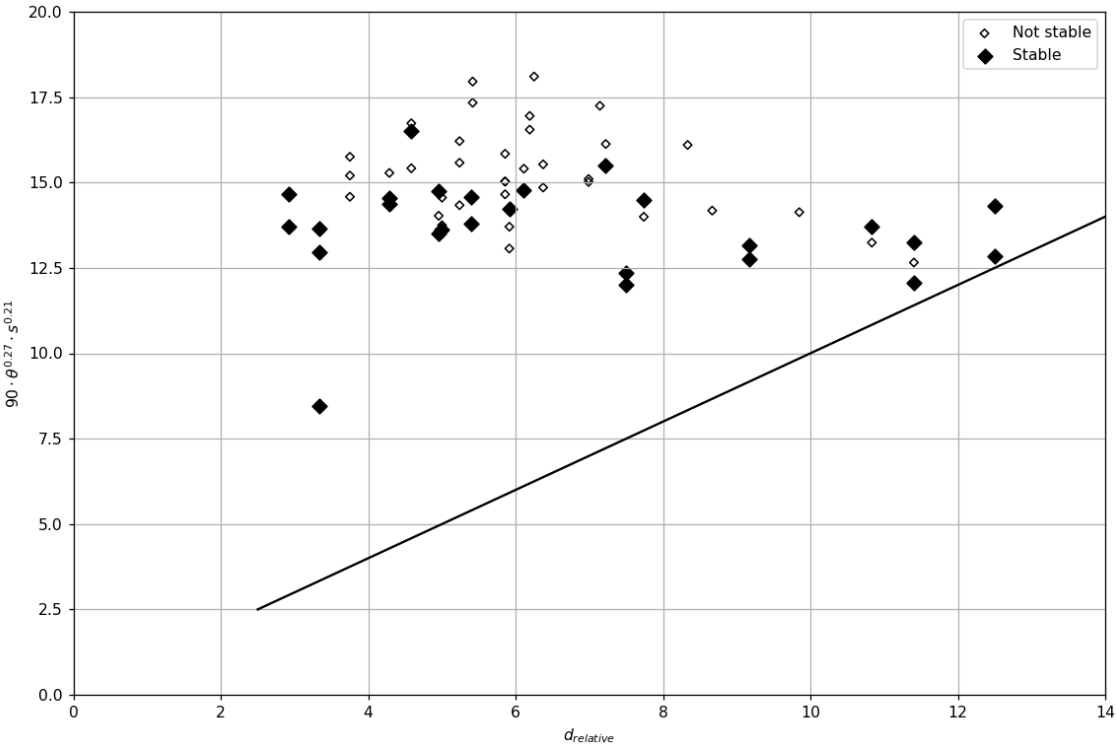

Figure E.5: Relation of the prediction method using the mobility parameter (from Section 4.4) with data points for the single plate (grey) reef using the spectral velocity determination

F

Best-estimate Morison graphs

To predict the stability of the single plate reef prototype at full size, Figure F.1 and Figure F.2 are given. These figures show the relationship between the required weight and the water depth and the significant wave height and water depth. For these graphs, no safety factor was used to obtain the best-estimate prediction of the reef prototype.

The used density is equal to 1025 kg/m^3 and the coefficient of friction μ is equal to 0.6. The remaining values used to generate the graphs in Figure F.1 and Figure F.2 are shown in Table F.1 and F.2 respectively.

Table F.1: Values used to determine the graphs in Figure F.1

C_d	C_m	C_l	μ	A_p [m^2]	V [m^3]	S [m^2]	$T_{m-1,0}$ [s]
2	3	2	0.6	3.6	1.3	4	10

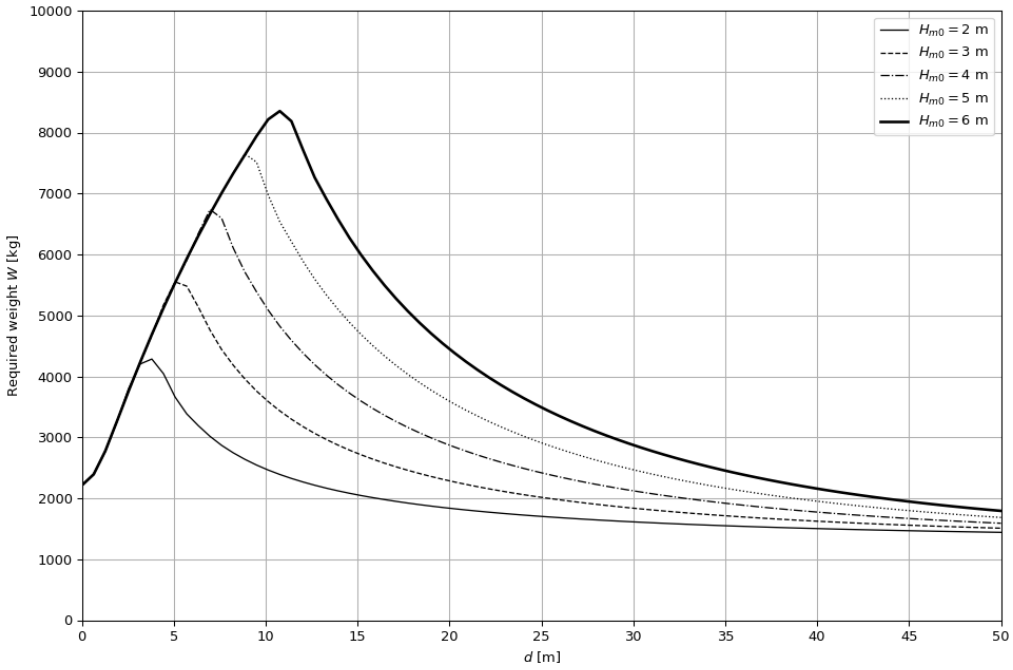

Figure F.1: Relation between the required dry weight of the single plate reef prototype and the water depth for several significant wave heights according to the Morison stability prediction without a safety factor. The spectral period $T_{m-1,0}$ is equal to 10 s.

Table F.2: Values used to determine the graphs in Figure F.2

C_d	C_m	C_l	μ	A_p [m^2]	V [m^3]	S [m^2]	W_{dry} [kg]
2	3	2	0.6	3.6	1.3	4	2444

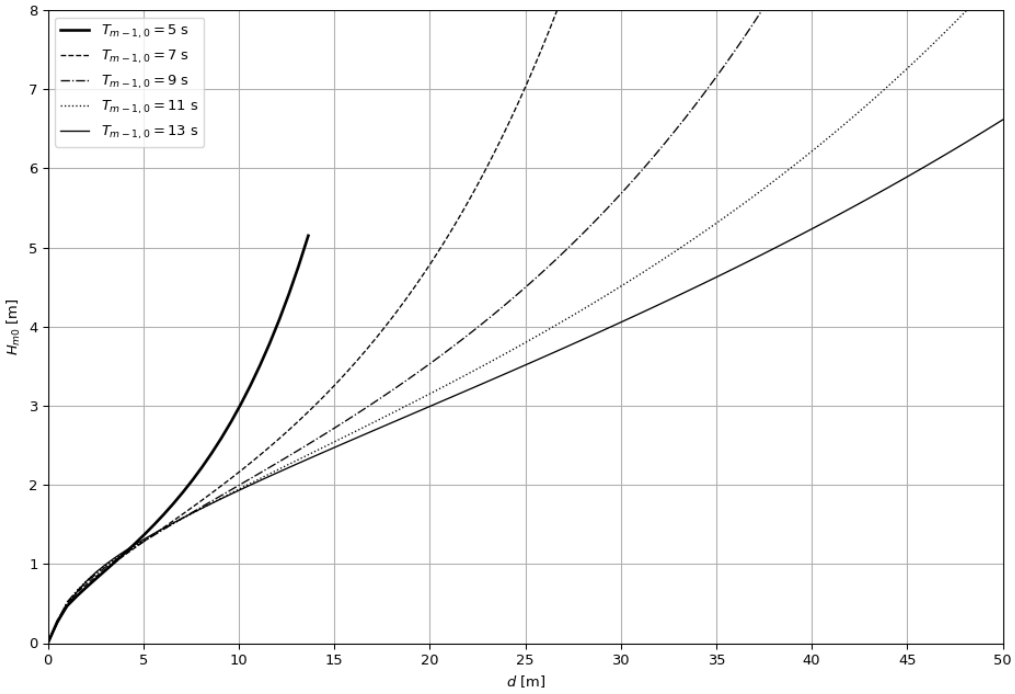

Figure F.2: Relation between the significant wave height and the water depth for several spectral periods for the single plate reef prototype according to the Morison stability prediction without a safety factor. Above a curve, the reef is unstable, while below a curve the reef is stable.

G

Suitability of prediction methods for variations in reef property

This appendix gives the suitability of the determined stability function (Section 4.2), the Morison prediction method (Section 4.3), and the mobility parameter prediction method (Section 4.4) for the double plate reef and the 2x2 reef which is made out of four single plate reefs. The prediction methods will be compared to the data points obtained from the irregular wave tests given in Table B. Six tests are performed for both the pink and 2x2 reef to test the stability.

G.1. The double plate pink reef

The pink reef consists of two Stelcon plates, so the height (0.07 m) is greater than the grey reef, and the weight (0.625 kg) is greater too. In this section, the prediction methods will be applied to the pink reef.

G.1.1. Applicability of the determined stability function

The procedure used to obtain the stability function from Section 4.2 is applied to the pink reef. Figure G.1 shows the data points through which trend lines are again drawn. The functions for these trend lines are given in Table G.1. Although only six data points are available, the trend lines were created based on the probabilities obtained from the grey reef trend lines.

The resulting stability function for the pink reef is given in Equation G.1, for which the comparison with the data points is given in Figure G.2. To determine the relative water depth $d_{relative}$, a reef height of 0.07 m is used. All stable points are below the stability line, and the only unstable point is above the line. From this, it can be concluded that the determined stability function for the pink reef gives a representative view of the stability of the reef.

$$\begin{aligned} \frac{H_{m0}}{d} &\leq (0.08 - s) \cdot \left((0.06 \cdot d_{relative})^{-1} + 0.94 \cdot (1.17 \cdot 10^{20})^{s} \right) \\ &\leq (1.33 - 16.6s) \cdot d_{relative}^{-1} + (0.075 - 0.94s) \cdot (1.17 \cdot 10^{20})^{s} \end{aligned} \tag{G.1}$$

Comparing the resulting stability function of the grey reef to the stability function of the pink reef, the only difference is the relation between the c_1 constant and the wave steepness s. For the grey reef, this is equal to $c_1 = 0.07 - s$, while for the pink reef this is equal to $c_1 = 0.08 - s$. This difference initiates that the pink reef is somewhat more stable than the grey one.

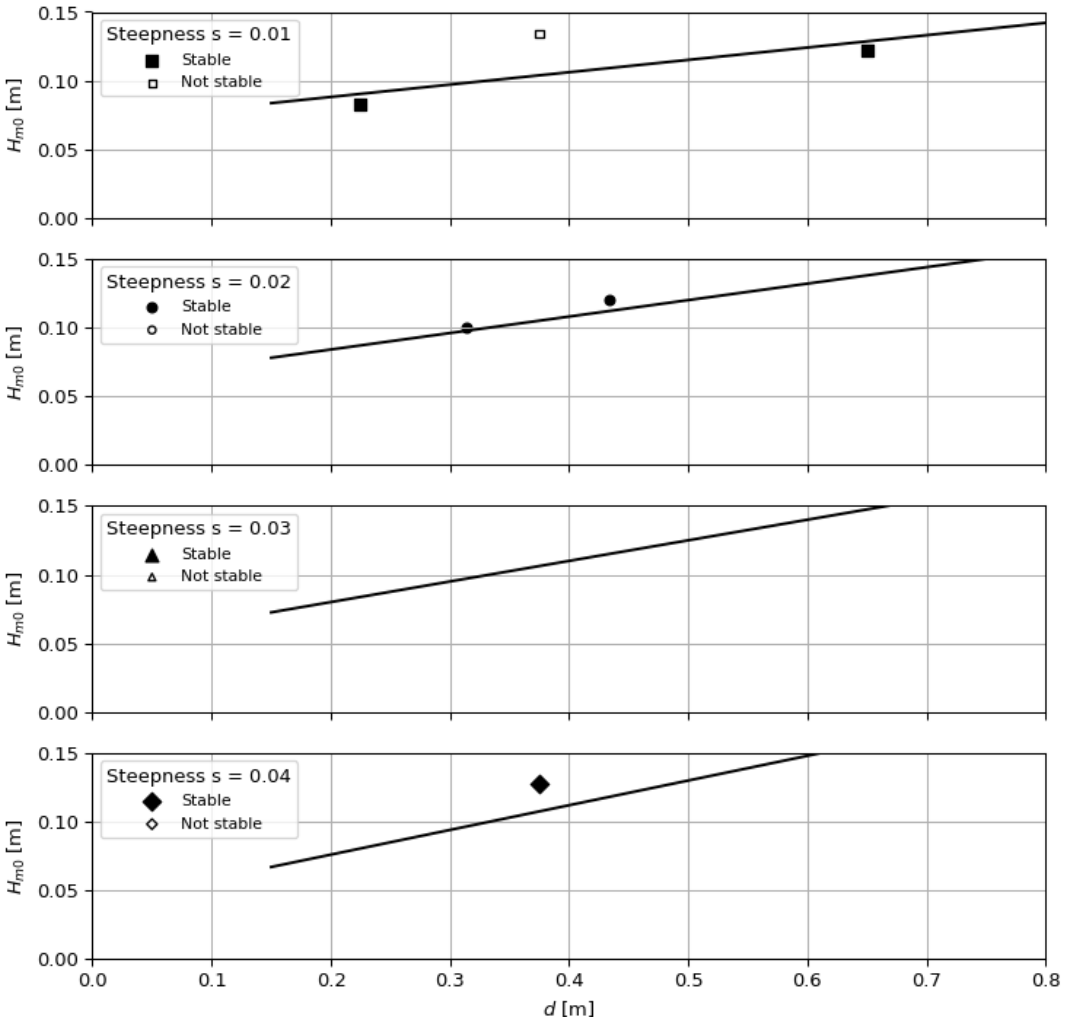

Figure G.1: Linear relation between the wave height H_{m0} and the water depth d for four different wave steepnesses. The plotted trend lines indicate the linear relationship, suggesting the extreme limit at which the reef just remains stable. The data points are obtained from the irregular wave tests for the pink reef model.

Table G.1: Four steepnesses with the corresponding trend line function and rewritten function for the relative wave height H_{m0}/d for the pink reef

Wave Steepness	**Function** Trend line	**Rewritten** Relative wave height
$s = 0.01$	$H_{m0} = 0.09d + 0.07$	$\frac{H_{m0}}{d} = 0.07\left(1.3 + \frac{1}{d}\right)$
$s = 0.02$	$H_{m0} = 0.12d + 0.06$	$\frac{H_{m0}}{d} = 0.06\left(2.0 + \frac{1}{d}\right)$
$s = 0.03$	$H_{m0} = 0.15d + 0.05$	$\frac{H_{m0}}{d} = 0.05\left(3.0 + \frac{1}{d}\right)$
$s = 0.04$	$H_{m0} = 0.18d + 0.04$	$\frac{H_{m0}}{d} = 0.04\left(4.5 + \frac{1}{d}\right)$

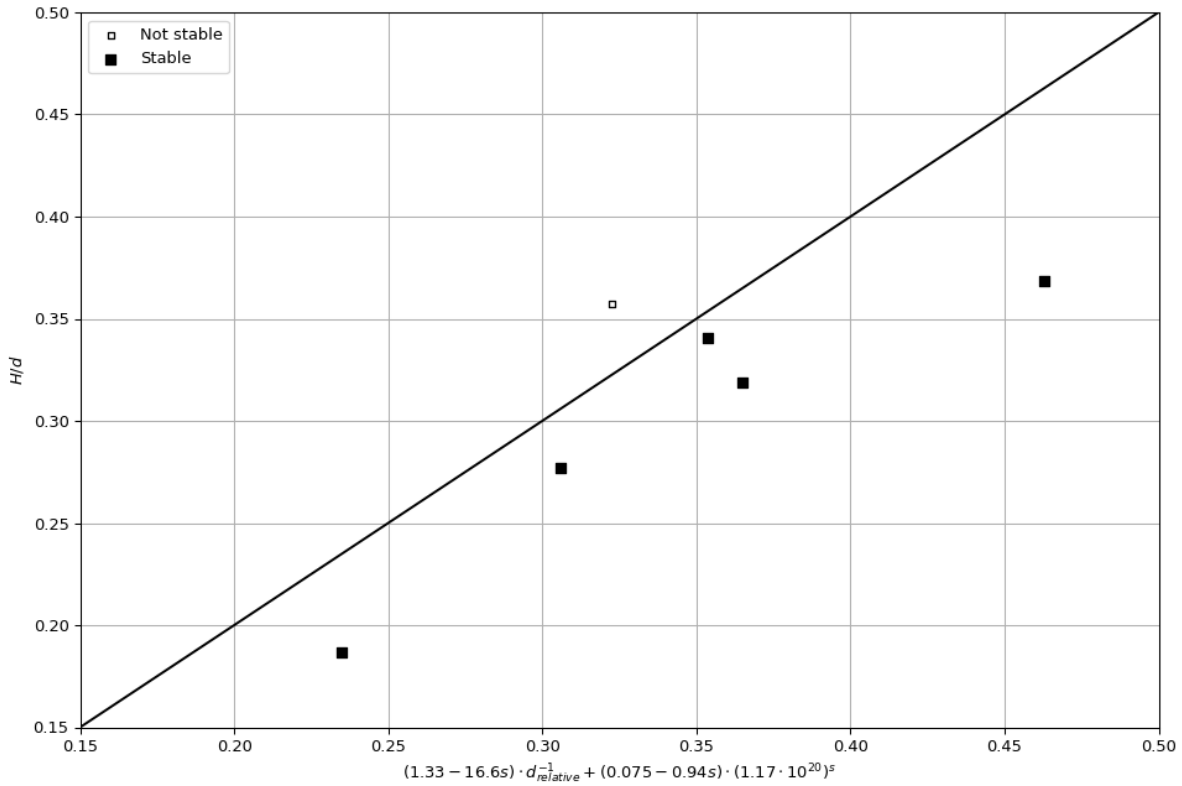

Figure G.2: Relation of the resulting stability function for the pink reef including data points, with the unstable points above the line and stable points below

G.1.2. Morison applicability

When applying the Morison method for the pink reef, the values of the parameters used are given in Table G.2. Compared to the single plate grey reef, the value of the projected cross-section seen from the flow direction A_p is slightly larger, as the pink reef is higher. The volume V and dry weight W_{dry} are determined in Section 3.3. The planform area S is equal to a 0.1 meter by 0.1 meter square, resulting in an area of 0.01 m^2, which is the same as for the grey reef.

Figure G.3 gives the Morison method applied to the pink reef model and the data points from the wave flume tests with the pink reef. Although the number of data points for the pink reef is small, the Morison method corresponds well to the points.

Table G.2: Values used to determine the graphs in Figure G.3

C_d	C_m	C_l	μ	A_p [m^2]	V [m^3]	S [m^2]	W_{dry} [kg]
2	3	2	0.5	0.01	0.000313	0.01	0.625

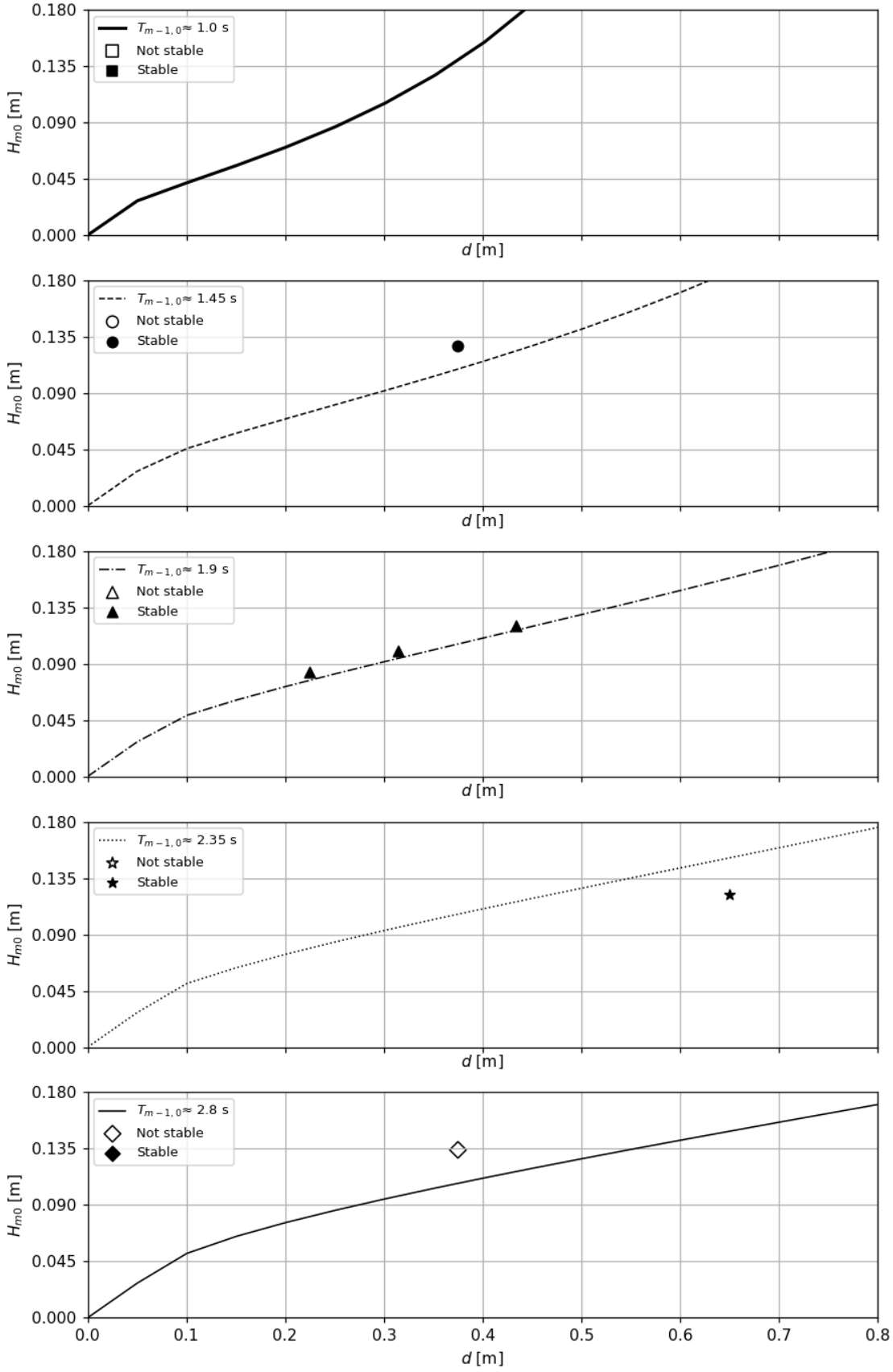

Figure G.3: Separate plots for the relation between the significant wave height and the water depth for several spectral periods for the double plate (pink) reef model according to the Morison stability prediction, including the data points of the flume tests

G.1.3. Applicability of prediction method using the mobility parameter

The prediction method using the mobility parameter (Equation 4.6) is applied to the pink reef as well, as can be seen in Figure G.4. As the density of the double plate pink reef is equal to 1997 kg/m^3 (Section 3.3), and assuming a water density of 1000 kg/m^3, the relative density is equal to 0.997. The mobility parameter θ depends on a characteristic diameter of the reef D_{reef} as well, which is assumed to be equal to 0.14 m for the pink reef. This diameter is based on the largest dimension of the surface of the reef, being the diagonal, and is, therefore, the same as for the grey reef. For the relative water depth $d_{relative}$ determination, a reef height of 0.07 m is used.

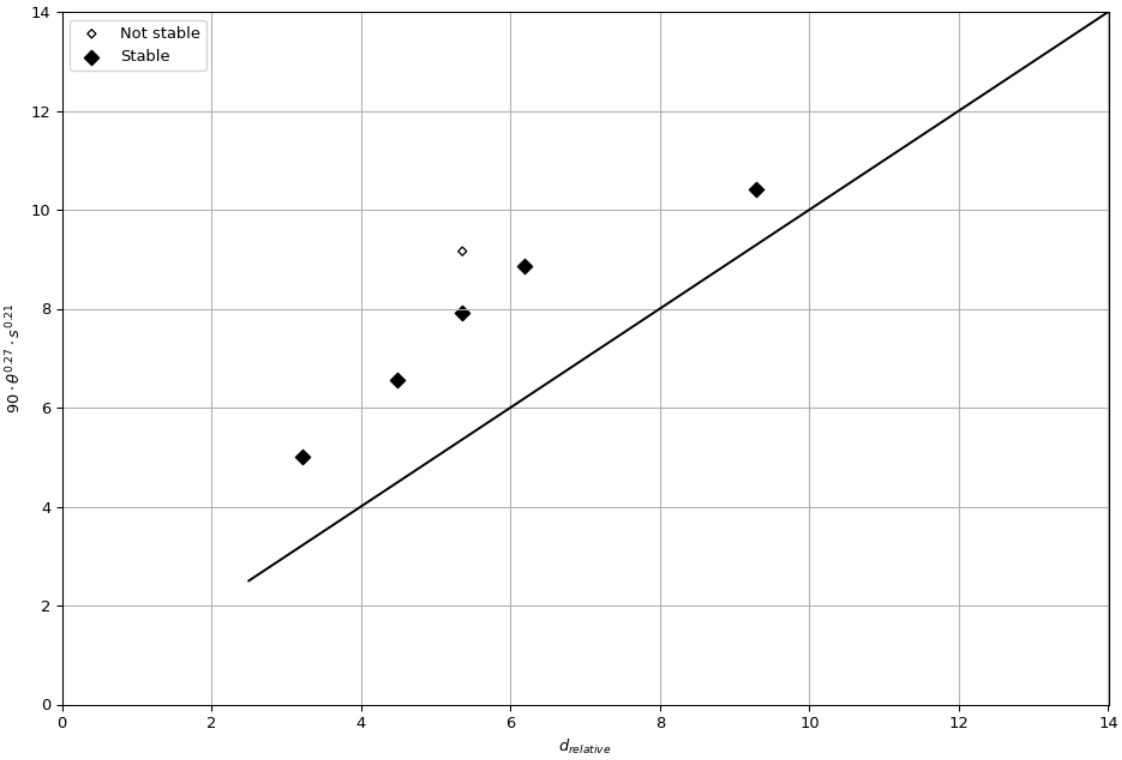

Figure G.4: Relation of the prediction method using the mobility parameter for the pink reef in which $r_1 = 90$ including data points

The data points, including the stable ones, are all located above the stability line. Since all stable tests are above the stability line while they should be below, the method underestimates the stability of the pink reef. Underestimating the stability is preferable to overestimating since an overestimation may lead to an unexpected instability of the reef. Redefining the values for the constants r_1, r_2, and r_3 can lead to a better fit through the data points of the pink reef. The linear relation between the relative water depth $d_{relative}$ and the y-axis, the θs-multiplication including constants, is still visible. Therefore, a reef-specific mobility parameter prediction method function is obtained by adjusting only the value of the constant r_1 from 90 to 55, as shown in Equation G.4. As shown in Figure G.5, this prediction method using the mobility parameter gives a representative view of the stability of the pink reef.

$$d_{relative} \leq 55 \cdot \theta^{0.27} \cdot s^{0.21} \tag{G.2}$$

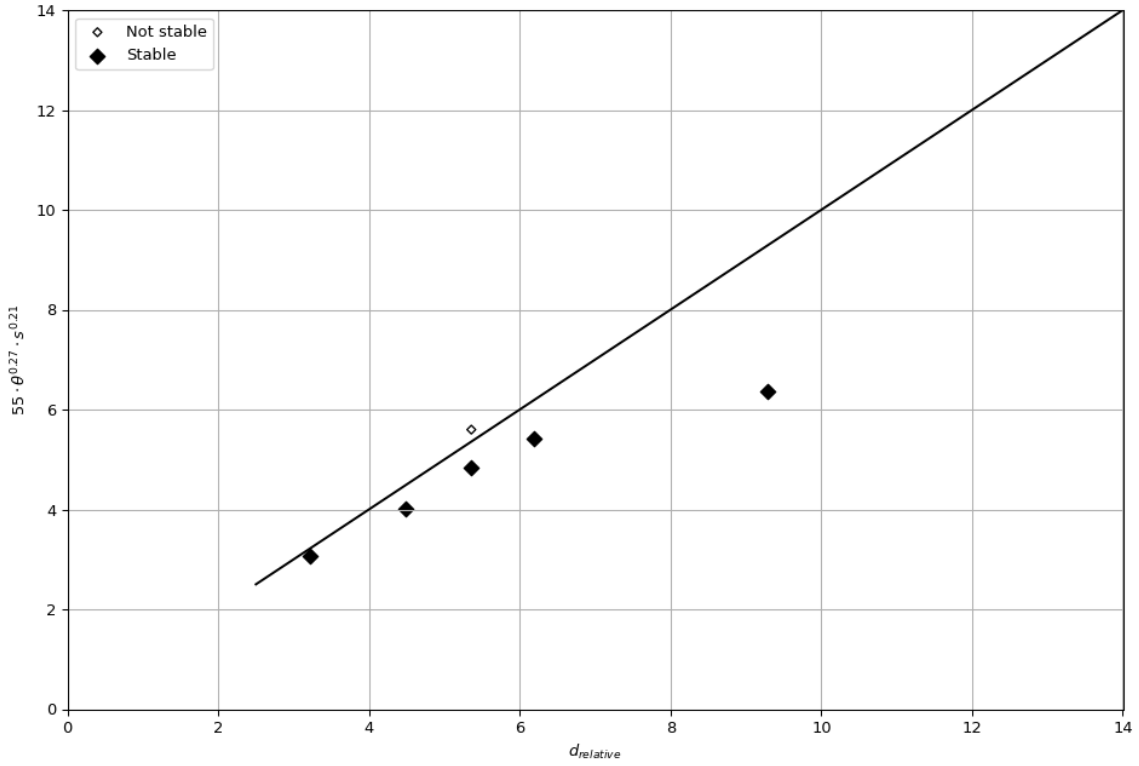

Figure G.5: Relation of the pink reef specific prediction method using the mobility parameter in which $r_1 = 55$ including data points

G.2. The 2x2 reef - four times the single plate grey reef

The 2x2 reef comprises four grey reefs (containing a single Stelcon plate). In this section, the prediction methods will be applied to the 2x2 reef.

G.2.1. Applicability of the determined stability function

The approach used to generate the stability function from Section 4.2 is also utilized to obtain the stability function for the 2x2 reef. The data points through which trend lines are constructed are shown in Figure G.6. Table G.3 contains the functions for these trend lines. The trend lines were generated using the probabilities gained from the grey reef trend lines, even though only six data points are available.

The resulting stability function for the 2x2 reef is given in Equation G.3, for which the comparison with the data points is given in Figure G.7. For determining the relative water depth $d_{relative}$, a reef height of 0.06 m is used, which is the same as for the grey reef. All stable points are below the stability line, and the only unstable point is above the line. From this, it can be concluded that the determined stability function for the 2x2 reef gives a representative view of the stability of the reef.

$$\begin{aligned} \frac{H_{m0}}{d} &\leq (0.09 - s) \cdot \left((0.06 \cdot d_{relative})^{-1} + 0.94 \cdot (1.17 \cdot 10^{20})^{s} \right) \\ &\leq (1.5 - 16.6s) \cdot d_{relative}^{-1} + (0.085 - 0.94s) \cdot (1.17 \cdot 10^{20})^{s} \end{aligned} \tag{G.3}$$

Comparing the resulting stability function of the grey reef to the stability function of the 2x2 reef, the only difference is the relation between the c_1 constant and the wave steepness s. For the grey reef, this is equal to $c_1 = 0.07 - s$, while for the 2x2 reef this is equal to $c_1 = 0.09 - s$. This difference initiates that the 2x2 reef is somewhat more stable than the grey one and even somewhat more stable than the pink reef.

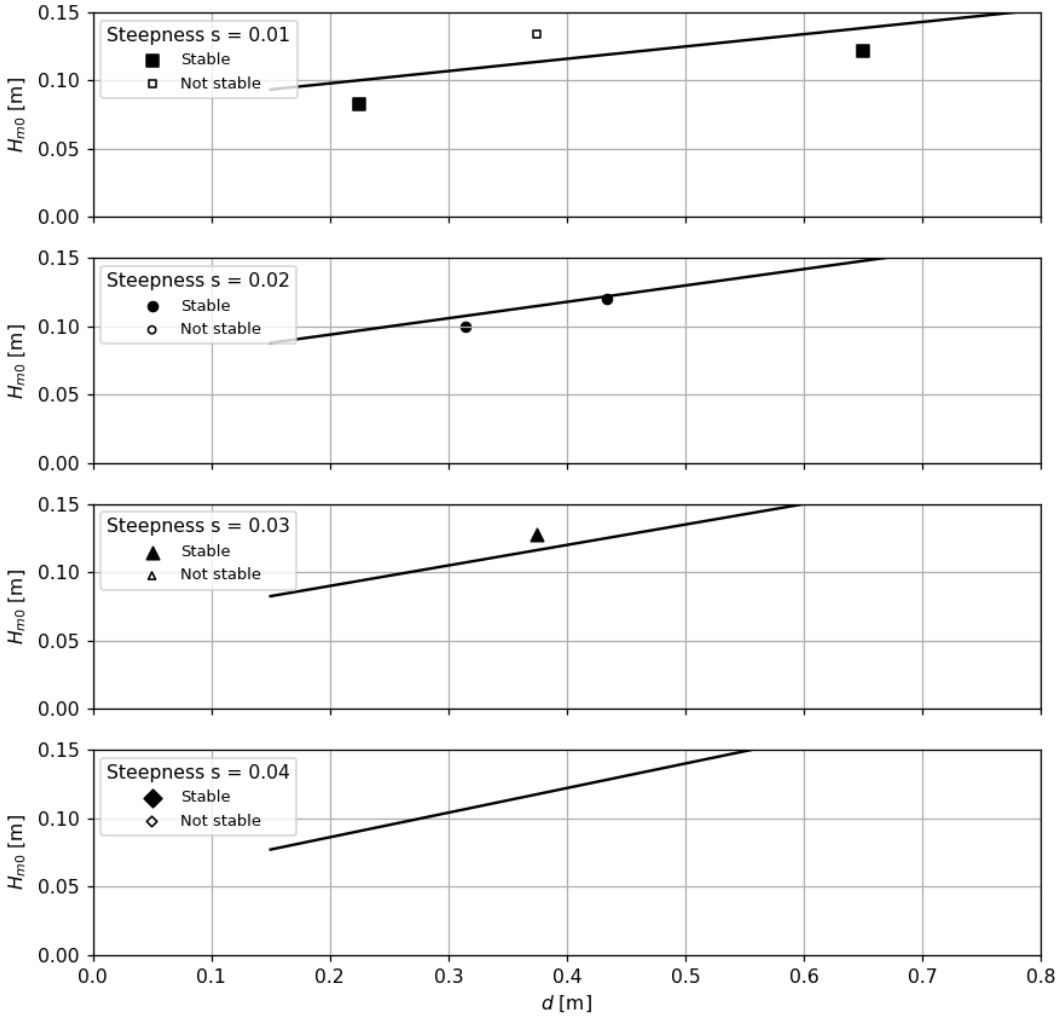

Figure G.6: Linear relation between the wave height H_{m0} and the water depth d for four different wave steepnesses. The plotted trend lines indicate the linear relationship, suggesting the extreme limit at which the reef just remains stable. The data points are obtained from the irregular wave tests for the 2x2 reef model.

Table G.3: Four steepnesses with the corresponding trend line function and rewritten function for the relative wave height H_{m0}/d for the 2x2 reef

Wave Steepness	**Function** Trend line	**Rewritten** Relative wave height
$s = 0.01$	$H_{m0} = 0.09d + 0.08$	$\frac{H_{m0}}{d} = 0.08\left(1.1 + \frac{1}{d}\right)$
$s = 0.02$	$H_{m0} = 0.12d + 0.07$	$\frac{H_{m0}}{d} = 0.07\left(1.7 + \frac{1}{d}\right)$
$s = 0.03$	$H_{m0} = 0.15d + 0.06$	$\frac{H_{m0}}{d} = 0.06\left(2.5 + \frac{1}{d}\right)$
$s = 0.04$	$H_{m0} = 0.18d + 0.05$	$\frac{H_{m0}}{d} = 0.05\left(3.6 + \frac{1}{d}\right)$

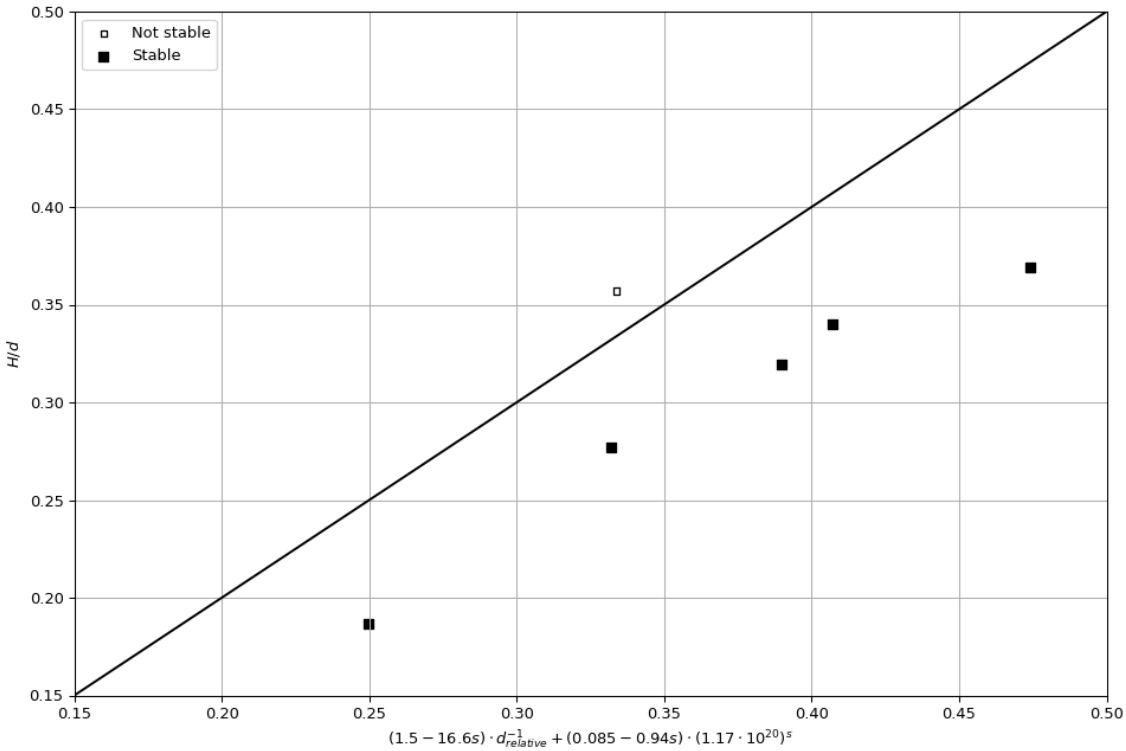

Figure G.7: Relation of the resulting stability function for the 2x2 reef including data points, with the unstable points above the line and stable points below

G.2.2. Morison applicability

The values of the parameters used in the Morison method for the 2x2 reef are listed in Table G.4. Compared to the single plate grey reef, the value of the projected cross-section seen from the flow direction A_p is three times greater, resulting in a value of 0.027 m^2. The volume V and dry weight W_{dry} are determined in Section 3.3. The 2x2 reef's planform area S is four times that of the grey reef's planform area.

The Morison approach applied to the 2x2 reef model, and the data points from the wave flume testing with the 2x2 reef are shown in Figure G.8. Since the same tests with irregular waves were conducted for the pink and the 2x2 reef, the data points for both comparisons do not differ. What is different are the graphs derived from the Morison method. It seems that the Morison method underestimates the stability of the reef for the 2x2 reef since four of the five data points for stable tests are above the prediction curves while they should be below.

Table G.4: Values used to determine the graphs in Figure G.8

C_d	C_m	C_l	μ	A_p [m^2]	V [m^3]	S [m^2]	W_{dry} [kg]
2	3	2	0.5	0.027	0.000707	0.04	1.417

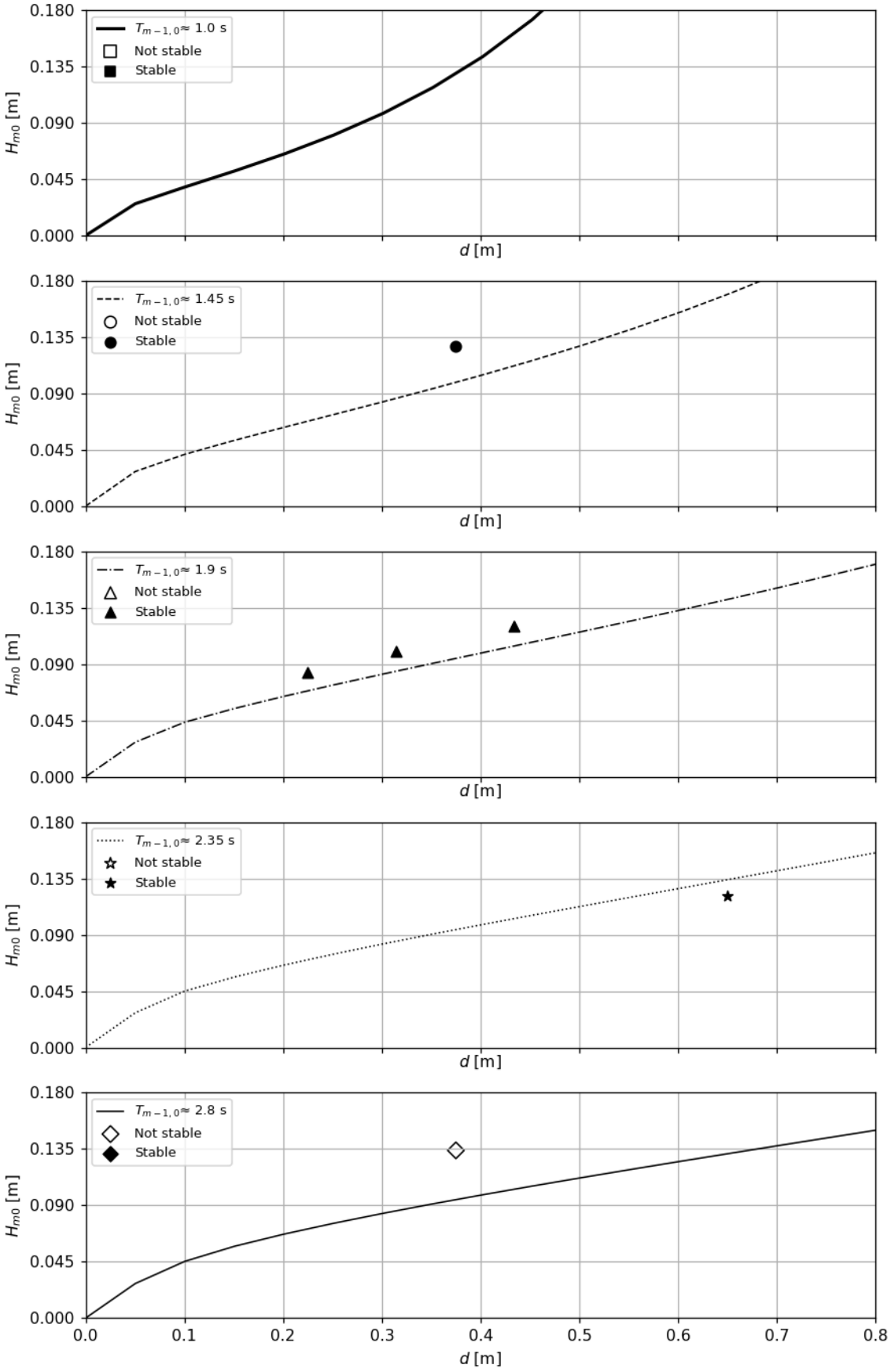

Figure G.8: Separate plots for the relation between the significant wave height and the water depth for several spectral periods for the 2x2 reef model according to the Morison stability prediction, including the data points of the flume tests

G.2.3. Applicability of prediction method using the mobility parameter

The prediction method using the mobility parameter is also applied to the 2x2 reef, as seen in Figure G.9. As the density of the double plate pink reef is equal to 2004 kg/m^3 (see Section 3.3), and assuming a water density of 1000 kg/m^3, the relative density will be equal to 1.004. The mobility parameter θ depends on a characteristic diameter of the reef D_{reef} as well, which is assumed to be equal to 0.28 m. This diameter is based on the largest dimension of the surface area of the reef, being the diagonal, and is the same as two times the diagonal of the grey reef. For the relative water depth $d_{relative}$ determination, a reef height of 0.06 m is used.

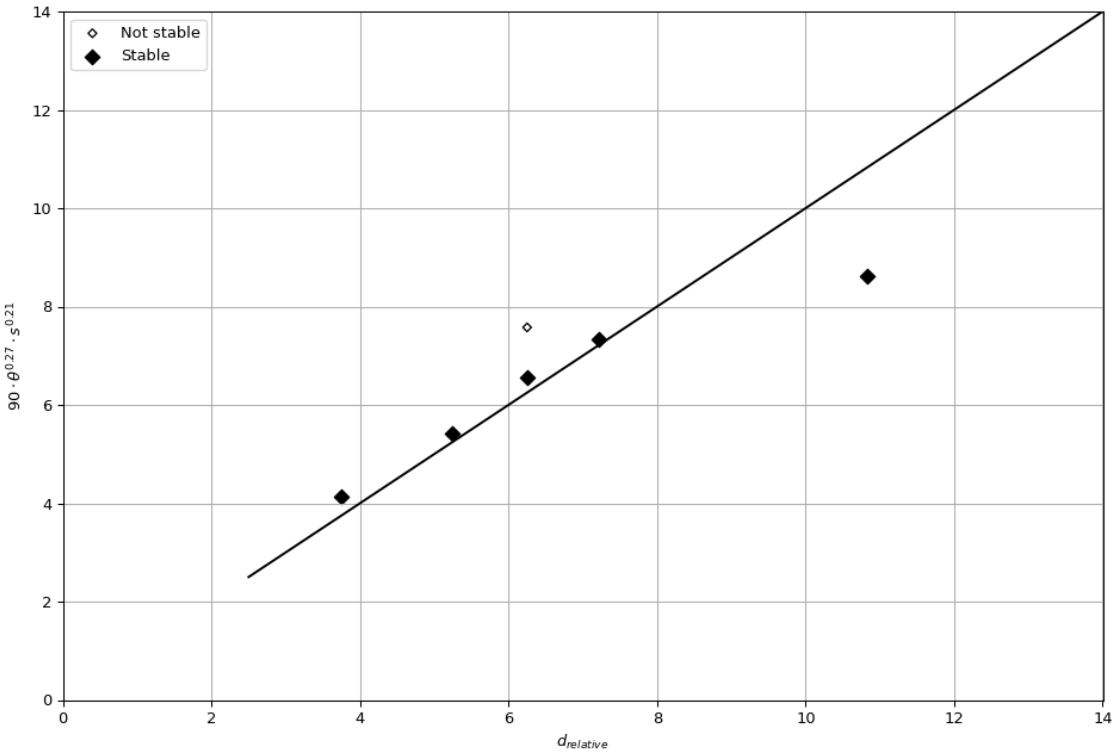

Figure G.9: Relation of the prediction method using the mobility parameter in which $r_1 = 90$ for the 2x2 reef including data points

The prediction method using the mobility parameter gives a pretty good estimation of the data points for the 2x2 reef, but a small underestimate is visible. This is because the stable points are below or slightly above the stability line, and the only unstable point is above. However, by adjusting only the value of the constant r_1 from 90 to 80, a reef-specific mobility parameter prediction method function is obtained for the 2x2 reef, as shown in Equation G.4. Figure G.10 shows this prediction method using the mobility parameter, which gives a representative view of the stability of the 2x2 reef.

$$d_{relative} \leq 80 \cdot \theta^{0.27} \cdot s^{0.21} \tag{G.4}$$

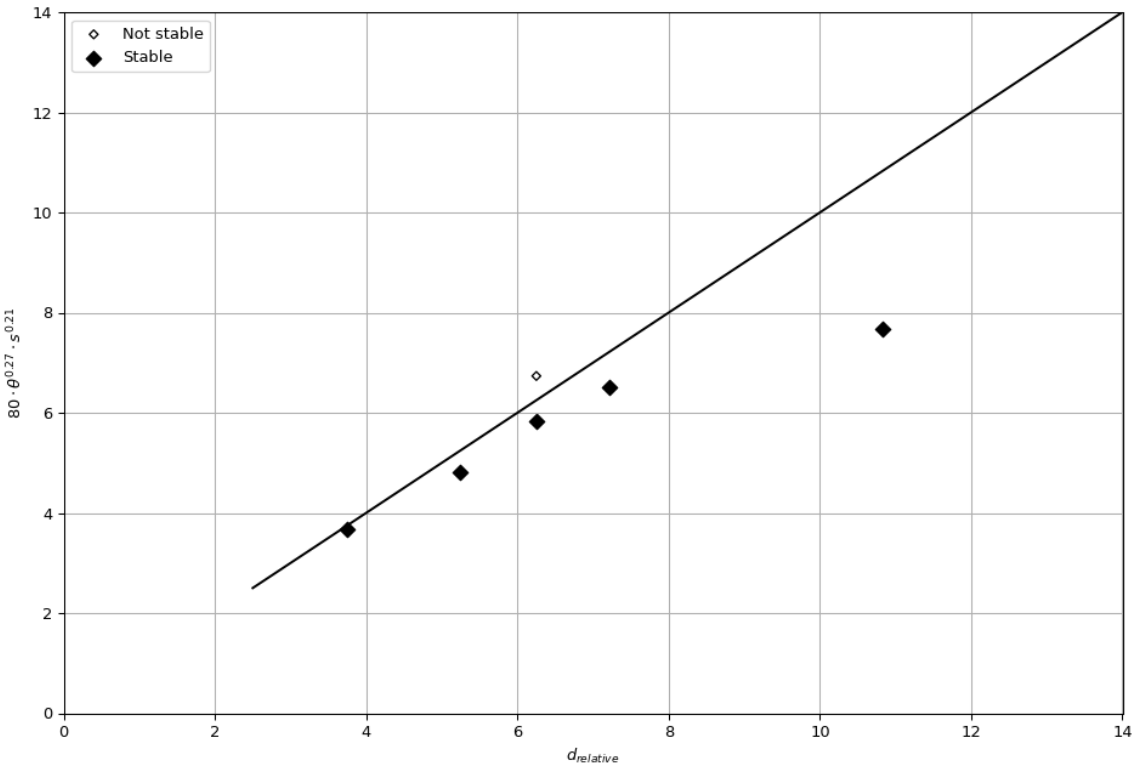

Figure G.10: Relation of the 2x2 reef specific prediction method using the mobility parameter in which $r_1 = 80$ including data points